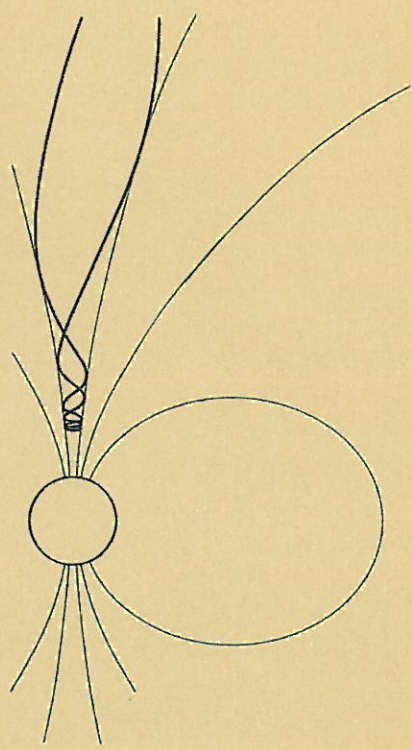


Dynamics of small satellites with gravity gradient attitude control



Julio Zorita



KTH Electrical Engineering

*Master of Science Thesis
Stockholm, Sweden 2011*



Space and Plasma Physics Department
KTH, Kungliga Tekniska Högskolan
SE-100 44 Stockholm
Sweden

DYNAMICS OF SMALL SATELLITES WITH GRAVITY GRADIENT ATTITUDE CONTROL

October 25, 2011

Author:
Julio Zorita

Supervisors:
Nickolay Ivchenko
Gunnar Tibert

Master of Science Thesis
Stockholm, Sweden 2011
XR-EE-SPP 2011:006

Abstract

SWIM (Space Weather using Ion Spectrometers and Magnetometers) is a CubeSat to be launched with the purpose of studying interaction between the Sun and the Earth. A magnetometer will be placed in a boom which provides gravity gradient stabilization. SWIM will be inserted in a 600 km circular orbit and it is required to maintain a LVLH (Local Vertical Local Horizontal) position. This master thesis analyses the dynamical behavior of SWIM. For doing so an attitude simulator and a mass model have been developed. Mass model has been designed according to linear stability analysis. Simulations with the mass model have been carried out from the most ideal environment to realistic orbit. As a result it has been deduced that gravity gradient stabilization propagates initial conditions which are perturbed by aerodynamic and magnetic torques. Magnetic torques could lead to uncontrolled yaw spin. Additionally the deployment of two solar panels to guarantee passive stabilization for yaw axes has been studied. Three axes stabilization and LVLH pointing can be achieved in an orbit lower than 600 km.

Acknowledgements

I would like to express my immense gratitude to Dr. Nickolay Ivchenko and Dr. Gunnar Tibert for their supervision and guidance while I was working on this thesis.

Similarly I would like to thank Dr. Troy Henderson from Virginia Tech who helped me while developing the attitude simulator, and the people from the Space System Laboratory at Virginia Tech, Robbie, Zack, Brad, Adam and Andrew for their warm welcome, fantastic work environment and friendship.

This thesis would have not been possible without my family, my mother María de la Paz, my sister Cayetana and my father Julio, who have always encouraged me throughout my university studies.

Also I would like to thank all the people of Space and Plasma Physics Department and the RAIN experiment team, who I have been working with since the beginning of this Master Thesis in a comfortable environment, in particular thanks to Will Reid for his advice.

I would like to thank Mario Valle for his assistance with the report structure and Israel Pons for his collaboration with the figures.

Last but not least I would like to thank all my friends for being supportive since the beginning of this thesis, in particular Enrique Mata with whom I have shared long working hours at KTH.

Contents

1	Introduction	1
1.1	CubeSat Technology	1
1.2	SWIM Project	2
1.2.1	Mission Experiments	2
1.2.2	Mission Specifications	2
1.3	KTH Participation	3
1.4	Gravity Gradient Stabilization	4
1.5	Active Control	4
1.6	Master Thesis Aim	5
2	Background	7
2.1	Orbital Mechanics	7
2.1.1	Two Body Problem	7
2.1.2	Spacecraft in Low Earth Orbit	8
2.1.3	Gravitational Potential Field Model	9
2.1.4	Atmospheric Drag	10
2.2	Attitude Kinematics	11
2.2.1	Finite Rotations	11
2.2.2	Direction Cosine Matrix (DCM)	12
2.2.3	Euler Angles	12
2.2.4	Eigenaxis Rotation	13
2.2.5	Euler Parameters, Quaternions	14
2.2.6	Kinematic Differential Equations	15
2.2.7	Attitude Definition	15
2.3	Rigid-Body Dynamics	17
2.3.1	Dynamic Equations	17
2.4	Disturbance Torques	18
2.4.1	Gravity Gradient Torque	18
2.4.2	Magnetic Torque	19
2.4.3	Aerodynamic Torque	20
2.5	Gravity Gradient Linear Stability Analysis	21
2.5.1	Circular Orbit	21
2.5.2	Circular Orbit Kinematics	21
2.5.3	Circular Orbit Equations of Motion	21
2.5.4	Linearized Equations	22
2.5.5	Linear Stability Analysis	23
2.5.6	Nadir and Zenith Position	24
3	Satellite Characterization	25
3.1	Mass and Geometric Properties	25
3.1.1	Center of Mass	26
3.1.2	Moments of Inertia	26
3.1.3	Boom Length	27
3.2	Aerodynamic Characterization	29

3.3	Magnetic Moment	29
4	Attitude Simulator	31
4.1	Simulator Layout	31
4.2	Initial Conditions for Propagation	31
4.2.1	Initial Conditions for Orbit Propagation	32
4.2.2	Initial Conditions for Attitude Propagation	34
4.3	ODE's Integrator	35
4.3.1	Attitude Simulator Results	35
4.3.2	Simulation Errors	37
4.4	Data Processing	38
4.4.1	Basis Vectors	38
4.4.2	Attitude Visualization	40
5	Circular Orbit and Gravity Gradient	43
5.1	Mass Model of SWIM	43
5.2	Circular Orbit	43
5.3	Pitch Propagation	44
5.3.1	Pitch Propagation Conclusions	48
5.4	Roll and Yaw Propagation	49
5.4.1	Roll and Yaw Periods	53
5.4.2	Angular Velocity	54
5.4.3	Conclusions	55
5.5	Boom Length	56
6	Non-Circular and Perturbed Orbits	59
6.1	Eccentricity Effect	59
6.1.1	Eccentricity in the Attitude Motion	61
6.2	Perturbed Orbits	63
6.2.1	Earth's Gravity Field	64
6.2.2	Atmospheric Drag	65
6.3	Conclusions	66
7	Attitude Disturbances	67
7.1	Aerodynamic Disturbances	67
7.1.1	Boom Length and Aerodynamic Torque	70
7.1.2	Aerodynamic Torque Conclusions	71
7.2	Magnetic Disturbances	72
7.2.1	Earth's Magnetic Field	72
7.2.2	Attitude Propagation with Magnetic Torque	73
7.2.3	Magnetic Torque Discussion	74
7.2.4	Magnetic Torque Conclusions	76
8	Mission Simulation	77
8.1	Mission Description	77
8.2	Uncontrolled Yaw Motion	81
8.3	Boom Position	82
8.4	Different Mass Configuration	84
8.5	Mission Conclusions	86
9	Aerostable Spacecraft	87
9.1	New Mass Distribution	87
9.2	Attitude Propagation	88
9.2.1	Attitude with Aerodynamic Torque	90
9.2.2	Attitude with Magnetic Torque	92
9.3	Propagation at Lower Altitude	93

9.3.1	Initial Deviations and Magnetic Torque	94
9.3.2	Aerodynamic Damping	95
9.4	Conclusions	95
10	Conclusions	97
10.1	Boom Length and Position	97
10.2	Dynamic Constrains	98
10.3	Future Work	98

List of Figures

1.1	CubeSat skeleton, [16].	1
1.2	SMILE magnetometer.	3
1.3	SIMPLE boom, [20].	3
1.4	Dragonsat 1 model with boom deployed.	4
2.1	Two body problem in an inertial reference frame.	8
2.2	Upper atmosphere density [7].	10
2.3	ECI N , A and B reference frames [4].	11
2.4	Axes definition.	16
2.5	Earth's magnetic field.	19
2.6	Stability regions of gravity gradient torque [4].	24
3.1	Models of hub and rod.	25
3.2	Auxiliary reference frame A'	26
3.3	Mass properties.	28
3.4	Gravity gradient torque as function of boom length.	28
3.5	Linear pitch period as function of boom length.	29
4.1	Attitude simulator layout.	31
4.2	ECI reference frame and orbit orientation, [5].	33
4.3	Perifocal and ECI N reference frames [5].	34
4.4	Position and velocity vectors in the ECI reference frame.	36
4.5	Orbit in 3D plot in the ECI reference frame.	36
4.6	Angular velocity.	37
4.7	Quaternions response.	37
4.8	Numerical error.	38
4.9	A frame along one orbit.	39
4.10	B frame along one orbit.	39
4.11	Attitude response.	40
4.12	A and B reference frames.	40
4.13	Attitude response.	41
5.1	Pitch motion for different initial angles.	45
5.2	Angular velocity for different initial angles.	45
5.3	Pitch motion for different $\omega_{2,t=t_0}$	46
5.4	Angular velocity for different $\omega_{2,t=t_0}$	46
5.5	Discontinuous pitch motion $\omega_{2,t=t_0} = 0.25n$ and $\theta_{2,t=t_0} = 0^\circ$	47
5.6	Basis vectors A and B reference frames.	47
5.7	Euler angles and linear theory for different $\theta_{1,t=t_0}$	49
5.8	Euler angles for different $\theta_{1,t=t_0}$	50
5.9	Angular velocity ω_i for different $\theta_{1,t=t_0}$	50
5.10	Angular velocity ω_i for different $\theta_{1,t=t_0}$	51
5.11	Linear equations angle motion, for different $\theta_{3,t=t_0}$	51
5.12	Euler angles θ_i , for different $\theta_{3,t=t_0}$	52

5.13	Linear equations angular velocity ω_i for different $\theta_{3,t=t_0}$	52
5.14	Angular velocity ω_i for different $\theta_{3,t=t_0}$	53
5.15	Euler angles θ_i for different $\omega_{i,t=t_0}$	54
5.16	Angular velocity ω_i for different $\omega_{i,t=t_0}$	55
5.17	Maximum deviation for $\theta_{1,t=t_0}$ and different boom lengths.	56
5.18	Maximum deviation for $\theta_{2,t=t_0} = 15^\circ$ and different boom lengths.	56
5.19	Maximum deviation for $\theta_{3,t=t_0}$ and different boom lengths.	57
6.1	Orbit trajectories for different eccentricities.	60
6.2	Eccentricity effect on the attitude.	60
6.3	Angular response for different $\theta_{1,t=t_0}$ and $e=0.01$.	61
6.4	Angular response for different $\theta_{2,t=t_0}$ and $e=0.01$.	62
6.5	Angular response for different $\theta_{3,t=t_0}$ $e=0.01$.	63
6.6	Earth oblateness effect on orbit altitude and roll axis.	64
6.7	Earth oblateness effect on the pitch and yaw axes	65
6.8	Orbit decay due to atmospheric drag.	66
7.1	Aerodynamic force and torque profiles.	68
7.2	Attitude propagation with aerodynamic torque and increasing $\theta_{1,t=t_0}$	68
7.3	Attitude propagation with aerodynamic torque and increasing $\theta_{2,t=t_0}$	69
7.4	Attitude propagation with aerodynamic torque and increasing $\theta_{3,t=t_0}$	70
7.5	Maximum deviation with aerodynamic torque with roll and yaw initial deviations.	70
7.6	Maximum deviation for $\theta_{2,t=t_0} = 15^\circ$, different boom length and aerodynamic torque.	71
7.7	Magnetic field in ECI and body reference frame for 98° inclination orbit.	72
7.8	Attitude propagation for different magnetic moments μ_1 .	73
7.9	Attitude propagation for different magnetic moments μ_2 .	73
7.10	Attitude propagation for different magnetic moments μ_3 .	74
7.11	Magnetic field in body frame for $\mu_2 = 0.5 \text{ mAm}^2$	75
7.12	Torque profiles for $\mu_2 = 0.5 \text{ mAm}^2$.	75
7.13	Yaw torques for $\mu_2 = 0.5 \text{ mAm}^2$.	76
8.1	Attitude response for mission simulation with initial roll $\theta_{1,t=t_0}$	78
8.2	Attitude response for mission simulation with initial pitch $\theta_{2,t=t_0}$	79
8.3	Attitude response for mission simulation with initial yaw $\theta_{3,t=t_0}$	79
8.4	Attitude response for mission simulation with $\mu = 0.1, 0.2 \text{ mAm}^2$	80
8.5	Magnetic and aerodynamic torques for $\mu = 0.2 \text{ mAm}^2$	80
8.6	Torques for $\mu = 0.2 \text{ mAm}^2$	81
8.7	Yaw response to different μ .	82
8.8	Maximum deviation with respect to boom position.	82
8.9	Maximum deviation with respect to boom position and initial roll.	83
8.10	Attitude response for new boom configuration and $\theta_{1,t=t_0} = 15^\circ$.	84
8.11	Attitude response for new boom configuration and $\theta_{2,t=t_0} = 15^\circ$.	85
8.12	Attitude response for mission new boom configuration and $\theta_{3,t=t_0} = 15^\circ$.	86
9.1	Aerodynamic torque about the yaw axis.	87
9.2	Attitude and angular velocity propagation for $\theta_{1,t=t_0} = 15^\circ$ in circular orbit.	89
9.3	Attitude and angular velocity propagation for $\theta_{2,t=t_0} = 15^\circ$ in circular orbit.	89
9.4	Attitude and angular velocity propagation for $\theta_{3,t=t_0} = 15^\circ$ in circular orbit.	90
9.5	Aerodynamic forces and torques for $\theta_{3,t=t_0} = 15^\circ$	90
9.6	Attitude with aerodynamic torque.	91
9.7	Yaw for different μ and panel length.	92
9.8	Yaw for different μ and panel length at 550 km.	93
9.9	Attitude with magnetic torque and initial deviation.	94
9.10	Attitude propagation at 500 km.	95

List of Tables

2.1	Zonal harmonics.	9
3.1	Center of mass of different elements.	26
3.2	Moments of inertia for different elements.	27
3.3	SWIM mass properties.	27
4.1	Initial conditions for orbit propagation.	35
4.2	Initial conditions for attitude propagation.	36
5.1	Mass Properties of SWIM model.	43
5.2	Orbit parameters.	44
5.3	Initial conditions pitch propagation.	44
5.4	Initial conditions for different ω_2 .	46
5.5	Initial conditions for different roll angles.	49
5.6	Initial conditions for different yaw angles.	51
5.7	Periods	54
5.8	Initial conditions for different angular velocities.	54
6.1	Initial conditions for eccentricity test.	60
6.2	Initial conditions about the roll axis, for elliptical orbits.	61
6.3	Initial conditions about the pitch axis, for elliptical orbits.	62
6.4	Initial conditions about the yaw axis, for elliptical orbits.	62
6.5	Perturbed accelerations at different altitudes.	63
6.6	Initial conditions Earth's oblateness test.	64
7.1	Mass properties for aerodynamic test.	67
7.2	Orbit parameters.	72
8.1	Initial conditions for orbit propagation	77
8.2	Initial conditions for roll mission analysis.	77
8.3	Initial conditions for pitch mission analysis.	78
8.4	Initial conditions for yaw mission analysis.	79
8.5	Mass Properties for boom deployed in 10×10 face.	84
9.1	Mass properties aerodynamic test.	88
9.2	Initial attitude conditions for new mass distribution.	88
9.3	Moments of inertia for different panel length.	92
9.4	Initial conditions for attitude propagation with magnetic torque.	94

Chapter 1

Introduction

Since the beginning of the Space era, technological advances brought by space research have had an extraordinary impact on people's lives. Furthermore, it is impossible to understand today's life without satellites orbiting the Earth. At first sight, outer space might be seen as a perfect environment to launch unmanned vehicles into. However, it is a hazardous environment for most satellite components. Therefore, improving our knowledge of the space environment is fundamental to advance in space technology.

There is only one way to do research in space. This is by sending measuring instruments into orbit. But major obstacles come from the high cost of designing, manufacturing, testing and, particularly, launching them into orbit. Reducing the size of scientific satellites in order to be able to launch them together with larger satellites is a way to make it more feasible. Based on this idea the CubeSat concept was created.

1.1 CubeSat Technology

In 1999 the CubeSat concept appeared as a collaboration between Professor Jordi Puig-Suari at California Polytechnic State University (Cal Poly) and Professor Bob Twiggs at Stanford University. The goal of the project is to provide a standard for design of picosatellites to reduce cost and development time, making space more accessible [1]. Currently the CubeSat Project is an international collaboration between universities, companies, and institutions worldwide.



Figure 1.1: CubeSat skeleton, [16].

The primary objective of building a CubeSat is to put into space small payloads within an affordable budget. Cubesats are launched as secondary payloads together with larger satellites (primary payload). Therefore, it is essential to assure the safety of the primary payload, launch vehicle and other CubeSats that could be on board. The best way to do so is standardizing its design and deployment system. There are some initiatives like the CubeSat Design Specification (CDS) from Cal Poly [2]. According to refer-

ence [2] a Cubesat is 10 cm cube with mass up to 1.33 kg. More specifically this is a 1U, one Cube or single CubeSat. Figure 1.1 shows the standard structure of a 1U CubeSat. Cubes can be joined to generate 2U or 3U Cubesats. Additional the specifications for materials and payloads are also considered in [2].

Although some companies have launched their own CubeSats, due to its low price it is a perfect platform for universities to launch scientific experiments. Moreover, collaborations between different universities on projects concerning CubeSats have appeared as a remarkable side effect. One example is the SWIM project, which this master thesis project is a part of.

1.2 SWIM Project

Space Weather using Ion Spectrometers and Magnetometers, (SWIM) is a student CubeSat project promoted by Dr. H. Vo from the InterAmerican University of Puerto Rico, IUPR. The preliminary concept of SWIM is to be a 3U CubeSat with a mass of 3.64 kg and gravity gradient passive control. Its scientific objectives are to:

- Acquire relevant Space Weather data to understand Sun-to-Earth coupling.
- To measure different time-constants in the Ionosphere-Thermosphere system.

Additionally, as a student project it provides an aerospace engineering experience to students by building a CubeSat. Although launching a CubeSat is one of the most affordable ways to launch payload into space, funding is required. The SWIM project is funded by:

- Puerto Rico Industrial Development Company PRIDCO: USD 570000.
- NASA Space Grant: USD 230000.
- IUPR Bayamon Matching Fund: USD 100000.

1.2.1 Mission Experiments

In order to achieve its scientific objectives, SWIM has to carry a number of different measuring instruments or experiments. A CubeSat is also a great opportunity to test new instruments in outer space. Universities and agencies collaborate to provide instruments in order to test their readiness. The SWIM payload include the following experiments:

- Wind Ion Neutral Composite Suite from F. Herrero, NASA Goddard, Space Flight Center.
- SMILE Fluxgate Magnetometer from N. Ivchenko at Royal Institute of Technology (KTH), Sweden.
- Deployable boom from G. Wiens, University of Florida.

1.2.2 Mission Specifications

To achieve the scientific objectives of the mission, relevant data have to be measured. This means that the spacecraft has to be inserted in a suitable orbit and maintain certain attitude requirements. The SWIM mission specifications are the following:

- The satellite will be inserted in a 600 km circular polar orbit
- The satellite will be required to have an attitude knowledge and pointing accuracy of less than 5 degrees.
- The satellite will maintain a Local Vertical Local Horizontal pointing.

There are additional requirements for the instruments, but they are beyond the scope of this master thesis.

1.3 KTH Participation

KTH takes part in the SWIM project. KTH is involved in the electronics, the deployable boom, and the satellite dynamics (ACS). The electronics involve SMILE (Small Magnetometer In Low mass Experiment). SMILE is a miniature digital fluxgate magnetometer, developed at KTH jointly with Lviv Centre of Institute of Space Research, Ukraine [19]. It measures three components of the magnetic field simultaneously.

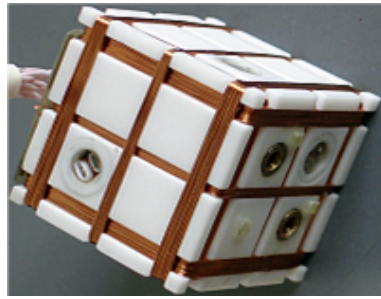


Figure 1.2: SMILE magnetometer.

To function properly, SMILE requires special onboard conditions. The magnetic moment of the satellite has to be low (magnetic cleanliness). This can be achieved by avoiding current loops and magnetic materials, but using shields or compensation magnets lead to measurement disturbance. In addition, to minimize measurement disturbances SMILE will be mounted on a boom, that also provides gravity gradient stabilization. Figure 1.2 shows SMILE. Its mechanical properties are dimensions of $20 \times 20 \times 21$ mm and mass of 20 grams.

KTH also participates in the boom development. SWIM will be equipped with a *self-contained linear meter-class deployable* (SIMPLE) boom, which is developed by the United States Air Force Research Laboratory (AFRL). SIMPLE has been designed due to the increasing capabilities demand for CubeSats, which lead to a highly compact deployable mechanism. SIMPLE is a motor-less self-deployment boom using the principle of controlled strain energy release of bi-stable tape springs [20]. Figure 1.3 shows the boom when is stored and fully deployed.

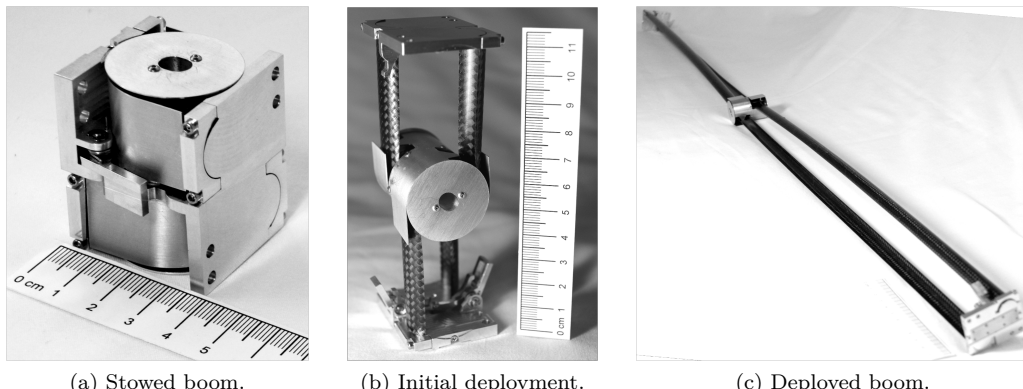


Figure 1.3: SIMPLE boom, [20].

The package dimensions of the SIMPLE boom are $50 \times 38 \times 38$ mm as depicted in Figure 1.3a. Its release mechanism is a single burn wire. The deployment actuation is at constant force, separating the two spacecraft masses (main structure and magnetometer) linearly in opposite directions, as shown in Figure 1.3b. The boom has its compact characteristics due to the use of composite bi-stable tape springs,

which act both as deployment mechanism and deployed element, like in Figure 1.3c

There is a collaboration of the University of Florida (UF), working on the boom mechanics and KTH, working on the composite materials testing.

Finally, the KTH participation also involves satellite dynamics. Having a deployed boom on a satellite has effects on the satellite motion. A study of the Cubesat dynamics with the boom deployed is carried out in this master thesis. In order to do so, collaboration between KTH and Virginia Polytechnic and State University (VT) was initiated.

1.4 Gravity Gradient Stabilization

Gravity gradient stabilization is a purely passive stabilization technique. This technique is mainly used to ensure pointing requirements towards the Earth. Pointing is achieved by deploying a boom along one of the spacecraft axes. As a consequence, the satellite tends naturally to align the boom in the direction towards the Earth's center.

Gravity gradient stabilization has been successfully employed in many Earth-pointing satellites. The major advantage of using gravity gradient is saving energy, no need of electric support or fuel, which assures long lifetime of the satellite and continuous pointing. On the other hand, its main drawback is poor pointing accuracy with respect to the orbiting reference frame [3]. A gravity boom is usually deployed along the yaw axis. Doing so provides gravity gradient Earth-pointing stabilization in the pitch and roll orientations. However the yaw motion is uncontrolled [3].

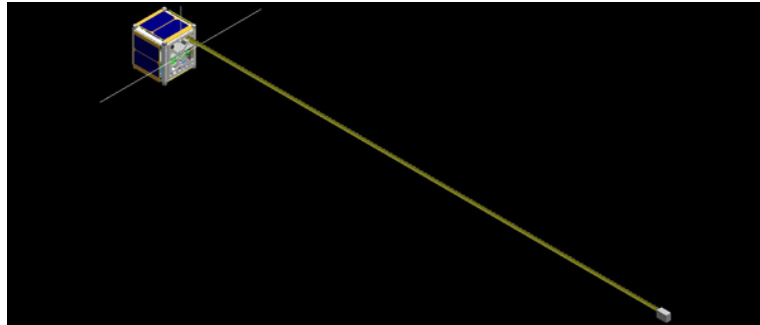


Figure 1.4: Dragonsat 1 model with boom deployed.

Figure 1.4 shows a 3D model of the Dragonsat 1, an undergraduate student project of the University of Texas, Austin. Dragonsat 1 is an example of a CubeSat with a gravity gradient boom deployed [22].

1.5 Active Control

Passive stabilization is desired if measuring devices are on board the satellite. However, depending on mission requirements it might not be suitable. Therefore, active control is applied. Attitude control with thrusters is not a suitable option due to the limited space in a CubeSat. Alternatively, the satellite can be spin-stabilized. However, it does not match with LVLH pointing requirements. Finally the spacecraft can be magnetically controlled, for which there are several options. For instance using a permanent magnet the spacecraft aligns with the Earth's magnetic field, which is not desired in this mission. Another option is to use torque coils in the three axes directions. These coils can be run by a control algorithm, which activates them when a restoring torque is required. However, how the magnetic torques affect on board experiments needs to be taken into account.

1.6 Master Thesis Aim

The aim of this Master Thesis is to analyze the dynamics of the SWIM CubeSat focusing on gravity gradient stabilization. In order to do this, an attitude simulator has been developed, which is presented in Chapter 4. A mass model of the spacecraft has been developed according to the linear stability analysis of a gravity gradient spacecraft in a circular orbit. Later attitude disturbances in terms of non ideal orbit and environmental torques are added and analyzed. Finally, simulations of the mission in a realistic environment are performed.

The objective of this document is to be a guideline for future work in the SWIM Attitude Control System (ACS) design and to understand the different aspects of small satellite attitude dynamics.

Chapter 2

Background

2.1 Orbital Mechanics

Spacecraft dynamics is composed of the study of the trajectory and attitude of the object. There is a strong relation between them. The position of the spacecraft defines perturbations which affect the attitude, and its orientation has long term effects on the trajectory. Orbital mechanics studies the trajectory of the spacecraft with respect to a reference frame.

2.1.1 Two Body Problem

The motion of two particles interacting with each other is described by the two body problem. A spacecraft orbiting the Earth could be approximated to describe a Keplerian orbit. This model assumes that planet and spacecraft are points of concentrated masses and only gravitational force is acting between them. With these assumptions, the equations of motion are called the two body problem. Later the model can be refined by adding disturbances to it.

Considering an inertial reference frame (S_1) and two particles with mass m_1 and m_2 , the gravitational force acting on both particles is:

$$\vec{F}_{12} = m_1 \ddot{\vec{r}}_1 = \frac{Gm_1m_2}{|\vec{r}_2 - \vec{r}_1|^3} (\vec{r}_2 - \vec{r}_1) \quad (2.1)$$

$$\vec{F}_{21} = m_2 \ddot{\vec{r}}_2 = -\frac{Gm_1m_2}{|\vec{r}_2 - \vec{r}_1|^3} (\vec{r}_2 - \vec{r}_1) \quad (2.2)$$

where $G = 6.67428 \times 10^{11} \text{ m}^3\text{kg}^{-1}\text{s}^{-2}$ is the gravitational constant.

Equations (2.1) and (2.2) describe the motion of both particles in inertial space. However, it is more interesting to see the motion of both particles with respect to their center of masses. So introducing a new reference frame (S_0) in the center of mass C_g , the motion of both particles with relative to this point can be studied. Therefore calculating the position of the center of mass:

$$\vec{r}_{C_g} = \frac{m_1 \vec{r}_1 + m_2 \vec{r}_2}{m_1 + m_2} \quad (2.3)$$

the motion of the first particle with respect C_g is:

$$\vec{r}'_1 = \vec{r}_1 - \vec{r}_{C_g} \rightarrow m_1 \ddot{\vec{r}}'_1 = -Gm_1m_2 \left(1 + \frac{m_1}{m_2}\right)^{-2} \frac{\vec{r}'_1}{|\vec{r}'_1|^3} \quad (2.4)$$

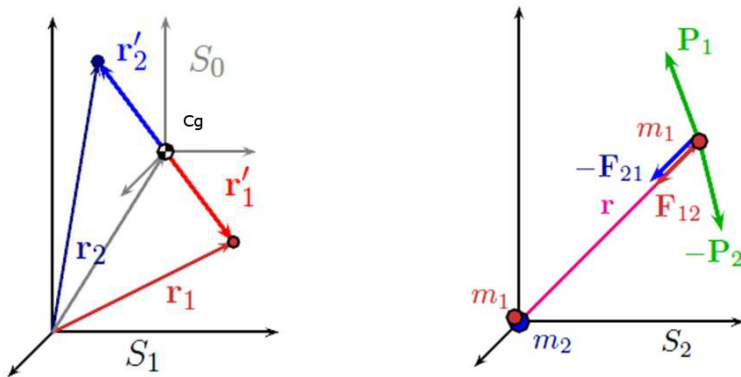


Figure 2.1: Two body problem in an inertial reference frame.

Finally the relative motion of one particle with respect to the other can be calculated. In order to do so a new reference frame (S_2) has to be established in one of the particles. This reference frame is non-rotating and non-inertial. The equations of motion depend on the relative position vector (\vec{r}_e), which is defined as follows:

$$\vec{r}_e = \vec{r}_1 - \vec{r}_2 \quad (2.5)$$

So, the motion is described by:

$$\ddot{\vec{r}}_e = \ddot{\vec{r}}_1 - \ddot{\vec{r}}_2 \quad (2.6)$$

$$\ddot{\vec{r}}_e = -G(m_1 + m_2) \frac{\vec{r}_e}{|\vec{r}_e|^3} \quad (2.7)$$

2.1.2 Spacecraft in Low Earth Orbit

The two body problem is used for calculating the orbit trajectory and velocity of a spacecraft orbiting the Earth. This fact allows us to make some simplifications in equation (2.7). Consider particle 1 to be a spacecraft with mass (m_s) and particle 2 to be the Earth with mass (M_E). Then:

$$M_E \gg m_s \rightarrow G(M_E + m_s) \approx GM_E = \mu \quad (2.8)$$

where μ is the standard gravitational parameter. The value of μ is more accurately known than G and M_E separately. Moreover, using μ the gravity formulas become simpler. From equation (2.8) it can be concluded that the center of mass of the system is located in the center of the Earth. Therefore, the reference frame of the relative motion can be considered inertial, and is called Earth Centered Inertial (ECI) reference frame.

Inserting equation (2.8) into (2.7) and defining $r_e = r$ to be the distance between the Earth and spacecraft, the equations of motion of the spacecraft with respect to the Earth in a Keplerian orbit are:

$$\ddot{\vec{r}} + \frac{\mu}{|\vec{r}|^3} \vec{r} = 0 \quad (2.9)$$

where the value of μ is $398600.4418 \text{ km}^3\text{s}^{-2}$ for the Earth.

The equations of motion (2.9) describe an ideal orbit where the Earth is assumed to be a point mass and disregarding space environment effects. However, a more realistic trajectory can be modelled adding disturbance effects in form of perturbing accelerations. By doing so equation (2.9) can be re-written as:

$$\ddot{\vec{r}} + \frac{\mu}{|\vec{r}|^3} \vec{r} = \vec{a}_j + \vec{a}_D + \vec{a}_{tb} + \vec{a}_{sp} + \vec{a}_{mag} \quad (2.10)$$

where the perturbed accelerations are:

\vec{a}_j	=	higher-order terms of the gravitational potential
\vec{a}_D	=	atmospheric drag
\vec{a}_{tb}	=	third body attraction
\vec{a}_{sp}	=	solar pressure
\vec{a}_{mag}	=	magnetic field

which can be classified as conservative and nonconservative. Conservative perturbations are explicit functions of position only, and there is no energy transfer. Therefore, the mean semimajor axis of the orbit remains constant [5]. This is the case for the gravitational potential. Nonconservative perturbations are functions of position and velocity, with energy exchange. Therefore, the mean semimajor axis changes with time. This occurs with solar pressure and atmospheric drag.

Since a Low Earth Orbit (LEO) is considered here, the predominant disturbances are the nonspheric shape of the Earth (gravitational potential) and atmospheric drag. With increasing altitude, the nonspheric effect is less important whereas gravitational attraction of the Moon and Sun become significant [5]. This is of essential importance for geosynchronous orbit, at around 35000 km altitude. In orbits below 2000 km, third body attraction can be neglected. Solar pressure effects will be neglected too, due to low orbit altitude.

2.1.3 Gravitational Potential Field Model

A Keplerian orbit is governed by a gravitational field like a potential function $\Phi(r) = -\frac{\mu}{r}$, where r is the distance from the spacecraft to the Earth's center, which produces an inverse square gravitational force. This model assumes the planet to be a point mass. Therefore, oblateness and mass distribution within the planet are neglected. For a more accurate model effects of the nonspherical shape of the Earth have to be added to the potential gravitational field. This has significant importance for LEO satellites.

To model this effect, it is convenient to express the corrected potential function of the Earth in the following form:

$$\Phi(r, \phi, \lambda) = -\frac{\mu}{r} + B(r, \phi, \lambda) \quad (2.11)$$

where $B(r, \phi, \lambda)$ is the spherical harmonic expansion used to correct the gravitational potential field for the Earth's nonspheric mass distribution, where r is the position of the spacecraft, ϕ the geocentric latitude, and λ the geographical longitude. Developing this model, the potential function takes the form [5][6]:

$$\Phi = -\frac{\mu}{r} \left[1 - \sum_{k=2}^{\infty} \left(\frac{a_e}{r} \right)^n J_n P_n(w) \right] \quad (2.12)$$

where a_e is the equatorial radius of the body, P_n Legendre polynomials, w is declination of the satellite and J_n are the zonal harmonics. The values of the harmonics depend on the shape and mass distribution of the planet. It is practically impossible to obtain J_n values by integrating its analytical expression, since no sufficiently accurate model of the Earth's mass distribution exists. Hence, the values of the harmonics are estimated by observing the motion of different spacecraft orbiting the Earth. The most widely used set of harmonics are the ones from the WGS 84 model [5] given in Table 2.1.

Zonal harmonics of the WGS 84 model	
J_2	$= 1082.63 \times 10^{-6}$
J_3	$= -2.52 \times 10^{-6}$
J_4	$= -1.61 \times 10^{-6}$
J_5	$= -0.15 \times 10^{-6}$
J_6	$= 0.57 \times 10^{-6}$

Table 2.1: Zonal harmonics.

The dominant harmonic is J_2 , being 400 times larger than the others. J_2 is often called oblateness perturbation. The acceleration due to oblateness perturbation in Cartesian coordinates is written as follows [4]:

$$\vec{a}_{J_2} = -\frac{3}{2} J_2 \left(\frac{\mu}{r^2} \right) \left(\frac{a_e}{r} \right)^2 \begin{pmatrix} \left(1 - 5 \left(\frac{z}{r} \right)^2 \right) \frac{x}{r} \\ \left(1 - 5 \left(\frac{z}{r} \right)^2 \right) \frac{y}{r} \\ \left(3 - 5 \left(\frac{z}{r} \right)^2 \right) \frac{z}{r} \end{pmatrix} \quad (2.13)$$

For high precision simulations higher order perturbation accelerations can be added. However, the main effect is the oblateness, described by J_2 .

2.1.4 Atmospheric Drag

The atmosphere influences spacecraft motion in the Earth surroundings. The interaction of Earth's atmosphere with a spacecraft produces drag forces over the vehicle's surface. Due to the nonconservative nature of aerodynamic forces the orbit trajectory is perturbed. Additionally, drag forces create aerodynamic torques which affect the attitude of the spacecraft, i.e. rotation dynamics.

The major effect of atmospheric drag in orbit propagation is the orbit decay. The exchange of energy results in a reduced eccentricity of the orbit. Therefore, the trajectory changes from an elliptical to a more circular orbit. There is also a decay in altitude, which eventually results in reentry of the spacecraft. Orbital decay rate depends on the atmospheric density and spacecraft geometry.

The major difficulty of drag prediction is the estimation of atmospheric density. Atmospheric density depends on the altitude, solar flux and variation between day and night. A mathematical model of density as a function of distance from the Earth can be formulated. The model assumes constant temperature of the upper atmosphere and models pressure and density as exponential functions:

$$\rho \propto e^{-mgh/kT} = e^{-\frac{h}{H}} \quad (2.14)$$

where h is altitude in km and $H = \frac{KT}{mg}$ is the scale height, where m is the molecular mass, T is temperature, g is the acceleration due to gravity and k is Boltzmann's constant. In the present work an empirical model will be used, which is based on measured data. Figure 2.2 shows the average atmospheric density with respect to altitude according to Werzt [7] and [8].

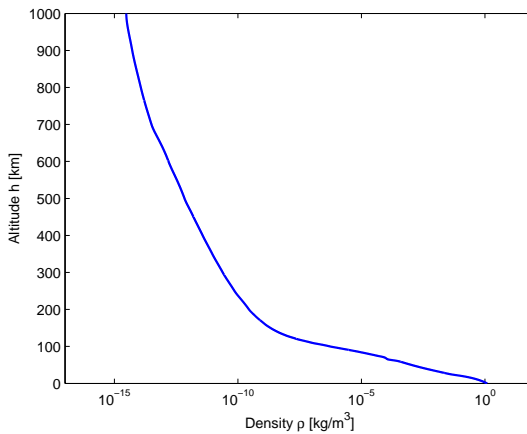


Figure 2.2: Upper atmosphere density [7].

Atmospheric drag is often taken into account for altitudes below 1000 km. However, its effect becomes significant only for orbits below 400 km altitude. Orbit decay is important for long term simulations. In order to model the effects of atmospheric drag an acceleration perturbation is defined [5] [9]:

$$\vec{a}_D = -\frac{1}{2}\rho V^2 \frac{C_D A}{m} \vec{n}_v \quad (2.15)$$

where ρ is the atmospheric density, V is the velocity of the spacecraft, A the satellite projected area, m the mass of the spacecraft, C_D is the drag coefficient and \vec{n}_v is the unit vector of satellite velocity.

2.2 Attitude Kinematics

Attitude kinematics describes the orientation of bodies. For a spacecraft it involves the orientation of a frame fixed in a body, in order to determine the orientation of the body itself. For a full understanding of rotational kinematics, it is necessary to establish the definition of the different reference frames which are involved in the project. Three different references frames are used in this work.

An Earth Centered Inertial (ECI) reference frame is used as fixed. It is defined by a right-hand set of three orthogonal unit vectors $N = (\vec{n}_1, \vec{n}_2, \vec{n}_3)$ with its center located at the Earth's center. This is a Cartesian reference frame, with basis vectors $\vec{n}_1 = (1, 0, 0)$ pointing towards the first point of Aries or vernal equinox, $\vec{n}_3 = (0, 0, 1)$ towards the Earth's North Pole and $\vec{n}_2 = (0, 1, 0)$ perpendicular to \vec{n}_1 and \vec{n}_3 .

The second reference frame is the orbit reference frame $A = (\vec{a}_1, \vec{a}_2, \vec{a}_3)$. The origin of this reference frame is located at the spacecraft's center of mass. Basis vectors are, \vec{a}_3 pointing towards the Earth, \vec{a}_2 perpendicular to the orbit plane and \vec{a}_1 perpendicular to both, which in a circular orbit corresponds to the spacecraft's velocity direction. Considering a spacecraft at a position \vec{R} with velocity \vec{V} , the unit vectors of the reference frame A are defined as follows:

$$\vec{a}_3 = -\frac{\vec{R}}{|\vec{R}|} \quad (2.16)$$

$$\vec{a}_2 = \frac{\vec{V} \times \vec{R}}{|\vec{V} \times \vec{R}|} \quad (2.17)$$

$$\vec{a}_1 = \vec{a}_2 \times \vec{a}_3 \quad (2.18)$$

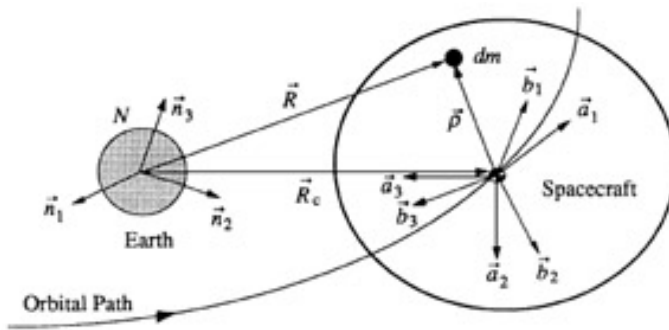


Figure 2.3: ECI N , A and B reference frames [4].

The last reference frame is the body-fixed $B = (\vec{b}_1, \vec{b}_2, \vec{b}_3)$. Its origin is again located at the spacecraft's center of mass. The unit vectors are aligned with the principal inertia axes. The orientation of the body is defined by the rotation between the body frame B and the orbit frame A .

2.2.1 Finite Rotations

A three-dimensional or spatial rotation is defined by a fundamental theorem stated by Euler: *The general displacement of a rigid body with one point fixed is a rotation about an axis which passes through that point.*

That means that a spatial rotation has both magnitude i.e. an angle and direction i.e. the axis of rotation [10]. Two rotations are not commutative except when they are infinitesimal or about the same axis.

Generally, a rotation can be represented by a rotation matrix R . Considering two reference frames $A = (\vec{a}_1, \vec{a}_2, \vec{a}_3)$ and $B = (\vec{b}_1, \vec{b}_2, \vec{b}_3)$, a rotation matrix $R^{B/A}$ makes the transformation to system B from system A ($B \leftarrow A$). So if there is a vector $\vec{r}_N = (r_{n1}, r_{n2}, r_{n3})$ expressed in the ECI frame N , the same vector expressed in the body reference frame is:

$$\vec{r}_B = R^{B/N} \vec{r}_N \quad (2.19)$$

A very important feature of a rotation matrix it is that is orthonormal [4]; hence, its inverse is equal to its transpose, which describes the inverse rotation.

$$R^{B/N'} = R^{N/B} \rightarrow \vec{r}_N = R^{N/B} \vec{r}_B \quad (2.20)$$

$$R^{B/N} R^{N/B} = R^{N/B} R^{B/N} = R^{B/N} R^{B/N'} = I \quad (2.21)$$

There are several ways to parametrize rotation matrices, which will be chosen depending on the situation. Following, different methods of generating a rotation matrix are presented.

2.2.2 Direction Cosine Matrix (DCM)

Having defined a pair of reference frames A and B with their respective right-hand set of orthogonal basis vectors $(\vec{a}_1, \vec{a}_2, \vec{a}_3)$ and $(\vec{b}_1, \vec{b}_2, \vec{b}_3)$, the rotation matrix to B from A has the form:

$$R^{B/A} = \begin{bmatrix} \vec{b}_1 \cdot \vec{a}_1 & \vec{b}_1 \cdot \vec{a}_2 & \vec{b}_1 \cdot \vec{a}_3 \\ \vec{b}_2 \cdot \vec{a}_1 & \vec{b}_2 \cdot \vec{a}_2 & \vec{b}_2 \cdot \vec{a}_3 \\ \vec{b}_3 \cdot \vec{a}_1 & \vec{b}_3 \cdot \vec{a}_2 & \vec{b}_3 \cdot \vec{a}_3 \end{bmatrix} = \begin{bmatrix} \vec{b}_1 \\ \vec{b}_2 \\ \vec{b}_3 \end{bmatrix} \cdot [\vec{a}_1, \vec{a}_2, \vec{a}_3] \quad (2.22)$$

which is called Direction Cosine Matrix (DCM), where the scalar product $\vec{b}_i \cdot \vec{a}_j$ is the cosine angle between vectors \vec{b}_i and \vec{a}_j . This construction of the rotation matrix is very convenient to change from the ECI frame N to the orbit frame A , because their basis vectors are known at all times, once the two body problem is solved.

2.2.3 Euler Angles

Two orthonormal coordinate frames can be related by other Euler theorem: *"Any two independent orthogonal coordinate frames can be related by a sequence of rotations (not more than three) about coordinate axes, where no two successive rotations may be about the same axis"* [11]. Having two coordinate system, this theorem states, that three successive rotations of the first coordinate about its axes, will make this coordinate rotate to the second coordinate system. The three angles of rotation about the coordinates axes are called the Euler Angles. Euler angles are frequently used to describe the orientation of a reference frame with respect to other. There are twelve possible rotation sequences that relate one coordinate to the other. If the three axes are named x y and z , the twelve possible rotation sequences are:

$$\begin{array}{lll} xyz & yzx & zxy \\ xzy & yxz & zyx \\ yzx & yzy & zxy \\ zxz & yxy & zyz \end{array} \quad (2.23)$$

Mathematically, three successive rotations are represented by a DCM, which is the product of three rotation matrices. Consider two orthonormal reference frames $A(\vec{a}_1, \vec{a}_2, \vec{a}_3)$ and $B(\vec{b}_1, \vec{b}_2, \vec{b}_3)$, a rotation to B from A can be divided into three successive rotations like:

$$B \leftarrow A : B \leftarrow A'' \leftarrow A' \leftarrow A \quad (2.24)$$

where $A' = (\vec{a}'_1, \vec{a}'_2, \vec{a}'_3)$ and $A'' = (\vec{a}''_1, \vec{a}''_2, \vec{a}''_3)$ are two intermediate reference frames. Introducing three Euler angles, $\theta_1, \theta_2, \theta_3$, and assigning each angle to one of the rotations as follows:

$$\begin{aligned} R(\theta_3) &: A' \leftarrow A \\ R(\theta_2) &: A'' \leftarrow A' \\ R(\theta_1) &: B \leftarrow A'' \end{aligned} \quad (2.25)$$

where each rotation matrix is defined like:

$$R(\theta_1) = \begin{bmatrix} 1 & 0 & 0 \\ 0 & \cos \theta_1 & \sin \theta_1 \\ 0 & -\sin \theta_1 & \cos \theta_1 \end{bmatrix} \quad (2.26)$$

$$R(\theta_2) = \begin{bmatrix} \cos \theta_2 & 0 & -\sin \theta_2 \\ 0 & 1 & 0 \\ \sin \theta_2 & 0 & \cos \theta_2 \end{bmatrix} \quad (2.27)$$

$$R(\theta_3) = \begin{bmatrix} \cos \theta_3 & \sin \theta_3 & 0 \\ -\sin \theta_3 & \cos \theta_3 & 0 \\ 0 & 0 & 1 \end{bmatrix} \quad (2.28)$$

the rotation matrix of the spatial rotation is defined as:

$$R^{B/A} = R(\theta_1)R(\theta_2)R(\theta_3) \quad (2.29)$$

with first rotation performed around \vec{a}_3 , second around \vec{a}'_2 and third around \vec{a}''_1 . Making the rotation sequence to be 123, equivalent to *xyz* from (2.23).

$$\theta_1 \vec{a}_1'' \leftarrow \theta_2 \vec{a}_2' \leftarrow \theta_3 \vec{a}_3$$

Giving the direct cosine matrix:

$$R^{B/A} = \begin{bmatrix} \cos \theta_2 \cos \theta_3 & \cos \theta_2 \sin \theta_3 & -\sin \theta_2 \\ \sin \theta_1 \sin \theta_2 \cos \theta_3 - \cos \theta_1 \sin \theta_3 & \sin \theta_1 \sin \theta_2 \sin \theta_3 + \cos \theta_1 \cos \theta_3 & \sin \theta_1 \cos \theta_2 \\ \cos \theta_1 \sin \theta_2 \cos \theta_3 + \sin \theta_1 \sin \theta_3 & \cos \theta_1 \sin \theta_2 \sin \theta_3 - \sin \theta_1 \cos \theta_3 & \cos \theta_1 \cos \theta_2 \end{bmatrix} \quad (2.30)$$

There is a different rotation matrix for each rotation sequence. Thus it is important to specified which sequence is chosen when Euler angles are employed.

2.2.4 Eigenaxis Rotation

Euler's eigenaxis rotation theorem states that if a rigid body is rotated about an axis which is fixed to the body and stationary in an inertial reference frame, the rigid body attitude can be changed from an initial orientation to any other orientation [4]. Such an axis that remains unchanged with respect to the inertial and body fixed reference frames throughout motion is called *Euler axis* or *eigenaxis*.

According to Euler's eigenaxis theorem two reference frames $A(\vec{a}_1, \vec{a}_2, \vec{a}_3)$ and $B(\vec{b}_1, \vec{b}_2, \vec{b}_3)$ are related by a unit vector $\vec{e} = (e_1, e_2, e_3)$ along the eigenaxis and a rotation angle θ such that:

$$\vec{e} = e_1 \vec{a}_1 + e_2 \vec{a}_2 + e_3 \vec{a}_3 = e_1 \vec{b}_1 + e_2 \vec{b}_2 + e_3 \vec{b}_3 \quad (2.31)$$

which leads to the following parametrization of the DCM [4] and [12]

$$R^{B/A} = \begin{bmatrix} \cos \theta + e_1^2(1 - \cos \theta) & e_1 e_2(1 - \cos \theta) + e_3 \sin \theta & e_1 e_3(1 - \cos \theta) - e_2 \sin \theta \\ e_2 e_1(1 - \cos \theta) - e_3 \sin \theta & \cos \theta + e_2^2(1 - \cos \theta) & e_2 e_3(1 - \cos \theta) + e_1 \sin \theta \\ e_3 e_1(1 - \cos \theta) + e_2 \sin \theta & e_3 e_2(1 - \cos \theta) - e_1 \sin \theta & \cos \theta + e_3^2(1 - \cos \theta) \end{bmatrix} \quad (2.32)$$

where $e_1^2 + e_2^2 + e_3^2 = 1$

2.2.5 Euler Parameters, Quaternions

From the Euler's eigenaxis theorem, Euler parameters or quaternions are defined:

$$\begin{aligned} q_1 &= e_1 \sin(\theta/2) \\ q_2 &= e_2 \sin(\theta/2) \\ q_3 &= e_3 \sin(\theta/2) \\ q_4 &= \cos(\theta/2) \end{aligned} \quad (2.33)$$

where $\vec{e} = (e_1, e_2, e_3)$ is the eigen axis and θ the rotation angle. Euler parameters or quaternions are another way to parametrize rotation matrices. The major advantage of quaternions comparing to Euler angles is that they present no discontinuities when the kinematic differential equations are integrated. However their major drawback is that there is no intuitive interpretation of their values.

Defining a vector $\vec{q} = (q_1, q_2, q_3)$, quaternions are constrained between them as follows:

$$\vec{q}^T \vec{q} + q_4^2 = q_1^2 + q_2^2 + q_3^2 + q_4^2 = 1 \quad (2.34)$$

which can be used to check the accuracy of the numerical integration. Additionally, a rotation matrix is parametrized in terms of quaternions like [4] [12]:

$$R^{A/B} = \begin{bmatrix} 1 - 2(q_2^2 + q_3^2) & 2(q_1 q_2 + q_3 q_4) & 2(q_1 q_3 - q_2 q_4) \\ 2(q_2 q_1 - q_3 q_4) & 1 - 2(q_1^2 + q_3^2) & 2(q_2 q_3 + q_1 q_4) \\ 2(q_3 q_1 + q_2 q_4) & 2(q_3 q_2 - q_1 q_4) & 1 - 2(q_1^2 + q_2^2) \end{bmatrix} \quad (2.35)$$

Giving a rotation matrix R the quaternion that defines it, can be obtained as follows:

$$q_4 = \frac{1}{2}(1 + R(1, 1) + R(2, 2) + R(3, 3))^{\frac{1}{2}} \quad (2.36)$$

$$\vec{q} = \frac{1}{4q_4} \begin{bmatrix} R(2, 3) - R(3, 2) \\ R(3, 1) - R(1, 3) \\ R(1, 2) - R(2, 1) \end{bmatrix} \quad (2.37)$$

Finally a last important feature of quaternions is their multiplication. Consider two successive rotations to B from A ($B \leftarrow A$). The rotation sequence performed is ($B \leftarrow A' \leftarrow A$) with rotation matrices:

$$\begin{aligned} R^{A'/A} &= R(\vec{q}_a, q_{4a}) \\ R^{B/A'} &= R(\vec{q}_b, q_{4b}) \end{aligned}$$

the resulting matrix of the entire rotation is:

$$R^{B/A} = R^{B/A'} R^{A'/A} = R(\vec{q}_b, q_{4b}) R(\vec{q}_a, q_{4a}) \quad (2.38)$$

Similarly the quaternion that defines the rotation matrix $R^{B/A}$ can be calculated as the multiplication of the quaternions that define the rotation matrices $R^{B/A'}$ and $R^{A'/A}$, which is calculated as:

$$\begin{aligned} \vec{q}_{AB} &= q_{4b}\vec{q}_a + q_{4a}\vec{q}_b + \vec{q}_a \times \vec{q}_b \\ q_{4ab} &= q_{4a}q_{4b} - (\vec{q}_a)^T \vec{q}_b \end{aligned} \quad (2.39)$$

which in matrix form is:

$$\begin{bmatrix} q_1 \\ q_2 \\ q_3 \\ q_4 \end{bmatrix} = \begin{bmatrix} q_{4b} & q_{3b} & -q_{2b} & q_{1b} \\ -q_{3b} & q_{4b} & q_{1b} & q_{2b} \\ q_{2b} & -q_{1b} & q_{4b} & q_{3b} \\ -q_{1b} & -q_{2b} & -q_{3b} & q_{1b} \end{bmatrix} \begin{bmatrix} q_{1a} \\ q_{2a} \\ q_{3a} \\ q_{4a} \end{bmatrix} \quad (2.40)$$

Equation (2.40) is also known as the quaternion multiplication rule.

2.2.6 Kinematic Differential Equations

So far, several methods of orientation of two orthogonal reference frames have been introduced as different ways to express a rotation matrix. But most important is to know how those reference frames are related with respect to time. That is described by the kinematic differential equations.

Consider two reference frames $A = (\vec{a}_1, \vec{a}_2, \vec{a}_3)$ and $B = (\vec{b}_1, \vec{b}_2, \vec{b}_3)$. A is stationary and B is moving with respect to A with an angular velocity $\vec{\omega} = \vec{\omega}^{B/A} = (\omega_1, \omega_2, \omega_3)$, which can be expressed in the B reference frame as:

$$\vec{\omega} = \omega_1 \vec{b}_1 + \omega_2 \vec{b}_2 + \omega_3 \vec{b}_3 \quad (2.41)$$

Both reference frames can be related as:

$$\begin{bmatrix} \vec{b}_1 \\ \vec{b}_2 \\ \vec{b}_3 \end{bmatrix} = R \begin{bmatrix} \vec{a}_1 \\ \vec{a}_2 \\ \vec{a}_3 \end{bmatrix} \leftrightarrow \begin{bmatrix} \vec{a}_1 \\ \vec{a}_2 \\ \vec{a}_3 \end{bmatrix} = R^T \begin{bmatrix} \vec{b}_1 \\ \vec{b}_2 \\ \vec{b}_3 \end{bmatrix} \quad (2.42)$$

In equation (2.42) the rotation matrix R is time dependent. Therefore taking time derivative of equation (2.42):

$$\begin{bmatrix} 0 \\ 0 \\ 0 \end{bmatrix} = \dot{R}^T \begin{bmatrix} \vec{b}_1 \\ \vec{b}_2 \\ \vec{b}_3 \end{bmatrix} + R^T \begin{bmatrix} \dot{\vec{b}}_1 \\ \dot{\vec{b}}_2 \\ \dot{\vec{b}}_3 \end{bmatrix} = \dot{R}^T \begin{bmatrix} \vec{b}_1 \\ \vec{b}_2 \\ \vec{b}_3 \end{bmatrix} + R^T \begin{bmatrix} \vec{\omega} \times \vec{b}_1 \\ \vec{\omega} \times \vec{b}_2 \\ \vec{\omega} \times \vec{b}_3 \end{bmatrix} = \dot{R}^T \begin{bmatrix} \vec{b}_1 \\ \vec{b}_2 \\ \vec{b}_3 \end{bmatrix} - R^T \begin{bmatrix} 0 & -\omega_3 & \omega_2 \\ \omega_3 & 0 & -\omega_1 \\ -\omega_2 & \omega_1 & 0 \end{bmatrix} \begin{bmatrix} \vec{b}_1 \\ \vec{b}_2 \\ \vec{b}_3 \end{bmatrix} \quad (2.43)$$

The skew symmetric matrix Ω can be defined from equation (2.43):

$$\Omega = \begin{bmatrix} 0 & -\omega_3 & \omega_2 \\ \omega_3 & 0 & -\omega_1 \\ -\omega_2 & \omega_1 & 0 \end{bmatrix} \quad (2.44)$$

combining equations (2.43) and (2.44), and after some mathematical manipulation (note: $\Omega^T = -\Omega$) the kinematic differential equations for a general case are defined [4]:

$$\dot{R} + \Omega R = 0 \quad (2.45)$$

So knowing the angular velocity as a function of time, the orientation of B relative to A is obtained by solving equation (2.45). In this project, the rotation matrix R is parametrized in terms of quaternions. This is done because quaternions do not present discontinuities comparing to Euler angles. Equation (2.45) in quaternion form is [4] [12]:

$$\begin{bmatrix} \dot{q}_1 \\ \dot{q}_2 \\ \dot{q}_3 \\ \dot{q}_4 \end{bmatrix} = \frac{1}{2} \begin{bmatrix} 0 & \omega_3 & -\omega_2 & \omega_1 \\ -\omega_3 & 0 & \omega_1 & \omega_2 \\ \omega_2 & -\omega_1 & 0 & \omega_3 \\ -\omega_1 & -\omega_2 & -\omega_3 & 0 \end{bmatrix} \begin{bmatrix} q_1 \\ q_2 \\ q_3 \\ q_4 \end{bmatrix} \quad (2.46)$$

which can be written as:

$$\dot{q} = \frac{1}{2}(q_4 \omega - \omega \times q) \quad (2.47)$$

$$\dot{q}_4 = -\frac{1}{2}\omega^T q \quad (2.48)$$

2.2.7 Attitude Definition

The attitude of a spacecraft is the orientation of the vehicle with respect to a defined reference frame. The orbit A and body B references frames have been chosen to define it. The result is expressed in Euler angles, because its interpretation is the easiest.

First the body axes motion has to be defined. To do so the *Roll*, *Pitch* and *Yaw* axes have to be designated. There is no standard definition of the rotation axes for spacecraft. In fact, depending on the spacecraft configuration, its axes are defined. Assuming the satellite to be aligned to with the orbit reference frame, i.e. A and B have the same basis vectors, the yaw axis is defined toward the nadir direction (\vec{a}_3), the pitch axis toward the negative orbit normal (\vec{a}_2) and the roll axis perpendicular to both (\vec{a}_1). Figure 2.4 shows the orbit and body references frames when they are not aligned.

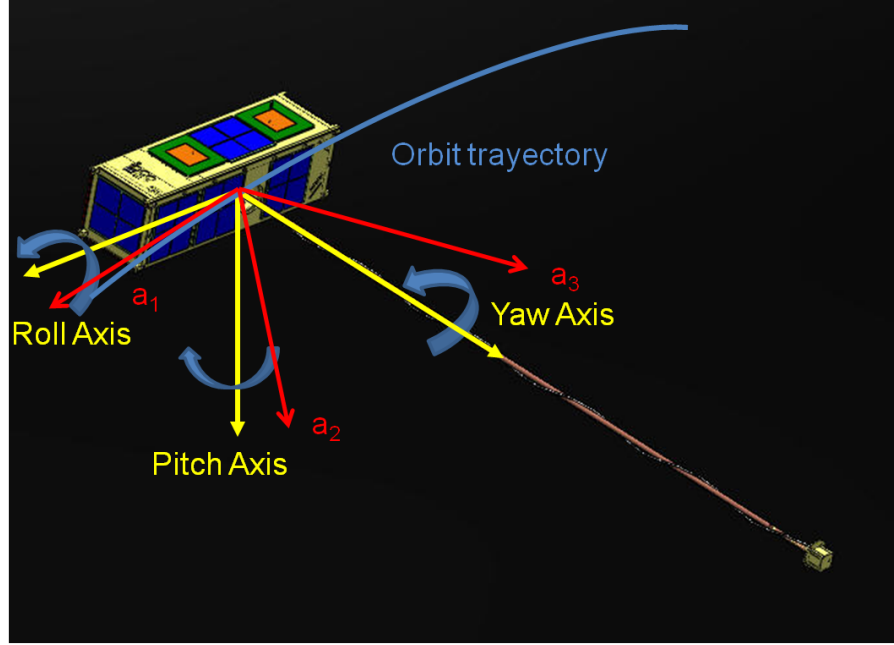


Figure 2.4: Axes definition.

Figure 2.4 shows the attitude definition of the CINEMA CubeSat. CINEMA has a deployed boom as SWIM. The red arrows represent the orbit reference frame and the yellow arrows the body reference frame. In Chapter 3 there is an explanation of the axes selection.

Now a rotation to go from reference frame A to B defines the attitude of the satellite. This is done by introducing three Euler angles $\theta_1, \theta_2, \theta_3$, Roll, Pitch and Yaw respectively in a 132 rotation sequence. Therefore the rotation sequence looks like:

$$\theta_1 \vec{a}_1'' \leftarrow \theta_3 \vec{a}_3' \leftarrow \theta_2 \vec{a}_2$$

which gives the spatial rotation matrix:

$$R^{B/A} = R_1(\theta_1)R_3(\theta_3)R_2(\theta_2) = \begin{bmatrix} \cos \theta_2 \cos \theta_3 & \sin \theta_3 & -\sin \theta_2 \cos \theta_3 \\ -\cos \theta_1 \cos \theta_2 \sin \theta_3 + \sin \theta_1 \sin \theta_2 & \cos \theta_1 \cos \theta_3 & \cos \theta_1 \sin \theta_2 \sin \theta_3 + \sin \theta_1 \cos \theta_2 \\ \sin \theta_1 \cos \theta_2 \sin \theta_3 + \cos \theta_1 \cos \theta_3 & -\sin \theta_1 \cos \theta_3 & -\sin \theta_1 \sin \theta_2 \sin \theta_3 + \cos \theta_1 \cos \theta_3 \end{bmatrix} \quad (2.49)$$

Although the attitude can be defined by Euler angles, the kinematic differential equations are expressed in quaternions. Hence, a transition from quaternions to Euler angles has to be performed. This is done by comparing matrices (2.35) and (2.49). Consider a generic rotation matrix R . R can be parametrized with both quaternions or Euler angles. Looking at matrix (2.49) it can be established that:

$$-\frac{R(3,2)}{R(2,2)} = \tan \theta_1 \quad (2.50)$$

$$-\frac{R(1,3)}{R(1,1)} = \tan \theta_2 \quad (2.51)$$

$$R(1, 2) = \sin \theta_3 \quad (2.52)$$

comparing equations (2.50), (2.51), and (2.52) with the parametrization of a rotation matrix in quaternions (equation (2.35)), the following relationships are established:

$$\theta_1 = \tan^{-1} \left(\frac{2(q_1 q_4 - q_2 q_3)}{1 - 2q_1^2 - 2q_3^2} \right) \quad (2.53)$$

$$\theta_2 = \tan^{-1} \left(\frac{2(q_2 q_4 - q_1 q_3)}{1 - 2q_2^2 - 2q_3^2} \right) \quad (2.54)$$

$$\theta_3 = \sin^{-1} (2(q_1 q_2 + q_3 q_4)) \quad (2.55)$$

Equations (2.53), (2.54) and (2.55) are only valid for the 132 rotation sequence. However, depending on the rotation sequence, similar relations can be found.

2.3 Rigid-Body Dynamics

Translational dynamics have been already discussed, where the satellite is modelled as point orbiting the Earth. After rotational kinematics the rotational dynamics of the spacecraft is introduced. Rotational dynamics studies how the spacecraft rotates around its center of mass. The satellite is assumed to be a rigid body i.e. the distance between particles remain constant. Although some parts of the satellite ,like the boom, have to be studied as elastic bodies, the rigid body approximation is the best way to start. This section describes how the satellite rotates depending on initial conditions and environmental effects.

2.3.1 Dynamic Equations

Considering a rigid body in motion with respect to an inertial reference frame N , the rotational dynamics of the body about a point O is given by the equation:

$$\left(\frac{d}{dt} \vec{H}_O \right)_N = \vec{M}_O \quad (2.56)$$

where the left-hand side is the time derivative of the angular momentum with respect to an inertial reference frame and the right-hand side is the total external torque applied to the body. The angular momentum of a rigid body about a point O is defined as follows:

$$\vec{H}_O = \int \vec{r} \times \dot{\vec{R}} dm = \int \vec{r} \times (\vec{\omega}^{B/N} \times \vec{r}) dm \quad (2.57)$$

where \vec{r} is the distance from O to a differential mass element dm and $\dot{\vec{R}}$ is the inertial velocity of the element dm . Considering $\vec{r} = (r_1 \vec{b}_1, r_2 \vec{b}_2, r_3 \vec{b}_3)$ and $\vec{\omega}^{B/N} = (\omega_1 \vec{b}_1, \omega_2 \vec{b}_2, \omega_3 \vec{b}_3)$, equation (2.57) can be developed in the body reference frame:

$$\vec{H} = \int \begin{bmatrix} y^2 + z^2 & -yz & -zx \\ -xy & x^2 + z^2 & -zy \\ -xz & -yz & x^2 + y^2 \end{bmatrix} dm \begin{bmatrix} \omega_1 \\ \omega_2 \\ \omega_3 \end{bmatrix} = \begin{bmatrix} J_{11} & J_{12} & J_{13} \\ J_{21} & J_{22} & J_{23} \\ J_{31} & J_{32} & J_{33} \end{bmatrix} \begin{bmatrix} \omega_1 \\ \omega_2 \\ \omega_3 \end{bmatrix} = \tilde{J} \vec{\omega}^{B/N} \quad (2.58)$$

where \tilde{J} is the inertia tensor. The inertia tensor provides information of the rotational characteristics of a rigid body. The diagonal terms J_{11}, J_{22} and J_{33} are called moments of inertia and off-diagonal terms products of inertia. Setting O to be the center of mass and making the body reference frame to be the principal inertia axes, \tilde{J} becomes a diagonal matrix and products of inertia are canceled.

The time derivative of the angular momentum under the assumption of body reference frame to be principal inertia axes is:

$$\left(\frac{d\vec{H}}{dt} \right)_N = \left(\frac{d\vec{H}}{dt} \right)_B + \vec{\omega}^{B/N} \times \vec{H} = \left(\frac{d\tilde{J}\vec{\omega}^{B/N}}{dt} \right)_B + \vec{\omega}^{B/N} \times \tilde{J}\vec{\omega}^{B/N} \quad (2.59)$$

and letting $\vec{\omega} = \vec{\omega}^{B/N}$, the equation of motion in the body reference frame in vector notation is:

$$\tilde{J} \cdot \dot{\vec{\omega}} + \vec{\omega} \times \tilde{J} \cdot \vec{\omega} = \vec{M} \quad (2.60)$$

which is also called Euler's equation, which can be expanded in the three axes directions:

$$\begin{aligned} J_1 \dot{\omega}_1 - (J_2 - J_3) \omega_2 \omega_3 &= M_1 \\ J_2 \dot{\omega}_2 - (J_3 - J_1) \omega_3 \omega_1 &= M_2 \\ J_3 \dot{\omega}_3 - (J_1 - J_2) \omega_1 \omega_2 &= M_3 \end{aligned} \quad (2.61)$$

It is seen that Euler's equations are three coupled, nonlinear ordinary differential equations. The result of their integration is the angular velocity as seen from the body reference frame B . Equations (2.61) together with (2.46) describe the rotational motion of a rigid body with three degrees of freedom. Together with the orbit dynamic equations (2.10) the entire dynamics of a spacecraft i.e. translation, rotation and orientation is defined.

2.4 Disturbance Torques

Rotational dynamics depends on initial conditions and disturbance torques applied to the spacecraft. By initial conditions it is meant the angular velocity of the spacecraft at starting time of simulation. Disturbance torques are represented in the left-hand side of equation (2.60). Similarly to acceleration disturbances, the most important environmental effects in LEO are gravity (\vec{M}_{grav}), magnetic (\vec{M}_{mag}) and aerodynamic (\vec{M}_{aero}) torques. Hence $\vec{M} = \vec{M}_{grav} + \vec{M}_{mag} + \vec{M}_{aero}$. In the following sections the torques are defined.

2.4.1 Gravity Gradient Torque

Gravity gradient torques are important when a satellite is orbiting close to a planet. They are produced because of different mass distribution across a satellite. In this sense the attraction force in a satellite is not constant along it. Attraction forces are proportional to mass, so difference in mass distribution produces gravity torques.

Considering a small mass element dm of a satellite orbiting the Earth, the force acting on it is equal to:

$$d\vec{f} = -\mu \frac{\vec{R}_{dm}}{|R_{dm}|^3} dm = -\mu \frac{(\vec{R}_{cm} + \vec{r})}{|\vec{R}_{cm} + \vec{r}|^3} dm \quad (2.62)$$

where μ is the gravitational parameter, \vec{R}_{dm} is the distance from the Earth to the mass element dm , \vec{R}_{cm} is the distance from the Earth to the center of mass of the satellite and \vec{r} is the distance from center of mass to the mass element dm . The gravity gradient torque is defined as:

$$\vec{M}_{grav} = \int \vec{r} \times d\vec{f} \quad (2.63)$$

letting \vec{R}_{cm} to be \vec{R} and developing equation (2.63) like in [4], [9] and [12] the gravity gradient torque is equal to:

$$\vec{M}_g = \frac{3\mu}{R^5} \vec{R} \times \tilde{J} \cdot \vec{R} \quad (2.64)$$

which depends on satellite's position (\vec{R}) and mass distribution properties (\tilde{J}). Considering \vec{R} to be (R_1, R_2, R_3) seen from the body reference frame, equation (2.64) can be expanded:

$$\begin{aligned} M_{g1} &= \frac{3\mu}{R^5} R_2 R_3 (J_3 - J_2) \\ M_{g2} &= \frac{3\mu}{R^5} R_1 R_3 (J_1 - J_3) \\ M_{g3} &= \frac{3\mu}{R^5} R_1 R_2 (J_2 - J_1) \end{aligned} \quad (2.65)$$

According to equation (2.65), differences between principal moments of inertia produces gravity gradient torques.

2.4.2 Magnetic Torque

The magnetic torque is the effect of the Earth's magnetic field and the magnetic moment of the spacecraft. Magnetic torque is modelled as [7]:

$$\vec{M}_{mag} = \vec{\mu} \times \vec{B} \quad (2.66)$$

where \vec{B} is the Earth's magnetic field and $\vec{\mu}$ the spacecraft magnetic moment, which is given in Am². The magnetic torque creates disturbances that the satellite experience in orbit [13]. On the other hand it can be used as an attitude control technique.

The magnetic moment of a satellite is the sum of magnetic moments of all individual parts of it. This represent all experiments, wires, steel screws and eddy currents over conducting bodies in the spacecraft. SWIM carries scientific instruments like magnetometer and particle instrument, so magnetical cleanliness is desired.

Regardless constrains required by the experiments, the magnetic moment will be used as a study parameter to check how the magnetic field affects the attitude. Therefore $\vec{\mu} = [\mu_1, \mu_2, \mu_3]^T$ represents the worst case magnetic moment in the body axes.

The Earth's magnetic field \vec{B} is estimated based on an *International Geomagnetic Reference Field* (IGRF) model. The IGRF models the Earth's magnetic field as the gradient of a scalar potential V , which can be calculated with the expression:

$$V(r, \theta, \phi) = a \sum_{n=1}^k \left(\frac{a}{r}\right)^{n+1} \sum_{m=0}^n (g_n^m m\phi + h_n^m \sin m\phi) P_n^m(\theta) \quad (2.67)$$

where a is the equatorial radius of the Earth, g_n^m and h_n^m are the *Gaussian* coefficients, (r, θ, ϕ) are the geocentric distance, coelevation, and east longitude from Greenwich and $P_n^m(\theta)$ are the associated Legendre functions [7].

The geomagnetic field approximates to a dipole at the Earth's surface, with magnetic field South pole near the Earth geographic north pole and the magnetic field North pole near the geographic south. Far from the Earth's surface the dipole approximation is not longer valid. The interaction between geomagnetic field and solar wind produces a shock wave as depicted in Figure 2.5.

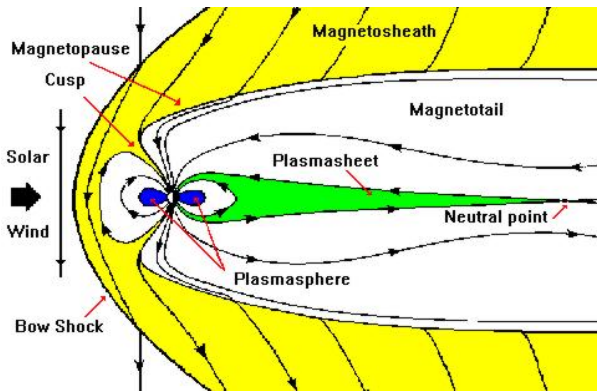


Figure 2.5: Earth's magnetic field.

In this work the Earth's magnetic field is estimated using the GEOPACK library by N. Tsyganenko [23], which is based on an IGRF model.

2.4.3 Aerodynamic Torque

The interaction between the upper atmosphere with a satellite produces changes in its rotation dynamics. There are particles impacting the satellite's surface, which induces forces and torques. The energy of the molecules is completely absorbed by the surface. These impacts generate aerodynamic forces $d\vec{f}_{aero}$ along surface elements dA [14]:

$$d\vec{f}_{aero} = -\frac{1}{2}C_D\rho V^2(\vec{n} \cdot \vec{v}_b)\vec{v}_b dA \quad (2.68)$$

where C_D is the drag coefficient, which is function of the surface structure and local angle of attack [7], ρ is the atmospheric density and dA is a surface element, \vec{n} is the unit vector normal to surface pointing outward and \vec{v}_b is a unit vector in the direction of translational velocity in the body frame. Integrating equation (2.68) over the spacecraft surface aerodynamic forces are calculated.

The aerodynamic torque is equal to the cross product of the distance of the center of mass to the center of pressure and the aerodynamic force. The center of pressure is the point where the aerodynamic force is generated. In order to calculate aerodynamic torques, it is common to divide the satellite into different geometrical elements, calculate the torque individually and summing them:

$$\vec{M}_{aero} = \sum_{i=1}^k \vec{r}_i \times \vec{F}_{aero,i} \quad (2.69)$$

where \vec{r}_i is the vector from the spacecraft center of mass to the center of pressure of the i th element and $\vec{F}_{aero,i}$ is the aerodynamic force along the i th element.

The aerodynamic torque is the major disturbance below 400 km altitude [7]. However, a satellite can be designed to be aerodynamically stable. This can be achieved by changing the position of the center of mass with respect of the center of pressure. Therefore, aerodynamic torque can be used as a passive stabilization technique.

2.5 Gravity Gradient Linear Stability Analysis

Gravity gradient is a passive attitude control technique. It is based on taking advantage of the satellite's mass distribution, making the gravity torque to restore the satellite to an equilibrium position. In order to find out which mass distribution produces such an effect, a linear stability analysis in a circular orbit is performed.

2.5.1 Circular Orbit

A satellite in a circular orbit rotates around the Earth with constant distance R and velocity V_c . The distance from the Earth (R) is defined as the radius of the Earth $R_e = 6378$ km plus the orbit altitude h , $R = R_e + h$. The orbit velocity is equal to $\sqrt{\mu/R}$. This model assumes the Earth to have homogeneous mass distribution and is represented as a point mass located at the center of the ECI reference frame N . This idealization allows us to change slightly the kinematic differential equations, and relate the body and orbit reference frames directly.

The orbit reference frame is local LVLH. The LVLH frame $A = (\vec{a}_1, \vec{a}_2, \vec{a}_3)$ is located at the spacecraft center of mass, with \vec{a}_1 tangent to the orbit in the velocity direction, \vec{a}_3 towards the Earth, (Nadir direction) and \vec{a}_2 perpendicular to the orbital plane. The body frame remains fixed to the spacecraft principal inertia axes.

2.5.2 Circular Orbit Kinematics

For this ideal case, the orbit frame is rotating with respect to N frame with angular velocity $\vec{\omega}^{A/N} = -n\vec{a}_2$. Where n is the orbital mean motion or angular frequency of the orbit, which for a circular orbit is:

$$n = \sqrt{\frac{\mu}{R^3}} \quad (2.70)$$

Since the angular velocity of the orbit reference frame is constant, the angular velocity of the body frame with respect to the Earth $\vec{\omega}^{B/N}$ is defined like [4]:

$$\vec{\omega}^{B/N} = \vec{\omega}^{B/A} + \vec{\omega}^{A/N} = \vec{\omega}^{B/A} - n\vec{a}_2 \quad (2.71)$$

So, developing equation (2.45) and taking into account equation (2.71) the kinematic differential equations relating A and B are:

$$\begin{bmatrix} \dot{q}_1 \\ \dot{q}_2 \\ \dot{q}_3 \\ \dot{q}_4 \end{bmatrix} = \frac{1}{2} \begin{bmatrix} 0 & \omega_3 & -\omega_2 + n & \omega_1 \\ -\omega_3 & 0 & \omega_1 & \omega_2 + n \\ \omega_2 - n & -\omega_1 & 0 & \omega_3 \\ -\omega_1 & -\omega_2 - n & -\omega_3 & 0 \end{bmatrix} \begin{bmatrix} q_1 \\ q_2 \\ q_3 \\ q_4 \end{bmatrix} \quad (2.72)$$

where $\vec{\omega} = (\omega_1, \omega_2, \omega_3)$ is the angular velocity of the rigid body.

2.5.3 Circular Orbit Equations of Motion

The equations of motion of a rigid spacecraft have been already presented, (2.61). It is assumed that Only gravity gradient torque is applied. The Gravity gradient torque is expressed in the body reference frame. Since the spacecraft is inserted into a circular orbit and the orbit reference frame A rotates with constant angular velocity, the gravity gradient torque can be related to the orbit reference frame (A) and later rotate it to the body (B). Using equations (2.16) and (2.70) gravity gradient torque in the orbit reference frame is:

$$\vec{M}_{grav,c} = 3n^2 \vec{a}_3 \times \tilde{J} \vec{a}_3 \quad (2.73)$$

after a transformation to the body reference frame has to be made. Knowing that $A = R^{A/B}B$, \vec{a}_3 is expressed like:

$$\vec{a}_3 = R(1,3)\vec{b}_1 + R(2,3)\vec{b}_2 + R(3,3)\vec{b}_3 \quad (2.74)$$

making the gravity gradient torque for a circular orbit in the body reference frame to be:

$$\vec{M}_g = 3n^2 \begin{bmatrix} 0 & -R_{33} & R_{23} \\ R_{33} & 0 & -R_{13} \\ -R_{23} & R_{13} & 0 \end{bmatrix} \begin{bmatrix} J_1 & 0 & 0 \\ 0 & J_2 & 0 \\ 0 & 0 & J_3 \end{bmatrix} \begin{bmatrix} R_{13} \\ R_{23} \\ R_{33} \end{bmatrix} \quad (2.75)$$

Introducing equation (2.75) into (2.61) and using the quaternion parametrization of a rotation matrix (2.35), the equations of motion are:

$$\begin{aligned} J_1\dot{\omega}_1 - (J_2 - J_3)\omega_2\omega_3 + 6n^2(J_2 - J_3)(q_1q_4 + q_2q_3)(1 - 2q_1^2 - 2q_2^2) &= 0 \\ J_2\dot{\omega}_2 - (J_3 - J_1)\omega_1\omega_3 + 6n^2(J_3 - J_1)(q_1q_3 - q_2q_4)(1 - 2q_1^2 - 2q_2^2) &= 0 \\ J_3\dot{\omega}_3 - (J_1 - J_2)\omega_1\omega_2 + 12n^2(J_1 - J_2)(q_1q_3 - q_2q_4)(q_1q_4 + 2q_2q_3) &= 0 \end{aligned} \quad (2.76)$$

Solving equations (2.72) and (2.76) simultaneously the motion of a rigid spacecraft and its orientation are determined. However, orientation is given in quaternions, which as it has been mentioned, do not give good physical interpretation. Therefore a change from quaternions to Euler angles is strongly recommended once the kinematic differential equations have been solved.

2.5.4 Linearized Equations

In order to linearized equations, Euler angles are used. Linear equations are made assuming small angles. Therefore, $\sin \theta_i \approx \theta_i$ and $\cos \theta_i \approx 1$. Additionally, the product between two angles is neglected. After all that process the equations of motion for small angles *Roll, Pitch and Yaw*, $(\theta_1, \theta_2, \theta_3)$ are:

$$\begin{aligned} J_1\dot{\omega}_1 - (J_2 - J_3)\omega_2\omega_3 &= -3n^2(J_2 - J_3)\theta_1 \\ J_2\dot{\omega}_2 - (J_3 - J_1)\omega_3\omega_1 &= 3n^2(J_3 - J_1)\theta_2 \\ J_3\dot{\omega}_3 - (J_1 - J_2)\omega_1\omega_2 &= 0 \end{aligned} \quad (2.77)$$

correspondingly the kinematic differential equations for small angles can be linearized as follows [4]:

$$\begin{aligned} \omega_1 &= \dot{\theta}_1 - n\theta_3 \\ \omega_2 &= \dot{\theta}_2 - n \\ \omega_3 &= \dot{\theta}_3 + n\theta_1 \end{aligned} \quad (2.78)$$

Putting the kinematic equations into the solid rigid equations (2.77), the linearized equations are obtained:

$$J_1\ddot{\theta}_1 - n(J_1 - J_2 + J_3)\dot{\theta}_3 + 4n^2(J_2 - J_3)\theta_1 = 0 \quad (2.79)$$

$$J_2\ddot{\theta}_2 + 3n^2(J_1 - J_3)\theta_2 = 0 \quad (2.80)$$

$$J_3\ddot{\theta}_3 + n(J_1 - J_2 + J_3)\dot{\theta}_1 + n^2(J_2 - J_1)\theta_3 = 0 \quad (2.81)$$

It can be seen that two of the equations are coupled together whereas equation (2.80) is not coupled to any. Hence, it is possible to calculate analytically the oscillation period for the pitch equation of motion by comparing equation (2.80) with an harmonic oscillator.

$$T_{pitch} = 2\pi \sqrt{\frac{J_2}{3n^2(J_1 - J_3)}} \quad (2.82)$$

Equation (2.82) shows that the period in pitch motion depends on the orbital rate and moments of inertia rather than initial deviations.

2.5.5 Linear Stability Analysis

The aim of the stability analysis is to know if deviations from an equilibrium configuration of a satellite are going to grow with time. If that happens the satellite is considered to be unstable. On the other hand, if deviations do not grow with time the satellite is stable.

First of all, equilibrium configuration has to be defined. By equilibrium configuration, it is considered that the Earth is seen stationary from the body reference frame. That happens when the body reference frame is aligned with the orbit reference frame i.e. $\theta_i = 0$. Also the satellite has to be spinning around the axis perpendicular to the orbit, with same frequency as the orbit rotation. Under these assumptions, there are three possible equilibrium configuration that depend on which of the principal axis of inertia i.e. maximum, minimum and intermediate is aligned with the orbit normal. However, not all three possible configuration may be stable. The linear stability analysis is performed to find which configuration is stable.

The stability analysis is based on seeking roots of linear dynamic equations (2.79), (2.80), and (2.81) in the frequency domain. Going to the frequency domain can be done by making a change of variable $\theta_i = e^{\lambda t} c$, where λ is a complex number or by taking the Laplace transform. Finally, the system is said to be asymptotically stable, if all of its roots have negative real parts $\text{Real}(\lambda_i) < 0$.

Since the pitch equation of motion is decoupled from the others, it can be investigated separately. The pitch equation in the frequency domain is:

$$e^{\lambda t} (\lambda^2 + 3n^2(J_1 - J_3)/J_2) = 0 \quad (2.83)$$

with roots:

$$\lambda_i = \pm \sqrt{-3n^2(J_1 - J_3)/J_2} \quad (2.84)$$

so, if $J_1 > J_3$ all roots are pure imaginary and therefore the equation is stable.

The roll and yaw equations can be written like a system of equations $M\ddot{\theta} + G\dot{\theta} + K\theta = 0$ where:

$$\begin{aligned} M &= \begin{bmatrix} J_1 & 0 \\ 0 & J_3 \end{bmatrix} \\ G &= (J_1 + J_3 - J_2)n \begin{bmatrix} 0 & -1 \\ 1 & 0 \end{bmatrix} \\ K &= n^2 \begin{bmatrix} 4(J_2 - J_3) & 0 \\ 0 & (J_2 - J_1) \end{bmatrix} \end{aligned}$$

After introducing the change of variable the roll/yaw equations are:

$$e^{\lambda t} [\lambda^2 M + \lambda G + K] c_0 = 0 \quad (2.85)$$

Grouping moments of inertia like $k_1 = (J_2 - J_3)/J_1$ and $k_3 = (J_2 - J_1)/J_3$, the characteristic equation of the system (2.85) is:

$$\lambda^4 + (1 + 3k_1 + k_1 k_3)n^2 \lambda^2 + 4k_1 k_3 n^4 = 0 \quad (2.86)$$

and the roots become pure imaginary if the following expressions are fulfilled:

$$\begin{aligned} k_1 k_3 &> 0 \\ 1 + 3k_1 + k_1 k_3 &> 0 \\ (1 + 3k_1 + k_1 k_3)^2 - 16k_1 k_3 &> 0 \end{aligned} \quad (2.87)$$

which are the stability condition for the roll and yaw axes. Together with the pitch condition can be represented in a stability diagram like depicted in Figure 2.6.

Figure 2.6 represents the stable regions in a $k_1 k_3$ plane. The stable regions are represented as clear zones whereas unstable regions are darker. Two different stable regions are distinguished, region 1 in the

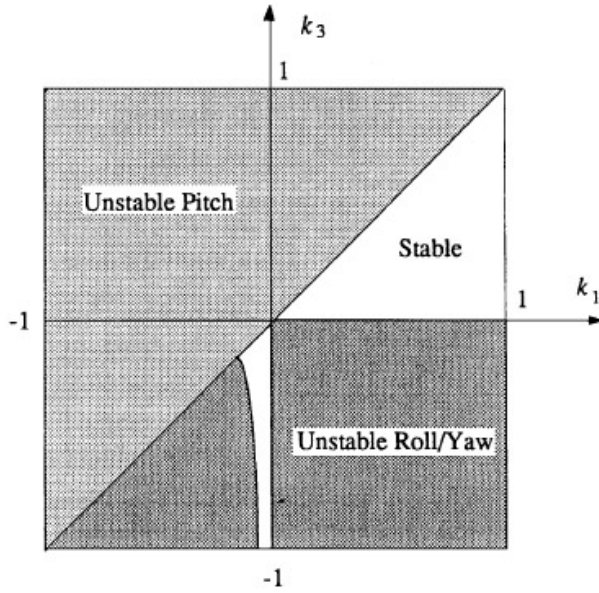


Figure 2.6: Stability regions of gravity gradient torque [4].

first quarter of the plane ($k_1 > 0, k_3 > 0$) and region 2 in the third quarter ($k_1 > 0, k_3 < 0$). Both regions can be expressed as functions of moments of inertia like:

$$\text{Stable} = \begin{cases} J_2 > J_1 > J_3 & , J_2 < J_1 + J_3 & \text{Region 1} \\ J_1 > J_3 > J_2 & , J_1 < J_2 + J_3 & \text{Region 2} \end{cases}$$

The region 1 represents a boom deployed along the yaw axis for a satellite model which is discussed in Chapter 3.

2.5.6 Nadir and Zenith Position

The linear stability analysis defines stable configuration in terms of mass distribution. In Chapter 3 SWIM geometry and mass distribution with deployed boom according to the stability analysis is defined. However, the stability analysis gives no information about how the satellite is pointing. In this sense two possible equilibrium positions can be defined. First equilibrium position has to be defined. The equilibrium position is the one that gravity gradient becomes zero. That happens when:

- The boom is pointing towards the Earth. If body and orbit reference frame are aligned, $\vec{M}_{grav} = 0$. This happens when the boom is aligned in the direction of the gravity force. In this position a satellite is called Nadir pointing.
- The boom is pointing opposite to the Earth. When the boom is perfectly aligned with the Earth but in a direction opposite to the gravity force. This position is called Zenith pointing.

When a deviation from the equilibrium position is very large, the satellite might become unstable and change its equilibrium position. For instance, if the satellite is nadir pointing but there is deviation in the roll or pitch axes larger than 90° from the equilibrium position, gravity torques would make it to rotate to zenith pointing position, therefore eventually the satellite turns around.

Finally, if the satellite starts the attitude in the equilibrium position and rotating with same frequency as the orbit reference frame, the Earth will be seen as stationary from the body reference frame. That happens for a circular orbit with only gravity gradient. This is referred as the equilibrium initial attitude conditions. The attitude analysis is done by adding deviation from the equilibrium initial attitude conditions.

Chapter 3

Satellite Characterization

The previous chapter summarizes and explains the physical principles that define spacecraft dynamics. Those principles are applicable to all kind of spacecraft. In order to apply them to a selected vehicle, a mechanical model has to be built. SWIM is a 3U CubeSat with a gravity gradient boom. A mass model is built by analyzing the different components of the spacecraft and joining them together. To do so, the spacecraft is divided into three main elements: hub, boom and magnetometer, which is placed at the tip of the boom. Other features involving dynamics like the magnetic moment and drag coefficient, have also to be defined.

The Hub is the main body of the CubeSat. The simplest model is an homogeneous rectangular parallelepiped or cuboid with dimensions width $w = 0.3$ m, height $h = 0.1$ m and depth $d = 0.1$ m. The mass of the hub is not yet decided, but due to requirements, the spacecraft has to have a mass of less than 4 kg [2]. Figure 3.1a shows a 3D model of a 3U CubeSat hub.

The boom is modelled as a slender rod of length L and uniform mass m_b . The boom length is one of the most important design parameters in terms of mass distribution and it will be modified during the design process until reach its final value. Hence, it is more useful to use density per unit length ρ_b that change the mass for every boom length. Figure 3.1b shows a slender rod model.

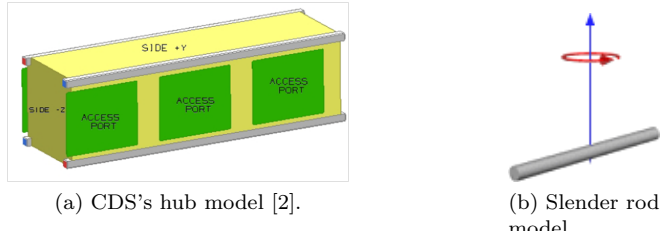
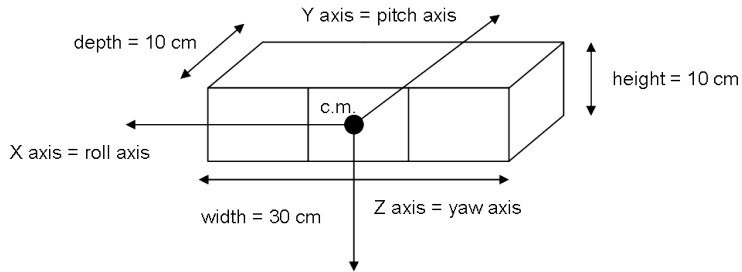


Figure 3.1: Models of hub and rod.

The magnetometer is modelled as a point mass m_t located at the tip of the boom. From now on, it will be referred as the tip mass. The tip mass includes the magnetometer and its casing. Some dummy mass could be added to the tip to reach a desired mass distribution. Therefore, m_t is also an important design parameter.

3.1 Mass and Geometric Properties

For calculating the mass properties an auxiliary reference frame $A' = (\vec{a}'_1, \vec{a}'_2, \vec{a}'_3)$ is established in the centroid of the hub, with \vec{a}'_1 along the width direction, \vec{a}'_2 along the depth and \vec{a}'_3 along the height direction as is represented in Figure 3.2.

Figure 3.2: Auxiliary reference frame A' .

The boom is assumed to be deployed from a point along a line that goes through \vec{d}'_1 . The best location to deploy the boom is the center of the hub, but that might be not possible due to systems' distribution inside the hub. The distance between point where the boom is deployed and the A' reference frame is considered to be l .

3.1.1 Center of Mass

In order to define a dynamic model of a rigid body the center of mass has to be found. The center of mass is the mean location of masses in a body. The dynamic equations are often referred to this point. For homogeneous mass distribution elements the center of mass corresponds with the centroid or geometrical center of the element. Nevertheless, a definition of the center of mass location for uniform mass distribution is given by:

$$\vec{R}_{c.m.} = \frac{\int \rho(\vec{r}) \vec{r} dV}{\int \rho(\vec{r}) dV} = \frac{1}{M} \int \rho(\vec{r}) \vec{r} dV = \frac{1}{M} \int \vec{r} dm \approx \frac{\sum m_i \vec{r}_i}{\sum m_i} \quad (3.1)$$

where $\vec{R}_{c.m.}$ is the position vector of the center of mass, \vec{r} is the position vector of element mass dm , $\rho(\vec{r})$ is the density function and M is the total mass of the system. In the last approximation of equation (3.1), m_i is the mass of element i and \vec{r}_i is the position of the center of mass of element i with respect to an arbitrary reference frame. This formula is used to find center of mass when the body is divided in many elements. Table 3.1 shows values of the location of the center of mass of the different elements of the spacecraft with respect to the auxiliary reference frame A' .

Element	Mass	$R_{c.m.,1}$	$R_{c.m.,2}$	$R_{c.m.,3}$
Hub	M	0	0	0
Boom	m_b	l	0	$L/2$
Tip	m_t	l	0	L

Table 3.1: Center of mass of different elements.

3.1.2 Moments of Inertia

Moments of inertia were introduced in the calculation of the angular momentum in equation (2.58). A moment of inertia measures resistance to rotation around an axis of a body. Considering an arbitrary axis and a position vector \vec{r} with respect to the axis, the moment of inertia is equal to:

$$J_i = \int r_i^2 dm \quad (3.2)$$

Moments of inertia are diagonal terms of the inertia tensor \tilde{J} , which measures mass distribution with respect to the coordinate axes. Inertia tensor changes for different coordinate axes of the same rigid body. Nevertheless, for any coordinate frame there is a unique orientation of axes which makes the inertia tensor diagonal [15]. These axes are called the principal inertia axes and their respective moments of inertia

are the principal moments of inertia. The principal moments of inertia for a given point represent the maximum, minimum and intermediate value of the moments of inertia. Table 3.2 shows values of moments of inertia for the various elements of the spacecraft with respect to their center of mass and axes parallel to A' auxiliary reference frame. In order to calculate moments of inertia for the entire satellite it is

Element	Mass	J_1	J_2	J_3
Hub	M	$\frac{M}{12}(h^2 + d^2)$	$\frac{M}{12}(w^2 + h^2)$	$\frac{M}{12}(w^2 + d^2)$
Boom	m_b	$\frac{m_b}{12}L^2$	$\frac{m_b}{12}L^2$	0
Tip	m_t	0	0	0

Table 3.2: Moments of inertia for different elements.

important to transfer moments of inertia to a parallel axis. The parallel-axis theorem states that if the moment of inertia of a body is known about an axis that goes through the center of mass, the moment of inertia about a parallel axis is equal to the moment of inertia at the center of mass plus the mass of the element times the distance of the axis square:

$$J = \bar{J} + md^2 \quad (3.3)$$

where \bar{J} is the moment of inertia at the center of mass and J is the moment of inertia for a parallel axis.

Finally parallel axis theorem has to be used for calculating moments of inertia in the center of mass of full body as follows:

$$\begin{aligned} J_1 &= \frac{M}{12}(h^2 + d^2) + Md_{1,hub}^2 + \frac{m_b}{12}L^2 + m_b d_{1,boom}^2 + m_t d_{1,tip}^2 \\ J_2 &= \frac{M}{12}(h^2 + w^2) + Md_{2,hub}^2 + \frac{m_b}{12}L^2 + m_b d_{2,boom}^2 + m_t d_{2,tip}^2 \\ J_3 &= \frac{M}{12}(w^2 + d^2) + Md_{3,hub}^2 + m_b d_{3,boom}^2 + m_t d_{3,tip}^2 \end{aligned} \quad (3.4)$$

where $d_{i,element}$ is the distance from the center of mass of element i to the center of mass of the spacecraft.

3.1.3 Boom Length

Mass properties of the spacecraft depend on the boom's location and length. The location of the boom depends more on the design of satellite systems than dynamic requirements. The place available between the different experiments will be used for the boom. Boom length is a trade off between CubeSat storage capability, experiment requirements and the dynamics of the spacecraft. For example, a magnetometer is placed at the tip of the boom, which requires a minimum distance in order to collect data without distortion from the spacecraft itself. Additionally, moments of inertia and gravity gradient torques produced by the spacecraft are functions of boom length, which affects the dynamics of the satellite

In order to check how mass properties change with boom length Figures 3.3 , 3.4 and 3.5 are displayed. Consider that the SWIN CubeSat has mass properties as summarized in Table 3.3 and variable boom length.

Mass properties		
Mass of hub M	=	3 kg
Mass of tip m_t	=	100 g
Boom density ρ	=	0.08 kg/m
Boom root location from A' origin	=	0.05 m along roll axis

Table 3.3: SWIM mass properties.

Figure 3.3a depicts the displacement of the center of mass for increasing boom length. As long as the boom is longer, the center of gravity is displaced along \vec{b}_3 axis and gets closer to the location of the boom in the \vec{b}_1 axis. The importance of the center of mass location recalls in the fact that a rigid body rotates around it. This is a crucial parameter for aerodynamic stabilization.

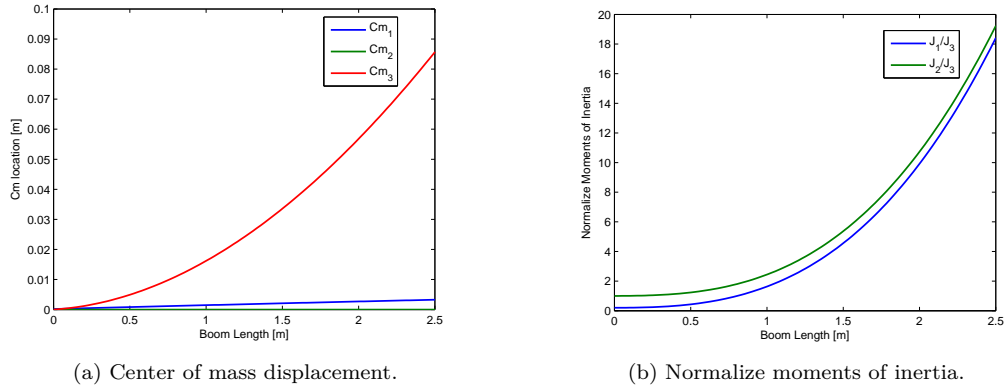


Figure 3.3: Mass properties.

Figure 3.3b shows how moments of inertia increase with boom length. Moments of inertia are normalized with respect to $J_3 = 0.025 \text{ kgm}^2$, which remains almost constant with boom length. It is seen that stability region 1 is reached for $L \approx 0.6$ meters, when $J_2/J_3 > 1$. After that, the moments of inertia grow sharply achieving almost 20 times their initial value for a 2 meters boom. Both J_1 and J_2 grow in the same fashion, approaching the same value. Comparing this fact with equation (2.65), it is deduced that a longer boom provides higher gravity torques about the roll and pitch axes, but almost equal torque about the yaw axis.

Figure 3.4 shows gravity gradient torques around the pitch axis, where linear theory and circular orbit are assumed. Figure 3.4 shows results for a 800 km circular orbit and three different deviations around the pitch axis $\theta_2 = 5^\circ, 10^\circ, 15^\circ$. It is seen that gravity gradient torques increase dramatically with boom length and deviation. Although stability has been treated only in terms of moments of inertia, once perturbations are added to the problem, the gravity gradient torques have to exceed the disturbance torques for a stable motion.

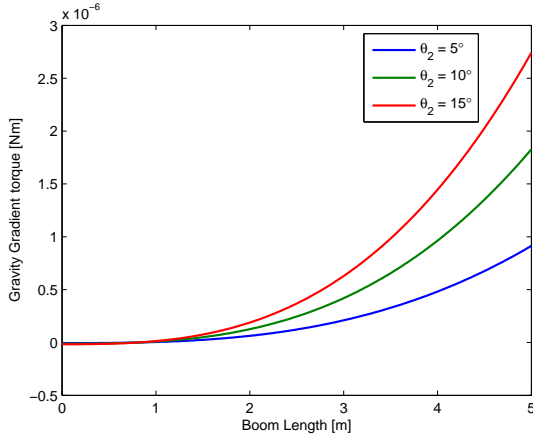


Figure 3.4: Gravity gradient torque as function of boom length.

Finally Figure 3.5 shows the linear period for a circular orbit of 800 km altitude. The figure has been done by evaluating equation (2.82) for different boom lengths.

The pitch linear period is an important feature of the satellite. It tells how fast the satellite restores its position. Therefore, it measures the stability capability of the spacecraft. The linear period decreases sharply for the first two meters. Then there is an asymptote around $T_{pitch} = 3500$ s. So, there is a boundary in terms of restoring capability. Looking at equation (2.80), when moments of inertia increase,

the gravity gradient torque increases and so does the rotatory inertia $J_2\ddot{\theta}_2$ of the spacecraft. Hence, there is a certain limit for the boom length where deploying a longer boom does not make the spacecraft restore its position faster.

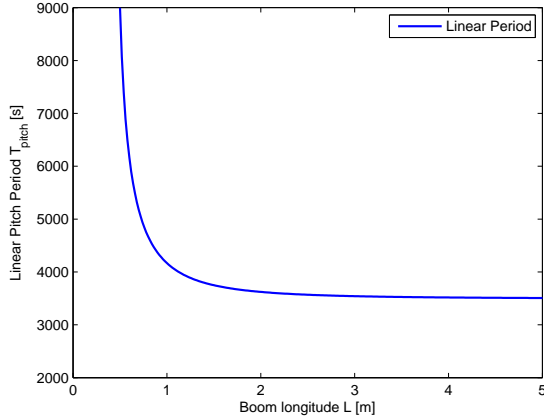


Figure 3.5: Linear pitch period as function of boom length.

3.2 Aerodynamic Characterization

According to the aerodynamic force equation (2.68), there are two parameters to be defined. These are drag coefficient C_D and area A . For the drag coefficient a conservative value of $C_D = 2.2$ is used [7].

The exposed area is calculated separately for the different three elements. The dimensions of the hub are already known. For the boom slender rod model is used again. The parameter that defines the area is the radius of the boom r_{boom} . Therefore boom area is calculated as:

$$A_{boom} = 2r_{boom}L \quad (3.5)$$

where L is the length of the boom. In order to calculate aerodynamic torques the boom is divided in several elements. In this way every element has the center of pressure at its geometric center.

The tip of the boom is modelled as a sphere for aerodynamic calculations. The parameter that defines the area is the radius of the tip r_{tip} . The area is modelled as a circle with the center of pressure at the center of the sphere. So, the area of the tip mass is:

$$A_{tip} = \pi r_{tip}^2 \quad (3.6)$$

In Chapter 1 the dimensions of SMILE were defined as $20 \times 20 \times 21$ mm. So including its casing a realistic value of r_{tip} is 25 cm.

3.3 Magnetic Moment

The magnetic moment is an unknown parameter. As it has been mentioned in section 2.4, the magnetic moment is used as a study parameter. Therefore, the vector $\vec{\mu}$ represent the three components of the magnetic torque in the body axes.

$$\vec{\mu} = [\mu_1, \mu_2, \mu_3]^T \quad (3.7)$$

Chapter 4

Attitude Simulator

An attitude simulator tool has been developed in order to investigate the spacecraft's attitude for different possible configurations, orbit trajectories and mission requirements.

4.1 Simulator Layout

The attitude simulator is a numerical tool made in MATLAB environment. It is divided in three principal packages, initial conditions for propagation, ODE's integrator and data processing as depicted in Figure 4.1. The aim of this simulator is to solve simultaneously the orbit propagation, Euler's equations of motion and kinematic differential equations, (2.10), (2.60) and (2.46) respectively. These equations make an initial value problem of system of ODE's, which is solved by a Runge-Kutta numerical integrator.

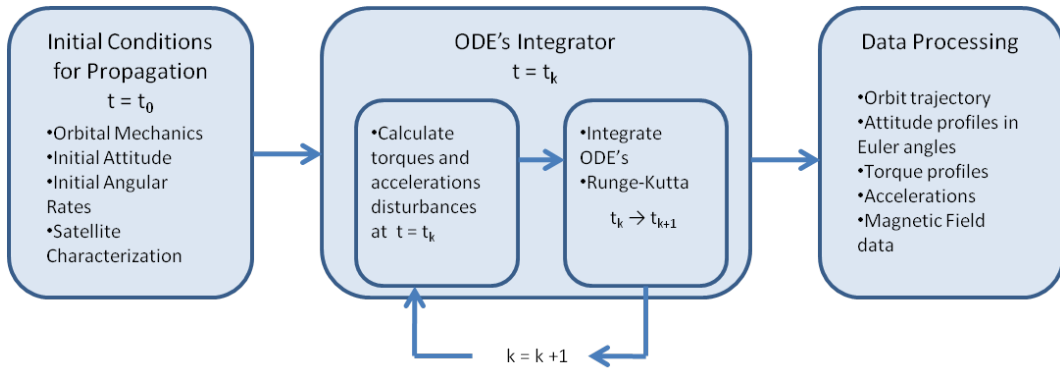


Figure 4.1: Attitude simulator layout.

There are several attitude propagators that separate orbital mechanics from the attitude propagation. However, since aerodynamic effects are included in the orbit calculation, the attitude is required at each iteration step of the orbit propagation.

4.2 Initial Conditions for Propagation

The attitude simulator solves one initial value problem (IVP) composed of a system of 13 equations. The general formulation of IVP is:

$$\frac{d\vec{u}}{dt} = \vec{f}(t, \vec{u}, \vec{p}), \quad \vec{u}_{(t_0)} = \vec{u}_0, \quad t \in [t_0, t_{end}] \quad (4.1)$$

where \vec{p} is the different parameters of the equations and \vec{u}_0 is the initial value of the system [17]. \vec{p} is the sum of the properties of the satellite discussed in Chapter 3. The aim of this section is to define \vec{u}_0 to start propagation. Ordinary differential equations can be solved in MATLAB by using some of the *ODE* functions. That requires to write the equations in state-variable form.

If \vec{r} from equation (2.10) is considered to be $\vec{r} = (x, y, z)$ in Cartesian coordinates the state-variable form of the equation is:

$$\begin{aligned}\dot{x}_1 &= x_2 \\ \dot{y}_1 &= y_2 \\ \dot{z}_1 &= z_2 \\ \dot{x}_2 &= -\mu \frac{x_1}{(\sqrt{x_1^2 + y_1^2 + z_1^2})^3} + a_x \\ \dot{y}_2 &= -\mu \frac{y_1}{(\sqrt{x_1^2 + y_1^2 + z_1^2})^3} + a_y \\ \dot{z}_2 &= -\mu \frac{z_1}{(\sqrt{x_1^2 + y_1^2 + z_1^2})^3} + a_z\end{aligned}\tag{4.2}$$

similarly the dynamic equations of motion (2.60) in state-variable form:

$$\begin{aligned}\dot{\omega}_1 &= (1/J_1)((J_2 - J_3)\omega_2\omega_3 + M_1) \\ \dot{\omega}_2 &= (1/J_2)((J_3 - J_1)\omega_3\omega_1 + M_2) \\ \dot{\omega}_3 &= (1/J_3)((J_1 - J_2)\omega_1\omega_2 + M_3)\end{aligned}\tag{4.3}$$

and the kinematic differential equations (2.46):

$$\begin{aligned}\dot{q}_1 &= 1/2(\omega_3 q_2 - \omega_2 q_3 + \omega_1 q_4) \\ \dot{q}_2 &= 1/2(\omega_1 q_3 + \omega_2 q_4 - \omega_3 q_1) \\ \dot{q}_3 &= 1/2(\omega_2 q_1 - \omega_1 q_2 + \omega_3 q_4) \\ \dot{q}_4 &= 1/2(-\omega_1 q_1 - \omega_2 q_2 - \omega_3 q_3)\end{aligned}\tag{4.4}$$

So, the attitude simulator consists in solving 13 non-linear coupled ordinary differential equations. Comparing equations (4.2), (4.3) and (4.4) with the general formulation of the IVP (4.1), the state vector \vec{u} is defined as follows:

$$\vec{u} = [x_1, y_1, z_1, x_2, y_2, z_2, \omega_1, \omega_2, \omega_3, q_1, q_2, q_3, q_4]^T\tag{4.5}$$

where the six first scalars correspond to the orbit propagation and the remaining seven to the attitude dynamics.

4.2.1 Initial Conditions for Orbit Propagation

The state vector for the orbit propagation is defined by six scalars. For a ECI reference frame it means position and velocity vector respectively $\vec{u} = (\vec{r}, \vec{v}) = (x_1, y_1, z_1, x_2, y_2, z_2)$. However, these values by themselves have no physical interpretation. Instead a set of classical elements of celestial mechanics is used.

The classical element set that defines an orbit is $(a, e, i, \Omega, \omega, \tau)$ [5], which are the semimajor axis, eccentricity, inclination, right ascension of the ascending node, argument of perifocal point and the time of perifocal passage. For convenience true anomaly (θ) is used instead of the time of perifocal passage. From the six elements, (a, e, θ) define magnitude and direction of \vec{r} and \vec{v} in the perifocal reference frame and (i, Ω, ω) the orientation from the perifocal to the ECI. So in order to calculate the position and velocity vector in the ECI reference frame, two steps are required. First, to calculate \vec{r} and \vec{v} in the perifocal coordinate frame and second, to rotate from the perifocal to the ECI frame [5].

The ECI reference frame has to be defined before starting calculations. Figure 4.2 shows the ECI reference frame and the orientation of the orbit frame with respect to the ECI frame.

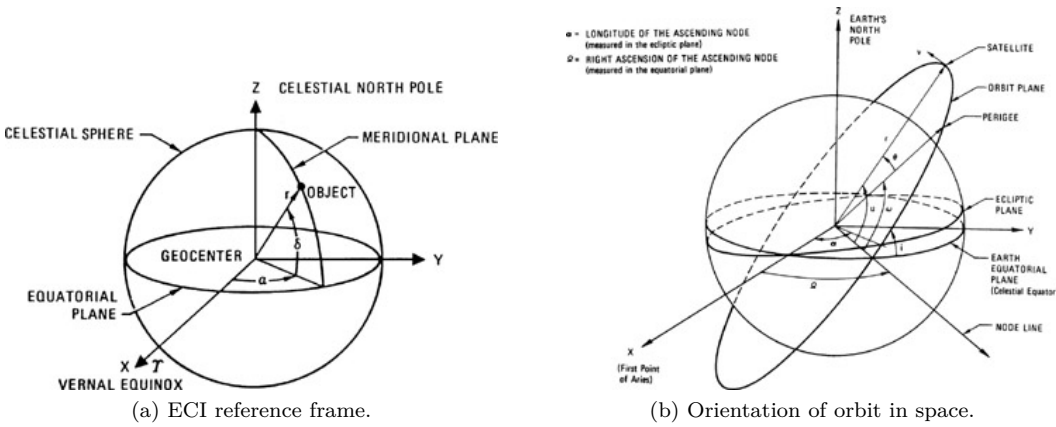


Figure 4.2: ECI reference frame and orbit orientation, [5].

Figure 4.2a shows the ECI reference frame. The origin of the coordinate system is located at the center of the Earth. The fundamental plane is the equator. The X axis points towards the vernal equinox. The Z axis goes through the North Pole and the Y axis is perpendicular to both.

Figure 4.2b shows the orientation of the orbit frame with respect to ECI. Orientation is defined by classical elements, which are defined as the following angles:

- Inclination (i): it is the inclination of the orbit with respect to the equatorial plane. It is measured counterclockwise from the equatorial plane to the orbit plane.
- Right ascension of the ascending node (Ω): it is measured counterclockwise in the equator plane. It is the distance from the X axis to the point where the orbit crosses the equator (line of nodes).
- Argument of the perigee (ω): it is measured in the orbit plane. Goes from the line of nodes to the perigee of the orbit.

And the elements that define size and shape:

- Eccentricity (e): it defines orbit shape, how elliptical the orbit is.
- True anomaly (θ): it is measured counterclockwise, it is the deviation from the perigee of the orbit.
- Semimajor axis (a): it defines the size of the orbit.

Although these parameters define the orbit shape, the altitude of the perigee h_{perigee} is to be used instead of the semimajor axis. Combining h_{perigee} and eccentricity (e), semimajor axis is calculated as:

$$a = (R_E + h_{\text{perigee}})/(1 - e) \quad (4.6)$$

where R_E is the radius of the Earth. Figure 4.3a depicts the position and velocity vector in the perifocal reference frame. The perifocal reference frame is located in the closer focus to perigee of the orbit with one axis perpendicular to the orbit plane. Figure 4.3b shows the orientation of the perifocal frame with respect to the ECI. From the conic equation, the position vector \vec{r} is calculated [9]:

$$\vec{r} = r \cos \theta \hat{P} + r \sin \theta \hat{Q} \quad (4.7)$$

where the radius vector magnitude is:

$$r = \frac{p}{1 + e \cos \theta} \quad (4.8)$$

Differentiating equation (4.7) the velocity vector is calculated as [5]:

$$\vec{v} = \sqrt{\frac{\mu}{p}} [(-\sin \theta \hat{P} + (e + \cos \theta) \hat{Q})] \quad (4.9)$$

where $p = a(1 - e^2)$ is the semilatus rectum of the orbit and μ is the standard gravitational parameter.

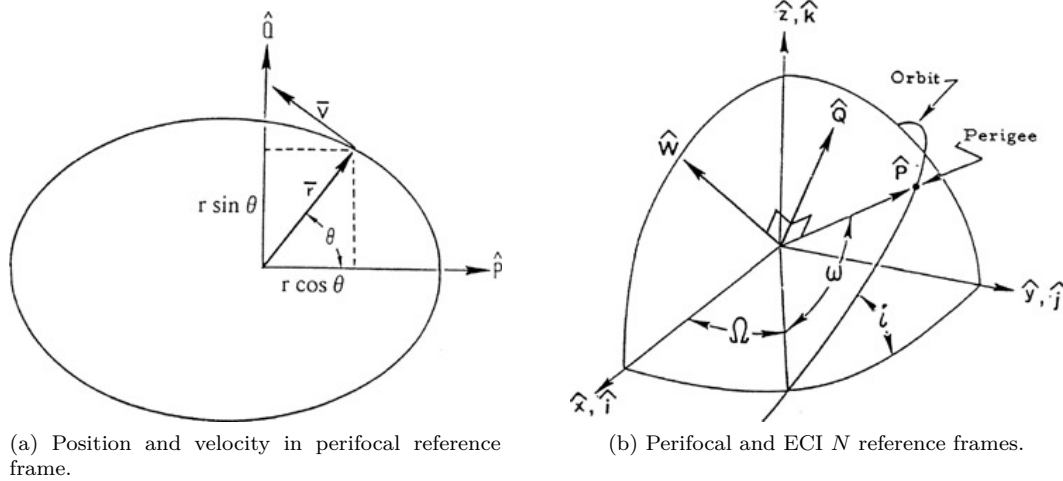


Figure 4.3: Perifocal and ECI N reference frames [5].

Then the position and velocity vector in the perifocal reference frame can be defined by eccentricity, true anomaly and altitude of the perigee, $(\vec{r}_p, \vec{v}_p) = f(e, \theta, h_{perigee})$. Now is time to rotate from the perifocal reference frame to the ECI. This is done by three successive rotations. It is easier to rotate from the ECI to the perifocal by rotating first about \hat{z} by Ω , second about \hat{x} by i and third about \hat{z} by ω (see Figure 4.3b), which gives the following rotation matrices:

$$R_1 = \begin{bmatrix} \cos \Omega & \sin \Omega & 0 \\ -\sin \Omega & \cos \Omega & 0 \\ 0 & 0 & 1 \end{bmatrix} \quad R_2 = \begin{bmatrix} 1 & 0 & 0 \\ 0 & \cos i & \sin i \\ 0 & -\sin i & \cos i \end{bmatrix} \quad R_3 = \begin{bmatrix} \cos \omega & \sin \omega & 0 \\ -\sin \omega & \cos \omega & 0 \\ 0 & 0 & 1 \end{bmatrix}$$

Multiplying the inverse of the rotation matrices i.e. $R'_1 R'_2 R'_3$ the following rotation matrix is calculated:

$$R^{perifocal/ECI} = \begin{bmatrix} \cos \Omega \cos \omega - \sin \Omega \sin \omega \cos i & -\cos \Omega \sin \omega - \sin \Omega \cos \omega \cos i & \sin \Omega \sin i \\ \sin \Omega \cos \omega + \cos \Omega \cos \omega \cos i & -\sin \Omega \sin \omega + \cos \Omega \cos \omega \cos i & -\cos \Omega \sin i \\ \sin \omega \sin i & \cos \omega \sin i & \cos i \end{bmatrix} \quad (4.10)$$

So the position and velocity vectors in Cartesian coordinates are calculated like:

$$\begin{bmatrix} x_1 \\ y_1 \\ z_1 \end{bmatrix} = R^{perifocal/ECI} \begin{bmatrix} r \cos \theta \\ r \sin \theta \\ 0 \end{bmatrix}; \quad \begin{bmatrix} x_2 \\ y_2 \\ z_2 \end{bmatrix} = R^{perifocal/ECI} \begin{bmatrix} -\sqrt{\frac{\mu}{p}} \sin \theta \\ \sqrt{\frac{\mu}{p}}(e + \cos \theta) \\ 0 \end{bmatrix} \quad (4.11)$$

4.2.2 Initial Conditions for Attitude Propagation

The state vector for the attitude propagation is formed by seven scalars, which correspond to the initial angular rates and initial quaternion, $\vec{u} = (\vec{\omega}, \vec{q}, q_4) = (\omega_1, \omega_2, \omega_3, q_1, q_2, q_3, q_4)$.

The initial angular rates need no transformation. This is because Euler's equations are expressed in the body reference frame.

This is different for the initial quaternion. The orientation of the spacecraft with respect to the ECI has to be defined for the first iteration. This is done by two successive changes of reference frame. First change of reference frame is from the ECI to the orbit A and second from the orbit to the body reference frame B .

$$R^{B/N} = R^{B/A} R^{A/N} = R(\vec{q}'', q_4'') R(\vec{q}', q_4') \quad (4.12)$$

The first rotation matrix $R^{A/N}$ is calculated by the definition of direction cosine matrix (DCM) from equation (2.22). Where N and A reference frames are defined in section 2.2. The basis vectors of A reference frame are calculated plugging initial values of the position and velocity vector into equations (2.16), (2.17) and (2.18).

The second rotation defines initial deviation from the orbit reference frame. Initial deviations are expressed in Euler angles roll, pitch and yaw, θ_1 , θ_2 and θ_3 . In order to work with Euler angles a 132 rotation sequence has been chosen. $R^{B/A}$ was introduced in equation (2.49). Once both matrices are calculated the quaternion that defines them can be calculated by applying equations (2.36) and (2.37). After both quaternions can be multiplied in order to get the quaternion at $t = t_0$, which from now on it will be referred as q_0 .

4.3 ODE's Integrator

The next package is the differential equations integrator. In order to solve equations (4.2),(4.3) and (4.4) an explicit Runge-Kutta (4,5) algorithm is used. Explicit methods for IVP problems need function value at the previous time step (u_{t-1}) to compute the solution.

The attitude simulator has been developed in MATLAB environment. Runge-Kutta (4,5) is introduced by the function `@ode45`. This function allows to adapt tolerance and minimum time step. The solution delivered by the integrator is a time vector \vec{t} and a solution matrix \tilde{u} with numerical values of the equations. The time vector has n components. The number of components depends on the time interval that is simulated $t \in [t_0, t_{end}]$ and step size taken by the solver, which depends on the tolerance selected. Solution matrix \tilde{u} has dimensions $(n \times 13)$, where each row corresponds to the solution corresponding at each time point.

$$\vec{t} = \begin{bmatrix} t_1 \\ t_2 \\ t_3 \\ \vdots \\ t_n \end{bmatrix} \quad (4.13)$$

$$\tilde{u} = \begin{bmatrix} x_{1,t1} & y_{1,t1} & z_{1,t1} & x_{2,t1} & y_{2,t1} & z_{2,t1} & \omega_{1,t1} & \cdots & q_{1,t1} & \cdots \\ x_{1,t2} & y_{1,t2} & z_{1,t2} & x_{2,t2} & y_{2,t2} & z_{2,t2} & \omega_{1,t2} & \cdots & q_{1,t2} & \cdots \\ x_{1,t3} & y_{1,t3} & z_{1,t3} & x_{2,t3} & y_{2,t3} & z_{2,t3} & \omega_{1,t3} & \cdots & q_{1,t3} & \cdots \\ \vdots & \vdots \\ x_{1,t_n} & y_{1,t_n} & z_{1,t_n} & x_{2,t_n} & y_{2,t_n} & z_{2,t_n} & \omega_{1,t_n} & \cdots & q_{1,t_n} & \cdots \end{bmatrix} \quad (4.14)$$

4.3.1 Attitude Simulator Results

One example of simulation results is displayed. This is done in order to get familiar with simulation result and their meaning. A spacecraft inserted into a circular orbit under gravity gradient torques is simulated. Moments of inertia of the simulation are $J_1 = 80$, $J_2 = 82$ and $J_3 = 4 \text{ kgm}^2$. Table 4.1 displays the initial conditions for the orbit propagation as they are selected in the simulator.

Orbit Propagation Initial Conditions		
Altitude of the perigee $h_{perigee}$	=	800 km
Eccentricity e	=	0
True anomaly θ	=	30°
Inclination i	=	30°
Right ascension of ascending node Ω	=	25°
Argument of the perigee ω	=	15°

Table 4.1: Initial conditions for orbit propagation.

Table 4.1 shows the orbital initial conditions in classical element set. Applying equation (4.11), initial conditions in Cartesian are found:

$$(\vec{r}, \vec{v}) = [3.0833, 5.3978, 3.5890, -0.0064, 0.0011, 0.0037] \times 10^3$$

The attitude initial conditions are delivered in Table 4.2.

Attitude Initial Conditions	
Angular velocity $\vec{\omega}$	= $(0, -0.001, 0)$ rad/s
Initial roll $\theta_{1,0}$	= 2°
Initial pitch $\theta_{2,0}$	= 6°
Initial yaw $\theta_{3,0}$	= 5°

Table 4.2: Initial conditions for attitude propagation.

For working with the simulator, the Euler angles have to be transformed to a quaternion. After transformation, the initial attitude conditions are:

$$(\vec{\omega}, q_0) = [0, -0.001, 0, -0.0123, -0.8421, 0.4513, 0.2951] \times 10^3$$

Finally the simulation is set to last 5×10^4 seconds.

Figure 4.4 depicts time evolution of the different components of the position and velocity vectors, seen from the ECI reference frame. That is equal to the first six columns of the solution matrix \hat{u} . Additionally, Figure 4.5 shows the orbit trajectory in a 3D plot where the point $(0,0,0)$ is the origin of the ECI reference frame.

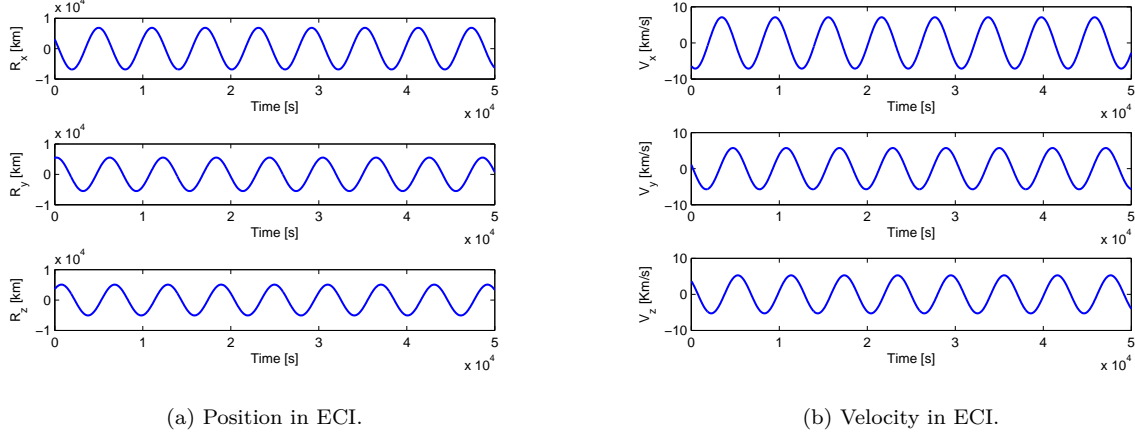


Figure 4.4: Position and velocity vectors in the ECI reference frame.

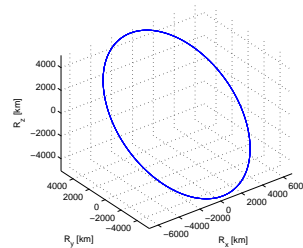


Figure 4.5: Orbit in 3D plot in the ECI reference frame.

Figure 4.6 shows time evolution of the angular velocity.

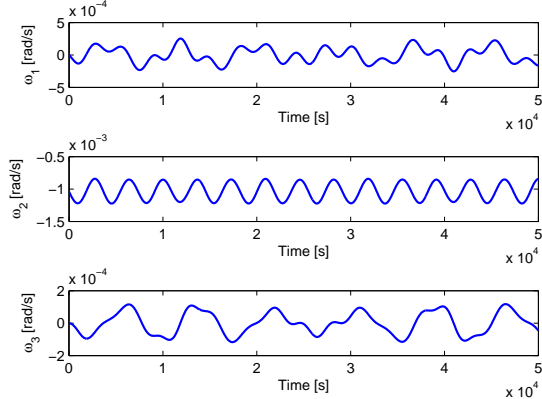


Figure 4.6: Angular velocity.

Figure 4.7 shows the solution of the kinematic differential equations (4.4). The quaternion response is a way to define the attitude, but as it has been mentioned, it is difficult to understand.

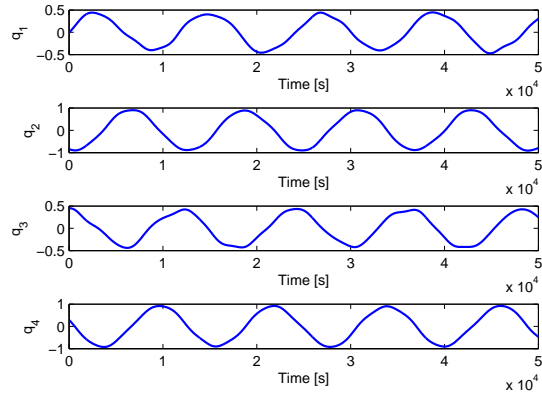


Figure 4.7: Quaternions response.

Summarizing, Figures 4.4, 4.6 and 4.7 show a total of 13 time dependent functions $f(\tilde{u}, t)$, corresponding to the values of matrix \tilde{u} with respect to time vector \vec{t} , which is the solution to the orbit and attitude propagation.

4.3.2 Simulation Errors

The attitude simulator is based on solving differential equations numerically. Doing that this, produces certain error. This error is the difference between the function real value and the numeric value. According to [17] truncation or local error e_k is defined as follows:

$$e_k = u(t_k) - u_k = O(h) \quad (4.15)$$

where $O(h)$ is the order of accuracy. The `@ode45` solver is a variable step, fifth order accuracy method. Additionally, it provides a tolerance parameter. The quaternion kinematic equations are used for checking numerical error. By definition, the norm of a quaternion is equal to the unit i.e. $norm(q) = 1$. Therefore,

the truncation error can be found by applying equation (4.15) to the quaternion norm :

$$e_k = \sqrt{q_1^2 + q_2^2 + q_3^2 + q_4^2} - 1 \quad (4.16)$$

In order to illustrate the truncation error Figure 4.8 has been generated. Two simulations with same initial conditions, Tables 4.1 and 4.2, and different relative tolerance parameters of the @ode45 solver have been run. The relative tolerance is defined as a measure of the error relative to the size of each solution component. In other words, it controls the number of correct digits in all solution components [18]. Once the simulations are finished equation (4.16) has been applied to the quaternion rates (Figure 4.7). Relative tolerance values are 10^{-6} and 10^{-9} respectively.

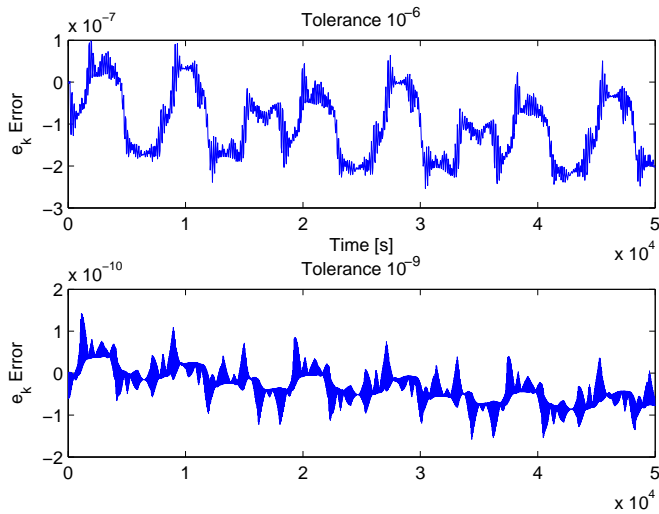


Figure 4.8: Numerical error.

Figure 4.8 exposes the difference in order of accuracy from one tolerance to other. However, increasing the tolerance means increasing the computing time. For instance, \tilde{u} dimension for 10^{-6} tolerance is 1249×13 whereas for 10^{-9} tolerance is 5317×13 for the same time interval. Therefore there is a trade off between the accuracy and computing resources.

4.4 Data Processing

The spacecraft's attitude is completely defined by the dynamic and kinematic equations, which solutions are represented in Figures 4.6 and 4.7 correspondingly.

The mission specifications demand a LVLH pointing. This is fulfilled by mass distribution. However, there is not possible interpretation of the angle deviations or satellite's pointing by looking at the quaternions response. Therefore, some mathematical manipulation of the ODE's integrator solution i.e. \vec{t} and \vec{u} is required.

4.4.1 Basis Vectors

The attitude with respect to LVLH pointing is defined as a rotation between the orbit frame A and the body frame B . So, a rotation matrix relating both frames has to be calculated. For doing so a DCM is used, but first the basis vectors of the A and B frames need to be calculated.

The Orbit reference frame basis vectors $A = (\vec{a}_1, \vec{a}_2, \vec{a}_3)$ are calculated using the orbit propagation information. Introducing data of Figure 4.4 into equations (2.16), (2.17) and (2.18) basis vectors of the orbit reference frame are defined for the entire time interval.

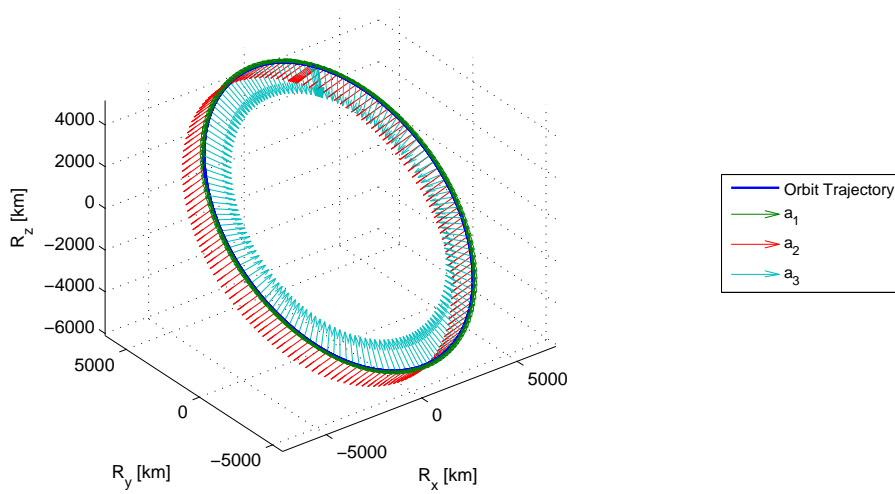


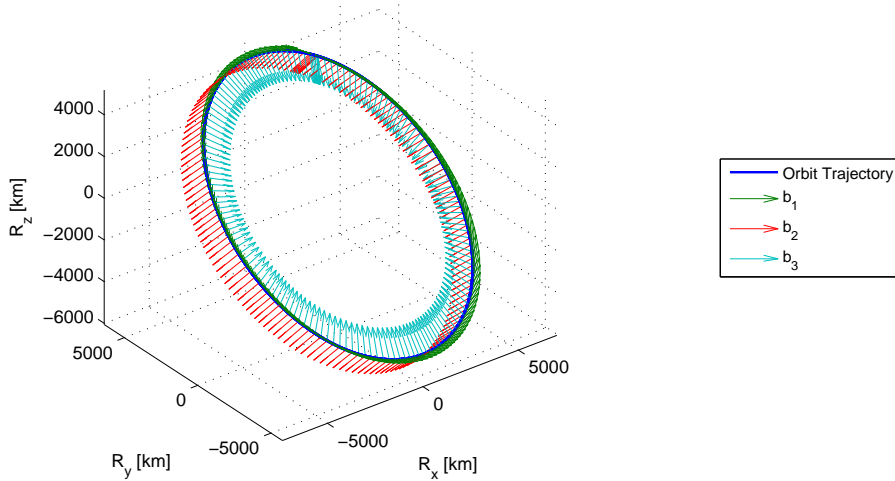
Figure 4.9: A frame along one orbit.

Figure 4.9 shows the A basis vectors over the first orbit. Green arrows represent \vec{a}_1 , red arrows \vec{a}_2 and blue arrows \vec{a}_3 .

A different path has to be used for getting the body reference frame basis vectors. A rotation to the B reference frame from the ECI N reference frame has to be made. For doing so the quaternion differential equations solution is used. Figure 4.7 delivers quaternion values for each time, i.e.

$$t_i \rightarrow q_i = (q_{1,i}, q_{2,i}, q_{3,i}, q_{4,i})$$

Inserting quaternion values into equation (2.35) the rotation matrix $R^{B/N}$ is defined. Finally rotation from N to B can be done. The N basis vectors were introduced in section 2.2 as $\vec{n}_1 = (1, 0, 0)$, $\vec{n}_2 = (0, 1, 0)$ and $\vec{n}_3 = (0, 0, 1)$. Figure 4.10 shows basis vectors of the body reference frame along the orbit for the same simulation as in Figures 4.6 and 4.7. Green arrows represent the roll axis (\vec{b}_1), red arrows the pitch axis (\vec{b}_2) and blue arrows the yaw axis (\vec{b}_3).

Figure 4.10: B frame along one orbit.

4.4.2 Attitude Visualization

After the calculation of the basis vectors of both reference frames a DCM matrix $R^{A/B}$ can be created. Euler angles can be extracted from a rotation matrix using equations (2.50),(2.51) and (2.52). Doing this operation for the entire time interval a clear picture of the attitude is generated.

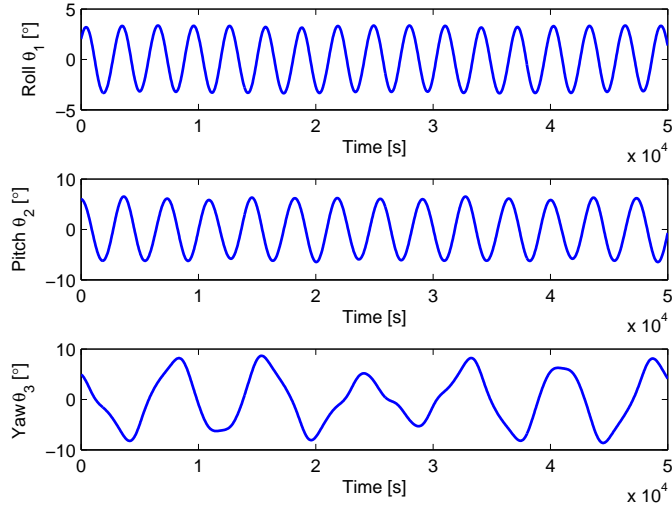


Figure 4.11: Attitude response.

Figure 4.11 shows the attitude representation, which is the angle deviation between the orbit and body reference frames. However, some clarifications need to be made. Euler angles are a clear way to represent attitude, but there are non-commutative. Therefore, for large angle rotations, the attitude representation vary with the Euler angle sequence. Nevertheless, for infinitesimal rotations, the chosen sequence is not important and differences in representation are neglected. On the other hand, very large rotations (90°) produce discontinuities in angle motion, which is difficult to analyze.

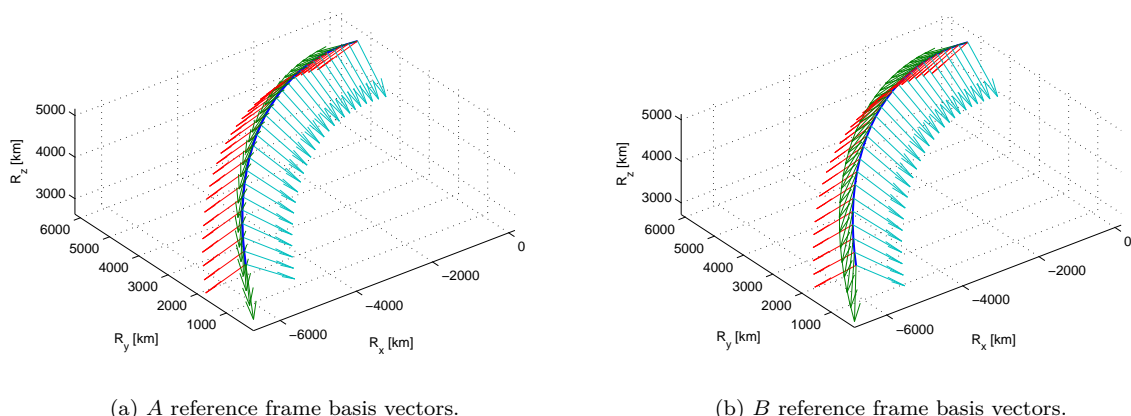


Figure 4.12: A and B reference frames.

For a better understanding of the attitude visualization Figures 4.12a and 4.12b are displayed. Figure 4.12 shows the orbit and body reference frames from $t = 6500$ s to $t = 7500$ s. Figure 4.13 is the attitude

representation in the same period of time.

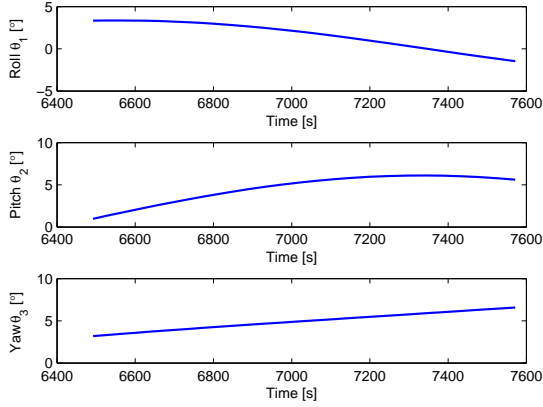


Figure 4.13: Attitude response.

To understand the attitude, several aspects have to be taken into account. The rotation sequence goes from A to B . It means from Figure 4.12a to 4.12b. The rotation sequence is 132, therefore first rotation is around axis \vec{a}_2 , second rotation around axis \vec{a}'_3 and the last rotation around \vec{a}'_1 . A positive rotation is counterclockwise.

Additionally, the torques profiles, aerodynamic forces, position vector and magnetic field data can be generated in this package.

Chapter 5

Circular Orbit and Gravity Gradient

After defining the simulator and the way to interpret the attitude, it is time to collect results and analyze them. The following method is used for the analysis of results. First simulation are run for the most ideal case, which is a circular orbit with only gravity gradient torque. After that, disturbances are added separately to the simulations and compared with respect to the circular orbit results. Finally some realistic simulations with all disturbances incorporated are performed and analyzed.

The most ideal case for starting analysis is a circular orbit with only gravity gradient torque. Furthermore the understanding of the gravity gradient torque regardless other environmental effect is of interest for SWIM stabilization. However, before starting, a mass model of the spacecraft has to be established.

5.1 Mass Model of SWIM

The satellite's model for a circular orbit with only gravity gradient torque, requires only mass distribution information. Table 5.1 shows the parameters used to model SWIM. It is assumed that the boom is deployed in the geometric center of the hub. These parameters have been decided after running multiple simulations, showing to be a good approximation for SWIM CubeSat and delivering results that help to analyze the different disturbances at the same time.

Mass properties		
Mass of hub M	=	3.5 kg
Density per length boom ρ_b	=	0.08342 kg/m
Mass of tip m_t	=	100 g
Length of boom L	=	0.9 m
Total mass of the spacecraft M_t	=	3.6834 kg
J_1	=	0.1029 kgm ²
J_2	=	0.1263 kgm ²
J_3	=	0.0292 kgm ²
$\vec{R}_{c.m.}$	=	(0,0,0.037) m
Linear pitch period T_{lin}	=	4.383×10^3 s

Table 5.1: Mass Properties of SWIM model.

The value of ρ_b is taken from a boom with similar characteristics from reference [21]. The moments of inertia of Table 5.1 satisfies stability criteria of region 1. Hence, the CubeSat has a stable configuration.

$$0.1263 > 0.1029 > 0.0292 \quad \text{and} \quad 0.1263 < 0.1029 + 0.0292 = 0.1321$$

5.2 Circular Orbit

The two body problem can be avoided, if only gravity gradient torque is affecting the spacecraft in a circular orbit. This is because the orbit and body reference frames can be related directly. Therefore

there is no need to calculate the basis vectors. Then, the circular orbit simulations are done by solving equations (2.76) and (2.72). That means that only 7 differential equations are solved, and therefore 7 initial conditions are required. For these simulations the initial quaternion defines rotation between the orbit and body reference frames. This simplification does not hold when aerodynamic or magnetic torques appear in the simulations, regardless of circular orbit. Nevertheless, some orbit parameters have to be defined. Table 5.2 defines the orbit parameters for the circular orbit simulations.

Orbit parameters	
Distance from Earth's surface h	= 600 km
Distance from Earth's center R	= 6978.1 km
Angular frequency n	= 1.1×10^{-3} rad/s
Orbital period T	= 5801.2 s

Table 5.2: Orbit parameters.

5.3 Pitch Propagation

The deviation about the pitch axis is of great interest. A stable nadir pointing spacecraft is expected to experience small deviation from the Nadir pointing equilibrium position. Focusing on the pitch behavior, the satellite is expected to move with a pendulum fashion with a period of 4.383×10^3 seconds. In order to verify this, several simulations are carried out with initial conditions summarized in Table 5.3. Simulations are run with linear and non-linear equations, to check the differences in the results between both theories.

$\vec{\omega}_0$ rad/s	Roll θ_1	Pitch θ_2	Yaw θ_3	q_0
(0, $-n$, 0)	0°	5°	0°	(0, 0.0436, 0, 0.9990)
(0, $-n$, 0)	0°	10°	0°	(0, 0.0872, 0, 0.9962)
(0, $-n$, 0)	0°	15°	0°	(0, 0.1305, 0, 0.9914)

Table 5.3: Initial conditions pitch propagation.

Table 5.3 delivers the initial deviation around the pitch axis from a Nadir pointing equilibrium configuration. The equilibrium configuration was defined in the linear stability analysis as the position in which the Earth is seen stationary from the body reference frame. In terms of initial condition it means $\vec{\omega}_{t=t_0} = (0, -n, 0)$ and $\vec{\theta}_{t=t_0} = (0^\circ, 0^\circ, 0^\circ)$.

Under initial conditions stated in Table 5.3, the roll and yaw deviations and angular velocity remain zero at all time i.e. $\omega_{1,3}(t) = 0$ and $\theta_{1,3}(t) = 0$. Therefore only the pitch angle motion θ_2 and angular velocity ω_2 are relevant.

Figure 5.1 shows that the pitch motion behaves like an undamped harmonic oscillator with amplitude equal to the initial deviation. Oscillations are around the equilibrium position, i.e. $\theta_2 = 0$. Time is normalized with respect to the orbital period. So keep in mind that one orbit is equal to 96 minutes. The amplitude of the angle propagation matches perfectly between the linear and non-linear equations, whereas there are small differences in the period. For the linear simulations, the period is equal to the linear period regardless of initial deviation. In the figure $T_{pitch}/T_{orbit} = 0.7558$. The period in non-linear equations becomes slightly larger for larger initial deviations. So there is a dependency with respect to the initial conditions. Therefore, agreement between the linear and non-linear equations decreases for growing initial deviation. As a consequence, it appears to be a phase shift between the linear and non-linear results. This effect is easy to see in the last orbits.

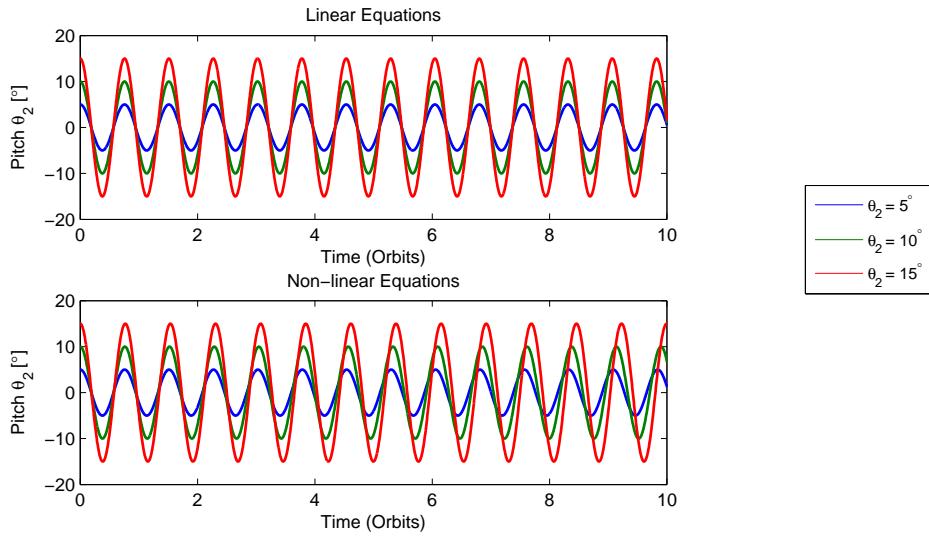


Figure 5.1: Pitch motion for different initial angles.

The angular velocity response, which is shown in Figure 5.2 has common features to the angle motion. It behaves as an undamped harmonic oscillator with respect to the equilibrium value $\omega_2 = -n$. The amplitude is proportional to the initial angle deviation. The period grows slightly with initial deviation for non-linear equations. Comparing Figures 5.1 and 5.2 it is noticed that maxima in one of the figures corresponds to the equilibrium position value in the other. This is because the gravity force is conservative, and therefore, there is an exchange of energy without dissipation between the angular velocity and angle motion. Therefore, there is no damping. In this energy exchange, the equilibrium position is the minimum energy configuration.

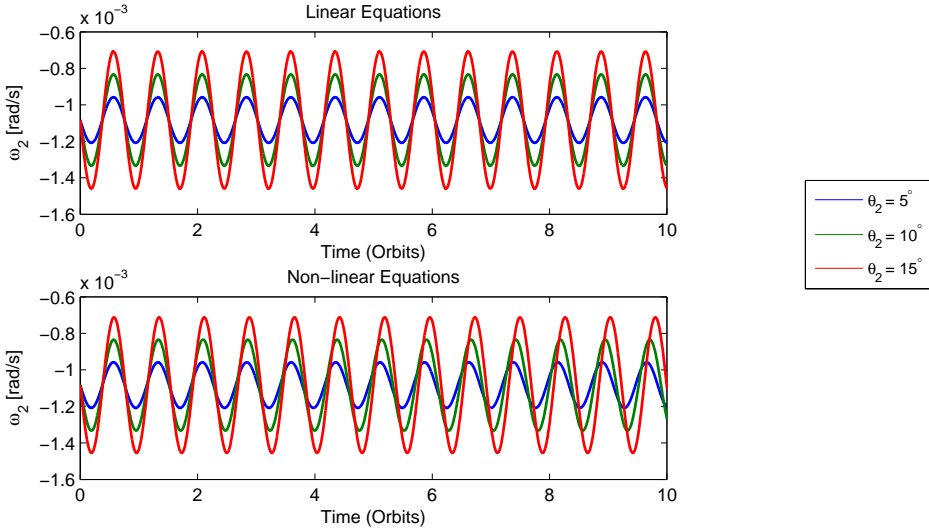


Figure 5.2: Angular velocity for different initial angles.

Figures 5.1 and 5.2 shows how initial deviations are propagated for the initial equilibrium angular velocity. However, how $\vec{\omega}_{t=t_0}$ affects the attitude have not been discussed yet. In doing so, some simulations with fixed initial angles in equilibrium i.e. $\theta_i = 0^\circ$ and different values of ω_2 have been done as displayed in Table 5.4.

$\vec{\omega}_0$ rad/s	Roll θ_1	Pitch θ_2	Yaw θ_3	q_0
(0, $-2.32n$, 0)	0°	0°	0°	(0, 0, 0, 1)
(0, $-2n$, 0)	0°	0°	0°	(0, 0, 0, 1)
(0, $-n$, 0)	0°	0°	0°	(0, 0, 0, 1)
(0, 0, 0)	0°	0°	0°	(0, 0, 0, 1)
(0, $0.32n$, 0)	0°	0°	0°	(0, 0, 0, 1)

Table 5.4: Initial conditions for different ω_2 .

Figure 5.3 shows the pitch motion. The third simulation starts at the equilibrium position i.e. $\omega_{2,t=t_0} = -n$. For the other simulations the pitch angle grows until get certain amplitude and propagates as an oscillator. The amplitude and period become larger with bigger difference with respect to the equilibrium angular velocity. Since small changes in the initial angular velocity produce big changes in the angular response, linear theory has not been applied. Finally, there is phase change of π radians between simulations with same difference with respect to the equilibrium velocity, i.e. between $\omega_{2,t=t_0} = -2n$ and $\omega_{2,t=t_0} = 0$.

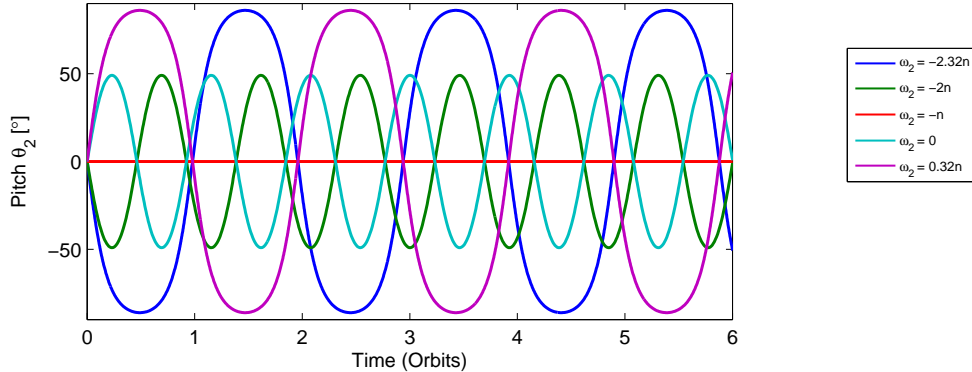
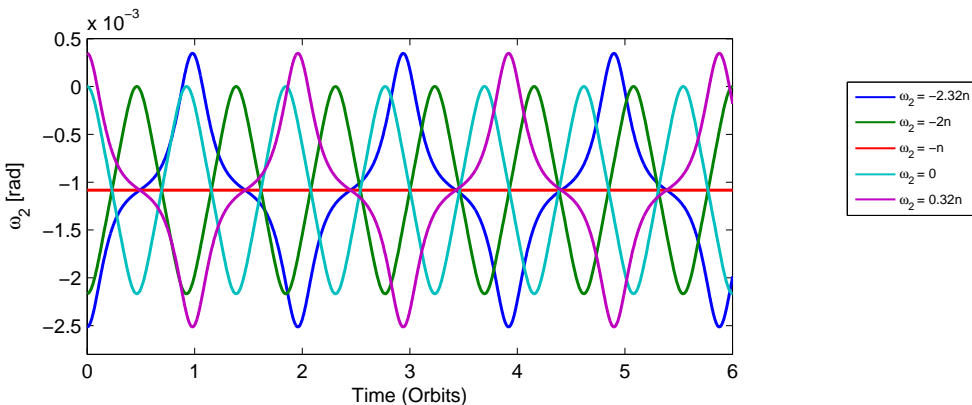
Figure 5.3: Pitch motion for different $\omega_{2,t=t_0}$.

Figure 5.4 shows the angular velocity response. As it was shown in Figure 5.1 there is a propagation of initial conditions around the equilibrium angular velocity. In this case the amplitude is equal to the deviation from the equilibrium velocity. The periods are different proportionally to the amplitude. Comparing figures 5.3 and 5.4 the energy exchange mechanism is recognized again. Therefore a pendulum motion holds. It is important to realize that for the biggest deviation in $\omega_{2,t=t_0}$, the shape of the angular velocity propagation changes. This is due to non-linearity of equations.

Figure 5.4: Angular velocity for different $\omega_{2,t=t_0}$.

Comparing simulations with $\omega_{2,t=t_0}$ and $\theta_{2,t=t_0}$ fixed, it is seen that the pitch motion is more sensitive to a change in the angular velocity than angle deviation.

In figures 5.3 and 5.4 $\omega_{2,t=t_0} = -2.32n$ and $0.32n$ are lower and upper bounds for a stable motion. As discussed in the stability analysis section, larger deviations than 90° change the equilibrium position. This leads to discontinuities in the angle motion representation due to the trigonometric nature of the Euler angles. In order to show this effect a last simulation has been run with $\theta_{2,t=t_0} = 0$ and $\omega_{2,t=t_0} = 0.25n$ which is depicted in Figure 5.5.

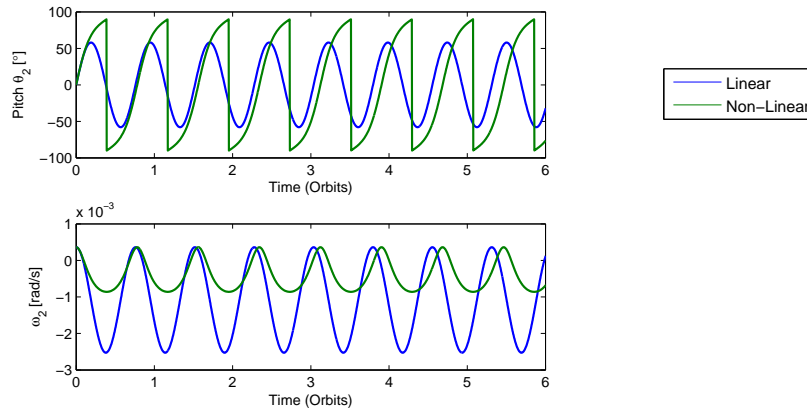


Figure 5.5: Discontinuous pitch motion $\omega_{2,t=t_0} = 0.25n$ and $\theta_{2,t=t_0} = 0^\circ$.

Figure 5.5 is a representation of an unstable motion, although the satellite's mass distribution is stable. Additionally, the linear simulation also appears. It is demonstrated that linear theory makes erroneous results for large angle deviation. The attitude propagation is shown again to be a periodic motion regardless of instability. However, in this case ω_2 never reaches its equilibrium value. Therefore, there is no harmonic oscillation around the equilibrium.

Special care must be taken when Figure 5.5 is analyzed. Every discontinuity has to be seen as a change in the equilibrium position. Moreover, the spacecraft motion is a continuous change from Zenith to Nadir pointing and the other way around. For a better understanding of the rotation mechanism Figure 5.6 is displayed.

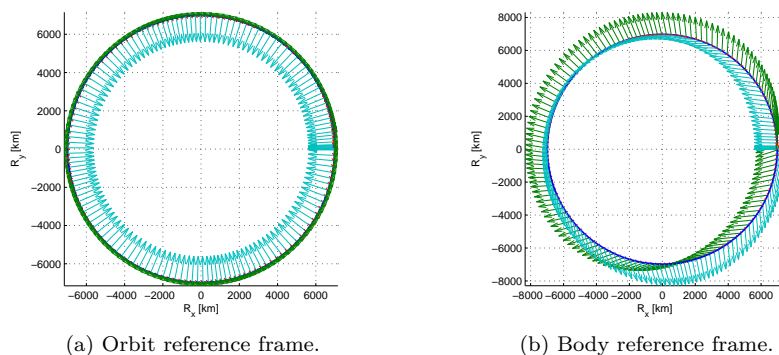


Figure 5.6: Basis vectors A and B reference frames.

Figure 5.6 shows the basis vectors for first orbit in the A and B reference frames for the simulation represented in Figure 5.5. First to notice is that for this figure, the 13 ODE's have been solved. Then,

the spacecraft trajectory is a circular, equatorial orbit starting at $\vec{r}_0 = (6978, 0, 0)$ km with velocity $\vec{v}_0 = (0, 7.56, 0)$ km/s. Like in Chapter 4, the green arrows represent the first axis, the red arrows the second axis and the blue arrows the third axis. The spacecraft starts aligned with the orbit frame but rotating in opposite direction comparing to the orbit reference frame. The pitch motion is defined as a rotation around the third axis (which is perpendicular to the equatorial plane in this particular simulation).

When the simulation begins, the spacecraft rapidly rotates getting positive deviation. Although the rotation to B from A looks clockwise, the third axis is pointing to the plane, and therefore, the rotation is counterclockwise. Once this happens the gravity gradient torques try to restore the position, but the angular velocity has bigger influence than gravity gradient torques, resulting in a larger deviation. Moreover, Figure 5.5 shows how the angular velocity never reaches the equilibrium value ($\omega_2 = -n$). Hence, the deviation is increasing until it reaches 90° . At this point Figure 5.5 shows a discontinuity and delivers -90° which is not correct. By looking at Figure 5.6b it is seen that the attitude is driven by the angular velocity rather than the gravity gradient.

This can be solved by deploying a longer boom. However, for the case of high deviation from equilibrium in the angular velocity there is a limit of boom length, were deploying a larger boom does not solve the problem. It happens the same as with the linear pitch period in Figure 3.5.

5.3.1 Pitch Propagation Conclusions

After analyzing the pitch propagation results, the most important conclusions can be summarized:

- A satellite under gravity gradient torque in a circular orbit behaves like a pendulum for the pitch motion. It propagates the initial conditions periodically, i.e. $\theta_{2,t=t_0}$ and $\omega_{2,t=t_0}$. The gravity gradient is conservative, and therefore there is an energy exchange with no damping of the angle motion.
- For small angles, the linear theory approximation matches accurately with the nonlinear equations.
- Small changes in the initial deviation $\theta_{2,t=t_0}$, produce small changes in the attitude propagation. Initial deviation has a small effect in the period of the propagation.
- Small changes in initial angular velocity $\omega_{2,t=t_0}$, produce large changes in the angle motion and period of the propagation.
- Deploying a longer boom reduces period propagation until certain limit. After this limit is reached, longer booms only changes mass properties of the satellite instead of its motion
- Severe restrictions have to be made for $\omega_{2,t=t_0}$ to have a stable motion. Only a small interval of values close to the angular frequency of the orbit gives a passive stable motion.

5.4 Roll and Yaw Propagation

When analyzing motion about the roll and yaw axes, all Euler angles (θ_i) and angular velocities (ω_i) have to be taken into account. This is due to coupling between the roll and yaw equations of motion. Same pattern as it has been used for the pitch propagation is followed for analyzing how initial conditions in the roll and yaw axes affect the attitude of the spacecraft.

First simulations are performed for fixed initial angular velocity and different angle deviations about the roll and yaw axes. After initial angle deviation is fixed, in order to understand how the angular velocity affects the spacecraft motion.

Simulations start with intial angle deviation about the the roll axis angle and the equilibrium angular velocity. Values are displayed in Table 5.5.

$\bar{\omega}_0$ rad/s	Roll θ_1	Pitch θ_2	Yaw θ_3	q_0
(0, $-n$, 0)	5°	0°	0°	(0.0436, 0, 0, 0.9990)
(0, $-n$, 0)	10°	0°	0°	(0.0872, 0, 0, 0.9962)
(0, $-n$, 0)	15°	0°	0°	(0.1305, 0, 0, 0.9914)

Table 5.5: Initial conditions for different roll angles.

For these simulations the linear and non-linear results have been divided into several figures. The reason is that for many inputs figures get difficult to understand.

Figures 5.7 and 5.8 show the angular response for the linear and non-linear equations respectively. Looking at the linear simulation with initial deviations about the roll axis, similat motion as with initial deviations around the pitch axis is found, but with a higher frequency. The yaw response does not look as an harmonic oscillator. The reason is is found in the coupling between the roll and yaw equationns of motion. The angular velocity response (Figure 5.7) magnitude is larger about the roll axis than the yaw. Therefore the yaw response is more influenced by the roll response than the other way around, and the harmonic oscillator behavior disappears. The angle motion in the yaw axis shows the largest period of all the angle responses. For both the roll and yaw linear simulations period is not a function of the initial deviations. Finally decoupling of pitch motion is observed.

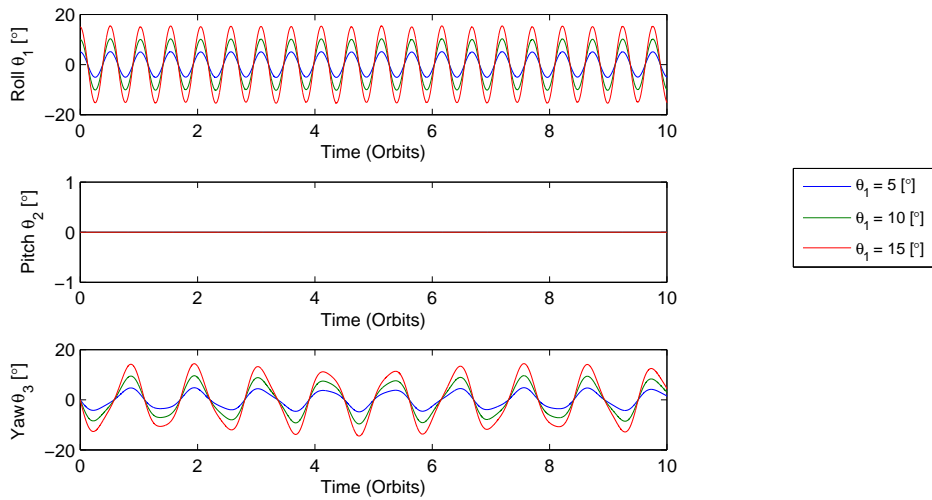


Figure 5.7: Euler angles and linear theory for different $\theta_{1,t=t_0}$.

The non-linear simulations differ much from linear than in the pitch motion case. For small initial

deviations ($\theta_1 < 10^\circ$) agreement between linear and non-linear responses is fairly good. For larger initial angles, non-linear effects start to appear after the second orbit. Then the period in the roll and yaw axis responses becomes larger. The amplitude increases considerably in the yaw axis, whereas in the roll axis it does not go beyond linear values. Moreover, for some orbit there is a slight drop in the angle amplitude. Significant angle deviations appear about the pitch axis. When non-linearity appears, the pitch shows a periodic behavior with $T_{pitch}/T_{orbit} \approx 0.78$, which is close to the linear period. However, now the spacecraft moves in a coning motion rather than a pendulum.

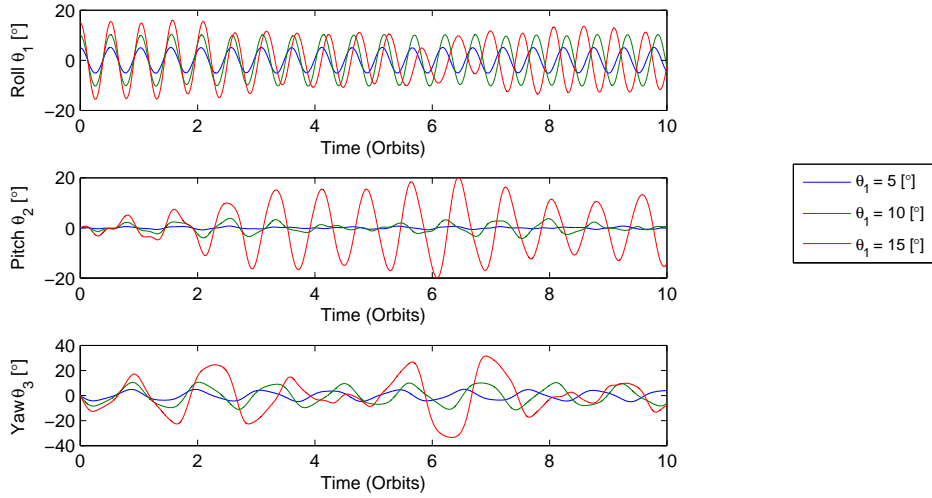


Figure 5.8: Euler angles for different $\theta_{1,t=t_0}$.

Figures 5.9 and 5.10 represent the linear and non-linear angular velocity response. Similar behavior as for the angle motion is found. Linear results show strong coupling between the roll and yaw axis and periodic response in time. An interesting fact is that now values of ω_1 sometimes exceed the linear values, which does not happen for the angular propagation. The amplitude in the roll axis response is twice the yaw axis one. Hence, the angular velocity about the roll axis has more impact about the yaw axis.

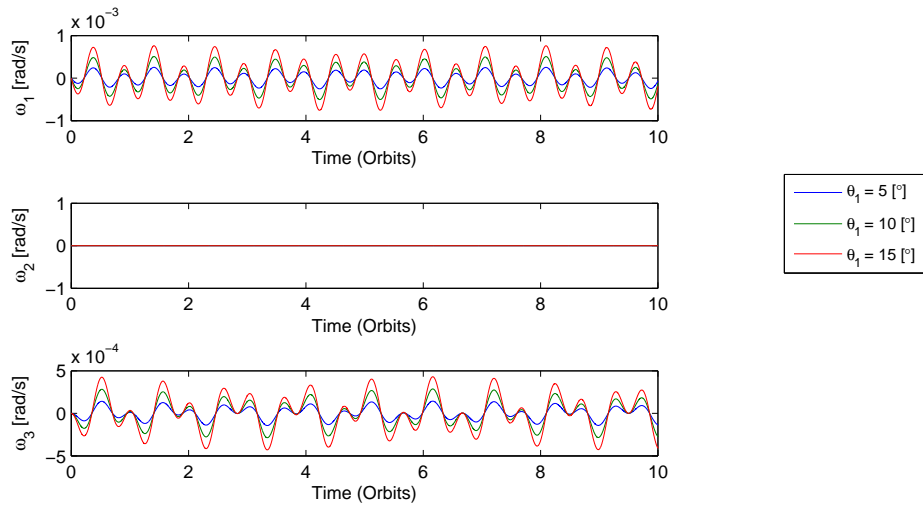


Figure 5.9: Angular velocity ω_i for different $\theta_{1,t=t_0}$.

Non-linearity appears after the second orbit for $\theta_{1,t=t_0} > 10^\circ$. The main difference between the linear and non-linear results is the coupling with the pitch motion. Amplitudes and periods change in the same fashion as in the angle motion.

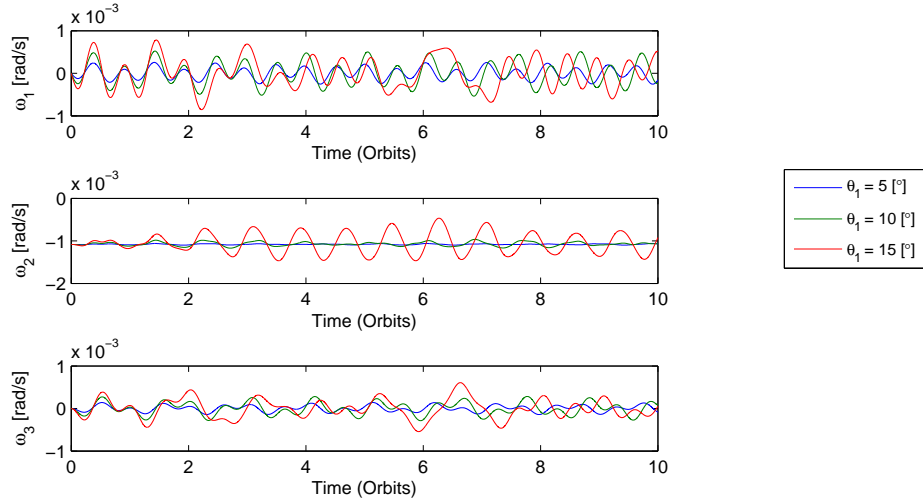


Figure 5.10: Angular velocity ω_i for different $\theta_{1,t=t_0}$.

The same exercise is done for initial deviations about the yaw axis. Table 5.6 shows initial conditions for the attitude propagation.

$\vec{\omega}_0$ rad/s	Roll θ_1	Pitch θ_2	Yaw θ_3	q_0
(0, $-n$, 0)	0°	0°	5°	(0, 0, 0.0436, 0.9990)
(0, $-n$, 0)	0°	0°	10°	(0, 0, 0.0872, 0.9962)
(0, $-n$, 0)	0°	0°	15°	(0, 0, 0.1305, 0.9914)

Table 5.6: Initial conditions for different yaw angles.

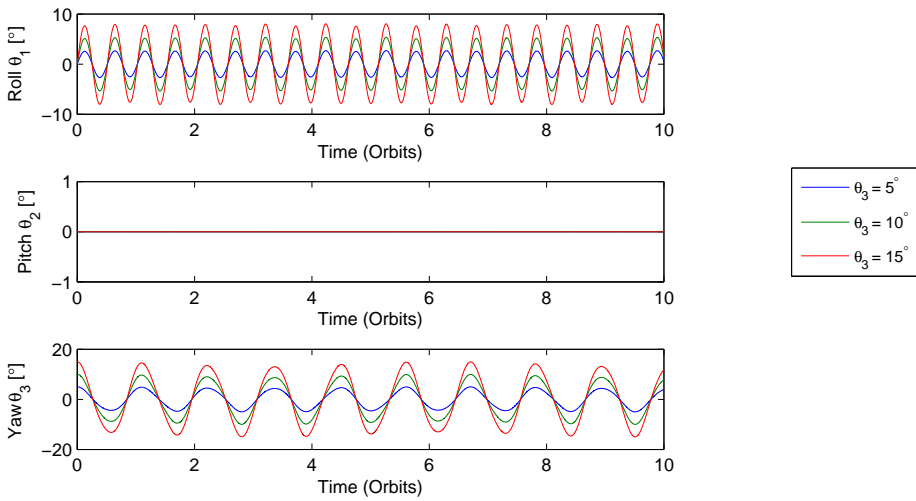


Figure 5.11: Linear equations angle motion, for different $\theta_{3,t=t_0}$.

Figure 5.11 depicts the angle motion according to the linear equations. Basically, there is an harmonic propagation in the roll axis with half the amplitude of the yaw initial conditions. In the yaw axis it is appreciated a smooth propagation of the initial deviations, which differs from an harmonic oscillator due to coupling between the roll and yaw equations of motion. The pitch motion is decoupled, and therefore, remains with zero value. Roll and yaw periods remain constant with growing initial amplitudes and similar to the ones with initial deviations about the roll axis.

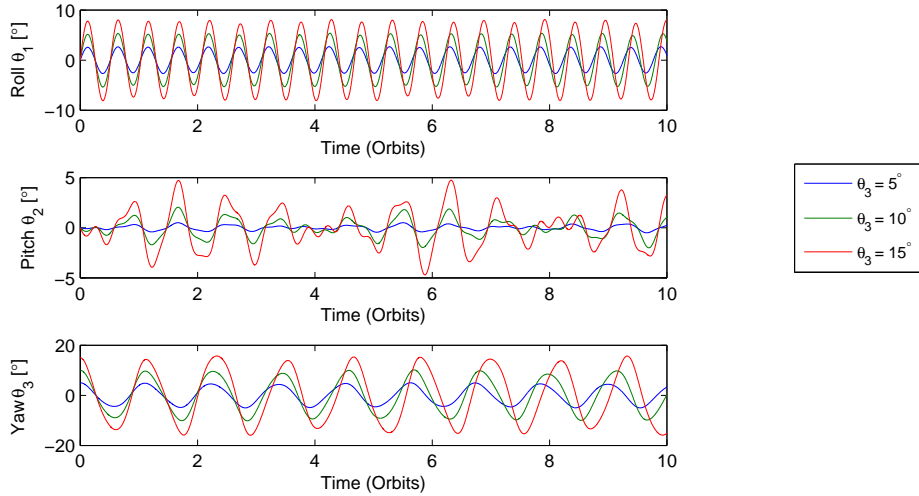


Figure 5.12: Euler angles θ_i , for different $\theta_{3,t=t_0}$.

Figure 5.12 shows the results of the non-linear simulations. Comparing with Figure 5.11 it is appreciate very good matching. In fact, compared to the simulations with initial conditions about the roll axis, there is a better agreement between the linear and non-linear solutions in this case. Differences in the amplitudes for the roll and yaw motion are negligible. Therefore, non-linearities have a low impact in the solution. The periods of motion become larger with larger initial deviations, which is a tendency shown for all non-linear simulations. Additionally, it is seen that the coupling between equations is smaller. Deviations about the pitch axis are small and irregular.

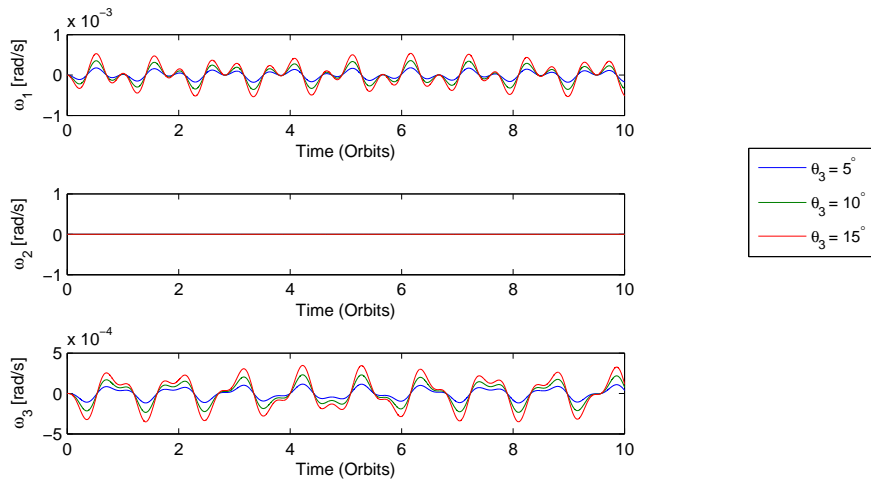


Figure 5.13: Linear equations angular velocity ω_i for different $\theta_{3,t=t_0}$.

Figures 5.13 and 5.14 show the linear and non-linear angular velocity responses. These figures have same features as the angle motion. At this point the trend of growing initial deviations is clearly defined.

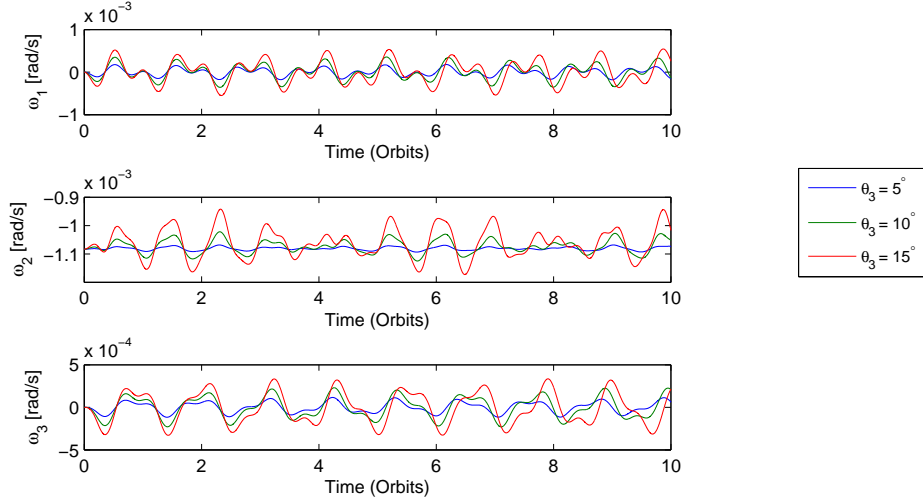


Figure 5.14: Angular velocity ω_i for different $\theta_{3,t=t_0}$.

It is concluded then, that agreement with the linear theory is better for simulations with initial deviations about the yaw axis than the roll axis. Therefore, non-linearity and coupling are more sensitive to initial conditions about the roll axis than the yaw.

5.4.1 Roll and Yaw Periods

According to the linear theory, the roll and yaw Euler's equations, (2.79) and (2.81) respectively, are coupled and a linear period cannot be calculated.

$$J_1 \ddot{\theta}_1 - n(J_1 - J_2 + J_3)\dot{\theta}_3 + 4n^2(J_2 - J_3)\theta_1 = 0$$

$$J_3 \ddot{\theta}_3 + n(J_1 - J_2 + J_3)\dot{\theta}_1 + n^2(J_2 - J_1)\theta_3 = 0$$

However, looking at the angular velocity of the linear response, Figures 5.9 and 5.13, it seems that the angular velocity magnitudes $\dot{\theta}_1$ and $\dot{\theta}_3$ are several orders of magnitude smaller than the roll and yaw angle deviations. In fact, values in equations are introduced in radians, so the angle motion amplitude reaches 0.2618 radians whereas the angular velocity is of the order of 0.001 radians/s. If the first derivatives are neglected in equations (2.79) and (2.81) similar expression as the linear pitch period can be calculated for the roll and yaw axis.

$$T_{Roll} \approx 2\pi \sqrt{\frac{J_1}{4n^2(J_2 - J_3)}} \quad (5.1)$$

$$T_{Yaw} \approx 2\pi \sqrt{\frac{J_3}{n^2(J_2 - J_1)}} \quad (5.2)$$

Equations (5.1) and (5.2) can be referred to as the quasi-linear periods. Inserting values from Table 5.1 into equations (5.1) and (5.2) it results that $T_{Roll} = 2985.2$ seconds and $T_{Yaw} = 6478.8$ seconds. Table 5.7 shows normalized periods for equations (5.1),(5.2), the solution of the linear equations, first orbits for the non-linear simulations with $\theta_{1,t=t_0} = 10^\circ$ and $\theta_{3,t=t_0} = 10^\circ$.

	Quasi-linear	Linear	$\theta_{1,t=t_0} = 10^\circ$	$\theta_{3,t=t_0} = 10^\circ$
$T_{\text{Roll}}/T_{\text{orbit}}$	0.5147	0.5145	0.522	0.5164
$T_{\text{Yaw}}/T_{\text{orbit}}$	1.1171	1.097	1.134	1.109

Table 5.7: Periods

Table 5.7 shows that period of the roll response according to equation (5.1) matches very accurately with the simulations, whereas the period of the yaw motion differs slightly more. This is due to the stronger influence of the roll axis to the yaw axis in the Euler's equations. Nevertheless, for a spacecraft with slow angular velocity like SWIM, this is a good approximation.

5.4.2 Angular Velocity

After initial deviations about axes have been analyzed, it is time to check the initial angular velocity. The same method as in the pitch motion is followed. Starting with no angular deviation, two simulations as displayed in Table 5.8 are run.

$\vec{\omega}_0$ rad/s	Roll θ_1	Pitch θ_2	Yaw θ_3	q_0
$(n/2, -n, 0)$	0°	0°	0°	$(0, 0, 0, 1)$
$(0, -n, n/2)$	0°	0°	0°	$(0, 0, 0, 1)$

Table 5.8: Initial conditions for different angular velocities.

The aim of these simulations is to analyze the attitude due to changes in the angular velocity components in the roll and yaw axes. Figure 5.15 shows the angle motion. First to be noticed is that the angle deviation is more affected in the axis where the angular velocity has been changed than in the other. In this sense, the same angular velocity has more effect in the yaw axis with amplitudes around 30° than in the roll with 15° amplitude. Both simulations produced similar deviations in the pitch axis, with the difference of few degrees larger deviation with initial conditions in the roll axis. Despite the fact that the initial angular velocity component in the yaw axis produces larger deviation ($\theta_{3,max} > 30^\circ$), a larger interval of velocities $[-n/1.1 \geq \omega_{3,t=t_0} \leq n/1.1]$ produce a stable motion compared with the roll axis $[-n/1.7 \geq \omega_{1,t=t_0} \leq n/1.7]$. With $\omega_{1,t=t_0} = \pm n/1.6$ the spacecraft becomes unstable after 14 orbits, due to large deviation in the yaw axis.

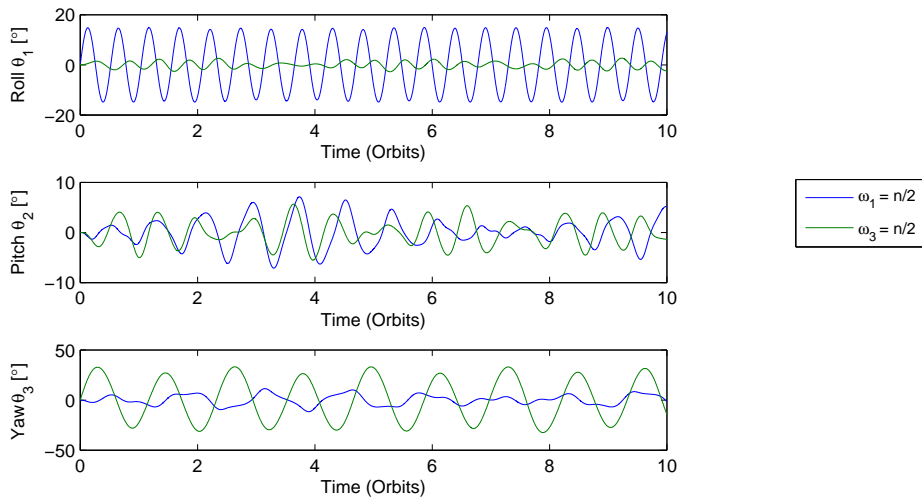
Figure 5.15: Euler angles θ_i for different $\omega_{i,t=t_0}$.

Figure 5.16 shows the angular velocity time response. What is noticed, is that initial conditions about

the roll axis produce responses with higher frequency than initial conditions in yaw. Comparing to initial angle deviations about the yaw axis, the amplitude doubles its values for $\omega_{3,t=t_0}$. However, looking at propagation with $\omega_{1,t=t_0}$, two different modes can be distinguished in the solution, so it has big coupling with the yaw motion. This coupling leads to smaller interval of stable motion.

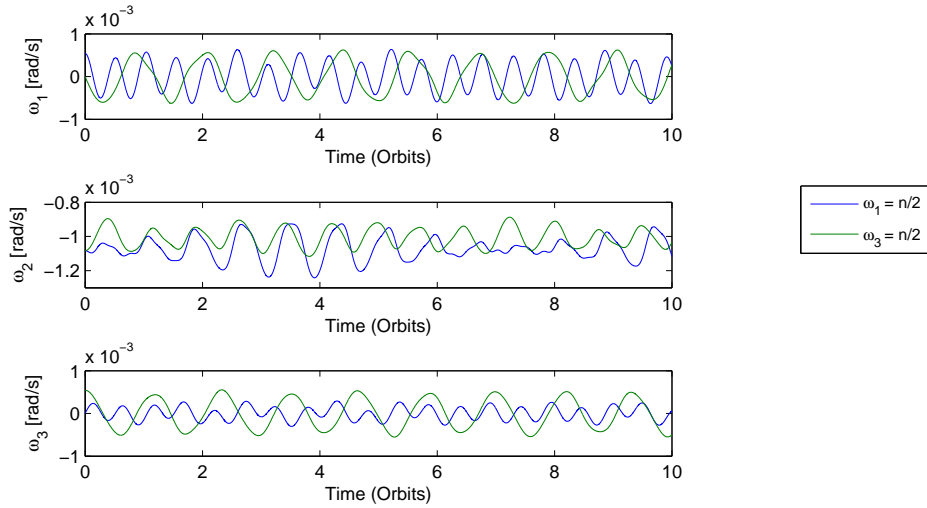


Figure 5.16: Angular velocity ω_i for different $\omega_{i,t=t_0}$.

5.4.3 Conclusions

Analyzing all figures, several conclusions are summarized:

- The motion about the yaw axis is more influenced by the motion about the roll, than the other way around.
- Angle motion is more sensitive to initial deviations about the roll axis than the yaw axis. Coupling and non-linearities appear faster for initial conditions about the roll axis, which lead to large deviation, specially in the yaw motion.
- Period of the pitch motion due to equation coupling, is similar to the linear period.
- Although linear equations in the roll and yaw axes are coupled, quasi-linear period can be calculated, that match for small angles.
- There is a bigger interval of values for the yaw axis than the roll, of the initial angular velocity that produce stable motion.

5.5 Boom Length

The circular orbit with gravity gradient torque analysis finishes with the study of the boom length. The idea is to know the maximum deviation of the Euler angles with respect to the boom length. To do so initial deviation is fixed and boom length is used as a free parameter. The boom length changes the mass distribution of the satellite, and therefore influences its dynamics.

Figure 5.17 shows the maximum deviation for initial conditions about the roll axis. Two values of $\theta_{1,t=t_0}$ have been used. The maximum deviation has been taken from simulations of 10^5 . So, the maximum deviation is calculated for more than the first 17 orbits.

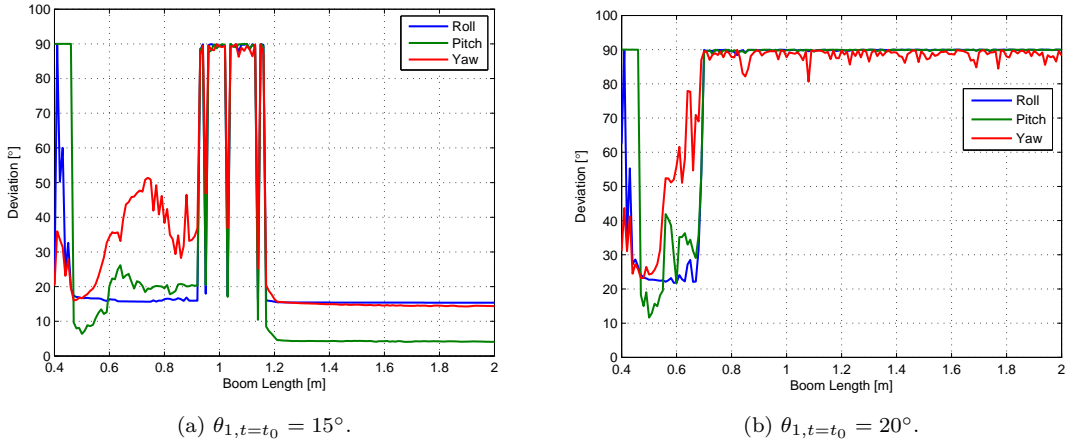


Figure 5.17: Maximum deviation for $\theta_{1,t=t_0}$ and different boom lengths.

Figure 5.17a has been done with $\theta_{1,t=t_0} = 15^\circ$ fixed. It can be divided into two areas, one with a boom smaller than 1.2 m and another with a boom larger than 1.2 m. For booms between 1 to 1.2 m the maximum deviations reaches 90° frequently. Therefore, that means that a combination between coupling and non-linearities produces high deviation for that range of mass distributions. For booms between 0.5 to 1 m, there are large deviations about the roll axis, but with a stable motion. For booms longer than 1.2 m motion is stable and the maximum deviations are equal to the initial deviations. Figure 5.17b has been done for $\theta_{1,t=t_0} = 20^\circ$ fixed. The motion is unstable for booms longer than 0.7 m. Hence, some damping is required for large initial deviations about the roll axis.

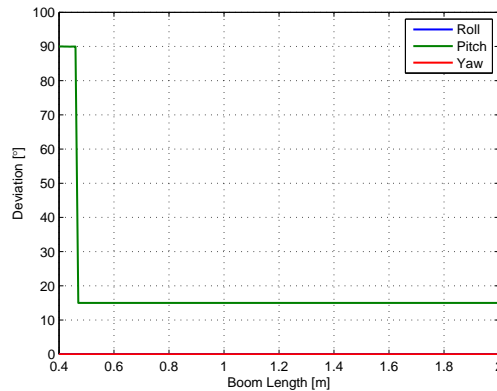


Figure 5.18: Maximum deviation for $\theta_{2,t=t_0} = 15^\circ$ and different boom lengths.

Figure 5.18 depicts maximum deviation for fixed initial deviation of 15° about the pitch axis. The gravity gradient torque produces very good pitch stabilization. Therefore, the propagation of initial conditions like an undamped harmonic oscillator starts for 0.5 m booms.

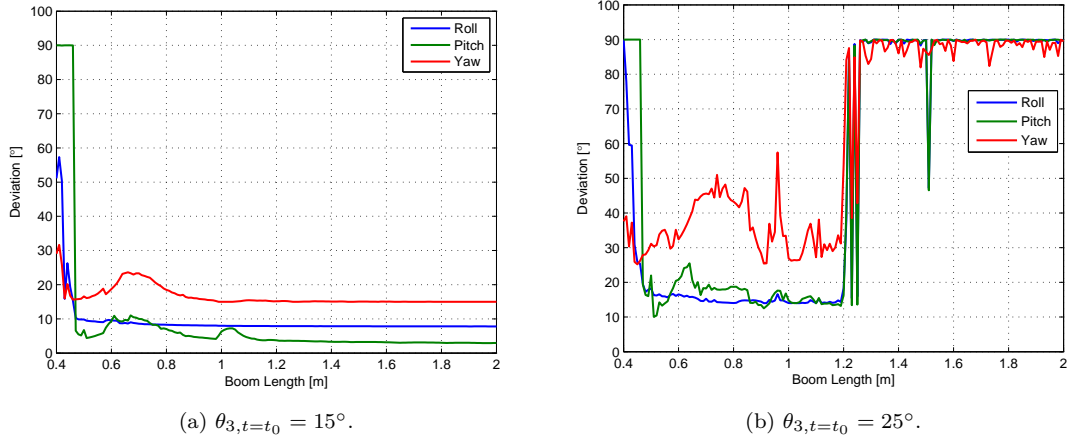


Figure 5.19: Maximum deviation for $\theta_{3,t=t_0}$ and different boom lengths.

Figure 5.19 shows maximum deviation for initial conditions about the yaw axis. For $\theta_{3,t=t_0} = 15^\circ$ the maximum deviations stabilize when the boom length reaches 1.2 m, being the lowest about the pitch axis, the intermediate about the roll and the largest about the yaw axis, which is equal to the initial deviation.

For initial deviations of $\theta_{3,t=t_0} = 25^\circ$, the maximum deviation behaves completely different. Once 1.2 m longitude is reached by the boom, unstable motion appears. For smaller booms, coupling and non-linearities occur, but the motion is stable. This time, the maximum deviation about the roll and pitch axis are similar and deviation about the yaw axis is the largest.

Finally some conclusions can be stated:

- Maximum deviation is more sensitive to initial roll angle than yaw and pitch.
- Large initial deviations for roll and yaw require damping systems to get stable motion.
- Severe, coupling and non-linearity of equations appear around 1 to 1.2 m long boom for initial conditions about the roll axis.
- For initial deviations below 10° , starting from 1.2 m boom length maximum deviations are equal to initial conditions.

Chapter 6

Non-Circular and Perturbed Orbits

The attitude propagation in a circular orbit has been studied. Now is time to check how orbit trajectory affects the attitude. To do so, some simulations for eccentric orbits are run and disturbances added separately. The sources of disturbance taken into account are the Earth's oblateness and atmospheric drag.

The eccentricity defines the orbit trajectory. It is a parameter which tells how elliptical an orbit is. The gravity gradient torques depend on the mass distribution and position. So, when the satellite gets further away from the Earth, the gravity attraction decreases. A range of different orbits with same perigee of 600 km are tested.

Oblateness of the Earth depends only on the position of the spacecraft. In this sense the inclination of the orbit is used as study parameter. A range of orbits from equatorial to polar are simulated.

The effect of the atmospheric drag is the orbit decay, which is a long term effect that depends mostly on the orbit altitude.

6.1 Eccentricity Effect

The Attitude propagation is expected to change once eccentricity is varied. First of all, the orbit reference frame A changes slightly from circular to elliptical orbits. In a circular orbit \vec{a}_1 goes always towards the velocity direction, i.e. position and velocity vector of the spacecraft are always perpendicular. This is not the case for an elliptic orbit, where the velocity vector is tangent to the trajectory making \vec{a}_1 to be different from the velocity direction.

Secondly, distance from the spacecraft to the Earth is not longer constant. That makes the orbit reference frame to rotate with no constant angular velocity, i.e. $\omega_2^{A/N} \neq \text{const}$. Therefore, even if the satellite starts rotating with the orbital frequency, is not longer possible to see the Earth stationary from the body reference frame. This fact makes \vec{a}_2 and \vec{b}_2 to rotate with different angular velocity, producing angle deviation between them.

Additionally, if the eccentricity makes the satellite to go far away from the Earth, the gravity gradient torque becomes smaller and eventually it is not able to restore the satellite to its equilibrium position.

Some simulations are run to analyze the eccentricity effects on the attitude of the spacecraft. The mass model is the same as for the circular orbit simulations, summarized in Table 5.1. This is done for a better comparison of the simulations. Equatorial orbits are selected for the simulations, with eccentricity as parameter. So the initial position is fixed for all simulations in the perigee of a 600 km altitude orbit i.e $h_{\text{perigee}} = 600$ km. Therefore, the right ascension of ascending node $\Omega = 0^\circ$, argument of perifocal point $\omega = 0^\circ$, true anomaly $\theta = 0^\circ$ and inclination $i = 0^\circ$, which gives the position vector $\vec{r} = (6978, 0, 0)$.

Table 6.1 summarizes the simulations for different eccentricities. Additionally, it gives the altitude of the apogee with respect to the Earth's surface, orbital period for the different orbits, initial velocity vector for orbit propagation in Cartesian coordinates \vec{v} and mean motion of the orbit, which is analogous to the orbital rate for a circular orbit.

Eccentricity	Apogee [km]	Orbital period [s]	\vec{v} [km/s]	Mean motion n [rad/s]
0	600	5801	(0, 7.557, 0)	1.10×10^{-3}
0.01	741	5889	(0, 7.595, 0)	1.10×10^{-3}
0.05	1335	6265	(0, 7.744, 0)	1.00×10^{-3}
0.08	1814	6573.9	(0, 7.8544, 0)	0.96×10^{-3}

Table 6.1: Initial conditions for eccentricity test.

Figure 6.1 shows the different orbits in a perifocal reference frame. As all orbits are equatorial ($i = 0^\circ$), the perifocal reference frame is equal to an xy Cartesian plane with origin located at the Earth's center. It can be seen how with growing eccentricity, the orbit trajectory becomes more elliptical. Also all orbits have the same perigee.

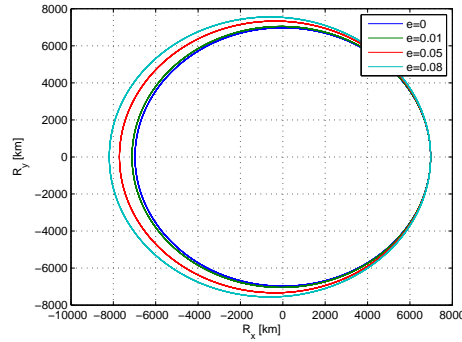
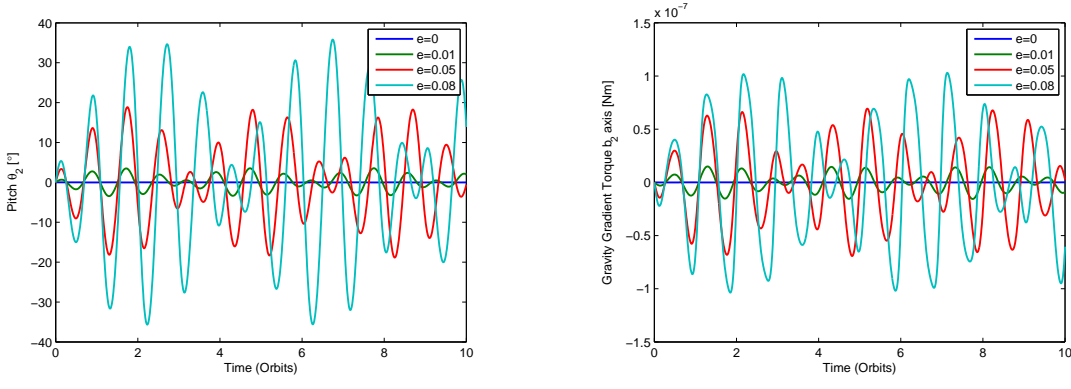


Figure 6.1: Orbit trajectories for different eccentricities.

Figure 6.2a shows the pitch motion and gravity gradient torque. Initially the orbit and body reference frames are aligned. Now the initial quaternion describes a rotation to B from N with value $q_0 = (-0.5, -0.5, 0.5, 0.5)$. The initial angular velocity is $\vec{\omega} = (0, -n, 0)$, where n is displayed in Table 6.1.



(a) Pitch deviation for different eccentricities.

(b) Gravity gradient torque for Different eccentricities.

Figure 6.2: Eccentricity effect on the attitude.

Figure 6.2a shows the angle deviation about the pitch axis. If the attitude motion starts with no deviation, only the pitch motion is affected by the eccentricity. It is important to realize that the orbital period is a function of the eccentricity. Therefore, the time axis has different value depending of the eccentricity. Angle deviation in the pitch axis increases with eccentricity. In fact, for this mass distribution an orbit of $e = 0.09$ produces unstable motion in the pitch axis. The periods and amplitudes are proportional to the eccentricity. The amplitude of deviations changes with time following a pattern of peaks. Nevertheless, a pendulum motion holds, but with variable amplitude.

Figure 6.2b shows the gravity gradient torque about the pitch axis \vec{b}_2 . The gravity torque looks like a mirror copy of the pitch deviation. This is because the gravity gradient torque is restoring and proportional to the angle deviation.

6.1.1 Eccentricity in the Attitude Motion

It has been seen that the eccentricity produces angle deviation about the pitch axis. The fact of bigger deviation about the pitch axis, spreads to the other two axes. For checking how the disturbance is spread, the same simulations as in Chapter 5 are run for an elliptic equatorial orbit with $e = 0.01$.

Low eccentricity has been selected due to mission requirements. SWIM is thought to be launch into a circular orbit. However, a perfect circular orbit does not exist. The orbit initial conditions are displayed in Table 6.1.

First simulations are for initial angles about the roll axis with the attitude initial conditions delivered by Table 6.2.

$\bar{\omega}_0$ rad/s	Roll θ_1	Pitch θ_2	Yaw θ_3	q_0
(0, $-n$, 0)	5°	0°	0°	(-0.4777, -0.4777, 0.5213, 0.5213)
(0, $-n$, 0)	10°	0°	0°	(-0.4545, -0.4545, 0.5417, 0.5417)
(0, $-n$, 0)	15°	0°	0°	(-0.4305, -0.4305, 0.5610, 0.5610)

Table 6.2: Initial conditions about the roll axis, for elliptical orbits.

Figure 6.3 depicts the angular response for different initial deviations about the roll axis.

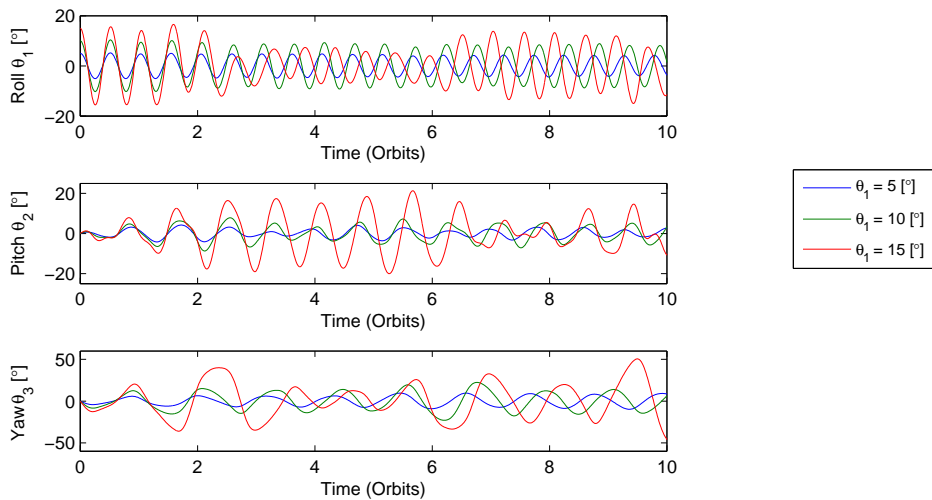


Figure 6.3: Angular response for different $\theta_{1,t=t_0}$ and $e=0.01$.

Figure 6.3 shows the attitude for an elliptic orbit with initial deviations about the roll axis . Figure 6.3

is compared with Figure 5.8 which delivers same simulations for a circular orbit. The elliptic orbit delivers larger deviations about the pitch axis for initial angles below 10° . That produces higher impact on the yaw amplitude of deviation than for the roll, which remains similar to a circular orbit. For $\theta_{1,t=t_0} = 15^\circ$, the amplitude in pitch is similar, but the elliptic orbit delivers more irregular shapes. There is not much difference in period for all initial Euler angles. This is due to a low eccentricity has been chosen.

The same exercise is repeated for initial pitch angles. Initial conditions for the attitude motion are described in Table 6.3.

$\bar{\omega}_0$ rad/s	Roll θ_1	Pitch θ_2	Yaw θ_3	q_0
(0, $-n$, 0)	0°	5°	0°	($-0.5213, -0.4777, 0.4777, 0.5213$)
(0, $-n$, 0)	0°	10°	0°	($-0.5417, -0.4545, 0.4545, 0.5417$)
(0, $-n$, 0)	0°	15°	0°	($-0.5610, -0.4305, 0.4305, 0.5610$)

Table 6.3: Initial conditions about the pitch axis, for elliptical orbits.

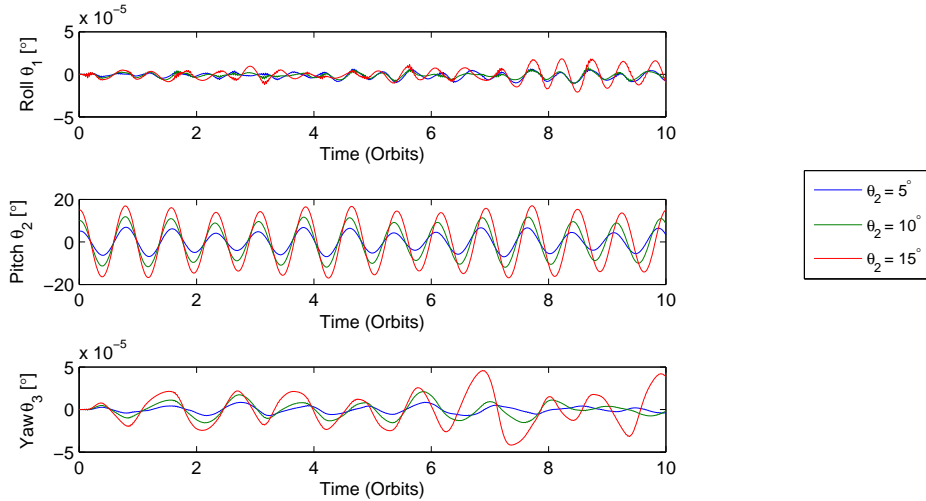


Figure 6.4: Angular response for different $\theta_{2,t=t_0}$ and $e=0.01$.

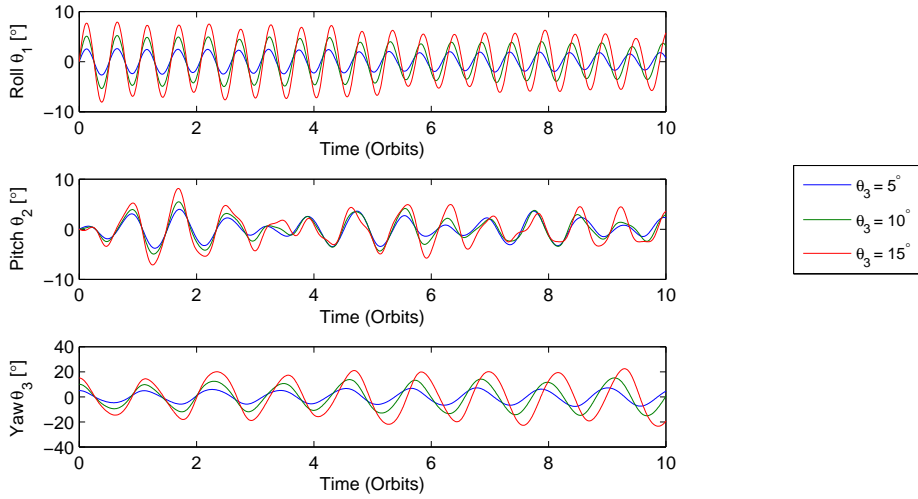
In the case of motion about the pitch axis, the difference that eccentricity creates is a slight variation in the amplitude deviation, whereas the period remain constant compare to the circular orbit simulation in Figure 5.1.

Finally yaw motion is tested. Initial conditions are depicted in Table 6.4.

Figure 6.5 shows elliptic orbit angle motion for initial yaw angle. Comparing to the circular orbit in Figure 5.12, there is a big difference in the pitch amplitude. An elliptic orbit produces twice the amplitude in pitch compare to a circular orbit. That produces changes in the roll motion, which its amplitude is not longer constant. Additionally, the angle amplitude about the yaw axis experiences a raise exceeding 20° at some points. There is no difference in period for all axes.

$\bar{\omega}_0$ rad/s	Roll θ_1	Pitch θ_2	Yaw θ_3	q_0
(0, $-n$, 0)	0°	0°	5°	($-0.5213, -0.4777, 0.5213, 0.4777$)
(0, $-n$, 0)	0°	0°	10°	($-0.5417, -0.4545, 0.5417, 0.4545$)
(0, $-n$, 0)	0°	0°	15°	($-0.5610, -0.4305, 0.5610, 0.4305$)

Table 6.4: Initial conditions about the yaw axis, for elliptical orbits.

Figure 6.5: Angular response for different $\theta_{3,t=t_0}$ $e=0.01$.

6.2 Perturbed Orbits

So far, only Keplerian orbits have been used to describe the spacecraft's trajectory. In order to improve the orbit model, some perturbing accelerations are added. Due to proximity to the Earth's surface only the Earth's mass distribution and atmospheric drag disturbances are modelled. How these disturbances affect the orbit is different.

The Earth's mass distribution or oblateness produces gyroscopic effects in the orbit motion [9]. The Earth bulges at the equator by around 20 km. Therefore, the effect of the oblateness depends strongly on orbit inclination. Orbit precession could lead to significant changes in the long term. For short time simulations, the oblateness effect on the satellite's attitude is not as important as the eccentricity, but necessary for an accurate model.

The major effect of the atmospheric drag for an orbit is its decay. This effect is almost negligible for short time simulations, specially over 400 km altitude with low eccentricity. Nevertheless, the orbit decay defines the satellite's life, especially for LEO spacecrafsts. However, accurate models require small perturbations.

In order to quantify the importance of these perturbations, the maximum norm of the acceleration vector of both disturbances is displayed in Table 6.5. The orbits selected are of 45° inclination with eccentricity of 0.01 and different altitudes of the perigee.

Altitude of Perigee [km]	Maximum \vec{a}_j [km/s ²]	Maximum \vec{a}_d [km/s ²]
800	2.313×10^{-4}	2.281×10^{-11}
700	2.496×10^{-4}	1.280×10^{-10}
600	2.656×10^{-4}	5.413×10^{-10}
500	2.836×10^{-4}	2.438×10^{-9}
400	3.065×10^{-4}	1.312×10^{-8}
300	3.266×10^{-4}	8.889×10^{-8}
200	3.535×10^{-4}	1.021×10^{-6}
150	3.684×10^{-4}	7.520×10^{-6}

Table 6.5: Perturbed accelerations at different altitudes.

Table 6.5 shows that the Earth oblateness is the predominant disturbance in the orbit propagation.

Acceleration due to Earth's oblateness (\vec{a}_j) increases gradually when the orbit gets closer to the Earth. Atmospheric drag acceleration increases sharply with decreasing distance from the Earth. This is due to large variations of the atmospheric density, which is modelled according to Figure 2.2.

Although the Earth's oblateness accelerations are bigger than atmospheric drag, there is an important fact that distinguish them. The atmospheric accelerations produce energy dissipation of the satellite, which is an accumulative process. Hence, this eventually makes more importance in the orbit propagation than the oblateness. This is relevant for altitudes below 400 km.

6.2.1 Earth's Gravity Field

It has been discussed that the Earth's mass distribution effect varies with inclination. Simulations for a 600 km circular orbit with different inclinations are run to study it. Table 6.6 shows the initial conditions for different inclinations and initial velocity vector for the orbit propagation. The spacecraft starts aligned with the orbit reference frame with $\vec{\omega} = (0, -n, 0)$.

inclination	Velocity \vec{v} km/s
0°	(0, 7.55, 0)
15°	(0, 7.30, 1.95)
30°	(0, 6.54, 3.78)
45°	(0, 5.34, 5.34)
60°	(0, 3.78, 6.54)
75°	(0, 1.95, 7.30)
90°	(0, 0, 7.55)

Table 6.6: Initial conditions Earth's oblateness test.

First variations in the orbit trajectory are displayed in Figure 6.6a. In this figure the altitude of the spacecraft with respect to the Earth is depicted.

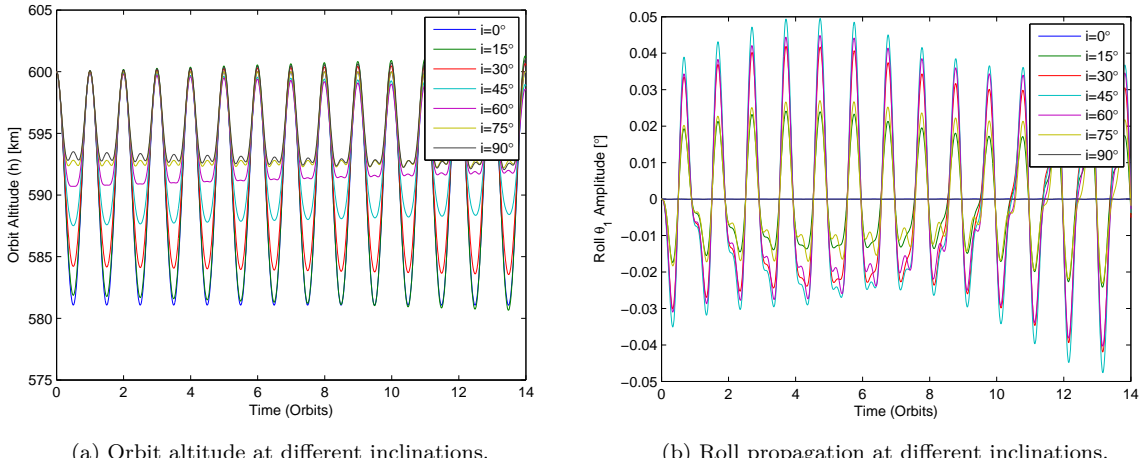


Figure 6.6: Earth oblateness effect on orbit altitude and roll axis.

A circular orbit in a model with homogeneous mass distribution of the Earth would be of constant altitude. As is shown in Figure 6.6a, the effect of the Earth's gravity field on the satellite trajectory is a slight variation of its distance with respect to Earth. The altitude variation happens periodically, once per orbit. Initially, the change in altitude is the lowest for polar orbit ($i = 90^\circ$), and increases gradually with lower inclination, with equatorial orbit ($i = 0^\circ$) having the largest change in altitude. In this sense, the oblateness of the Earth appears to have an effect similar to a small change in eccentricity. There is a change of amplitude with time for orbits that are not equatorial. The angle amplitude increases or

decreases depending on the inclination. For orbits with inclination higher than 45° , the altitude has a bulge at half of the orbit.

Figure 6.6b shows angle propagation about the roll axis for different inclinations. First to notice is that deviations are of very small amplitude. Therefore, if the satellite starts propagation with some angle deviation, the motion due to Earth's oblateness could be ignored. Nevertheless, it is important to realize that for equatorial and polar orbits, i.e. $i = 0^\circ$ and $i = 90^\circ$ the harmonics effect is almost non-existent. The maximum amplitude is for a 45° inclination orbit, decreasing the amplitude for orbits which go closer to the equatorial or polar. There is a periodic behavior in the motion.

Figure 6.7a shows pitch motion for different inclinations. The Earth's oblateness has a bigger impact on the pitch axis than the roll. Amplitudes could reach a quarter of angle $\theta = 0.25^\circ$. The biggest deviation is for an equatorial orbit, decreasing with inclination until get the lowest value in a polar orbit. Motion is again periodic.

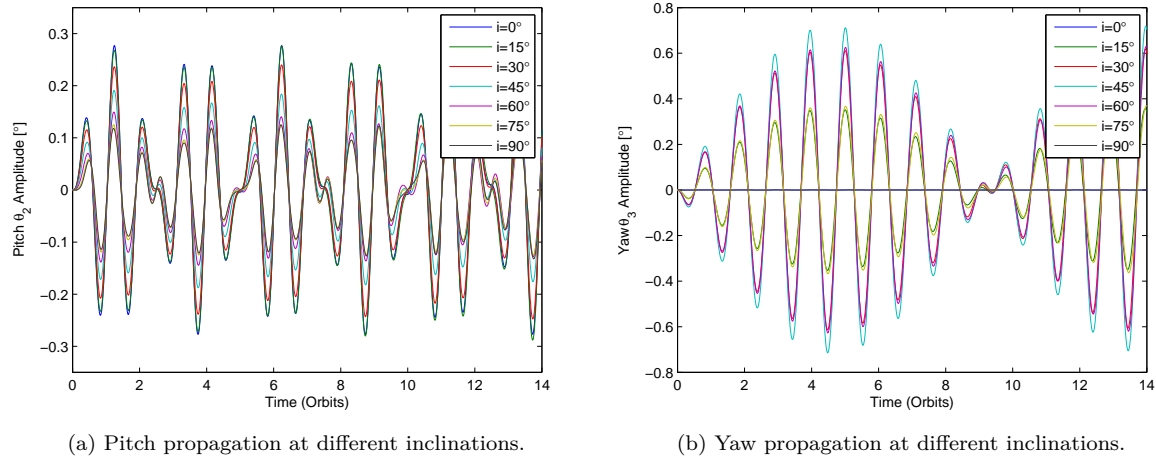


Figure 6.7: Earth oblateness effect on the pitch and yaw axes

Angle motion about the yaw axis is depicted in Figure 6.7b. The Earth's harmonics produce the largest deviations about this axis, reaching values close to 1° . Yaw motion is periodic and every 9 orbits same pattern is repeated. During that time yaw amplitude increases for the first half and decreases for the second. The largest amplitude is reached for a 45° orbit and lowest for polar and equatorial orbits. There is a gradual growth in amplitude from polar or equatorial to a 45° inclination orbit.

6.2.2 Atmospheric Drag

According to Table 6.6, the aerodynamic accelerations for a 600 km altitude orbit are six orders of magnitude smaller than the accelerations due to the Earth's gravity field. Therefore, the attitude for short simulations is not studied. However, the aerodynamic accelerations do affect the orbit trajectory. So, in order to verify their influence a long term simulation is run.

Figure 6.8 shows magnitude of the position vector (\vec{r}) with time. An equatorial orbit with perigee at 400 km and eccentricity $e=0.002$ is simulated. The initial position vector is $\vec{r} = (6778, 0, 0)$ km and the velocity vector $\vec{v} = (0, 7.676, 0)$ km/s. The attitude information is not important for this figure. The simulation last 10^7 seconds, which is equivalent to 115 days.

The orbit decay is observed in Figure 6.8. The position vector starts with 27 km amplitude and finishes with 17 km. This drop in amplitude means decrease in eccentricity. Additionally, the position vector norm values decrease throughout the entire simulation, which is the orbit decay.

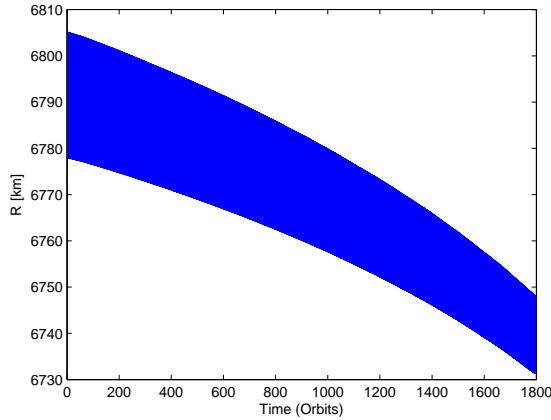


Figure 6.8: Orbit decay due to atmospheric drag.

6.3 Conclusions

The main conclusions for the attitude motion of SWIM due to orbit trajectory are summarized:

- Main source of change of the attitude motion due to orbit trajectory is the eccentricity.
- The Earth's gravity field is not a major source of disturbance. For polar orbit, the most significant disturbance is about the pitch axis.
- Alterations due to atmospheric drag could be ignored for a 600 km altitude orbit.

Chapter 7

Attitude Disturbances

The gravity gradient torques restore the satellite to its equilibrium position. The disturbance torques make the satellite to rotate in an uncontrolled fashion. In order to be stable, the satellite has to produce gravity torques that exceed disturbance torques. For a LEO spacecraft only the aerodynamic and magnetic torques are modeled. The influence of these disturbances are analyzed separately.

7.1 Aerodynamic Disturbances

The aerodynamic torque depends on the satellite's shape, position i.e. altitude with respect to the Earth, velocity and its attitude. More specifically, the angle deviation with respect to the velocity direction.

For the aerodynamic torque, the satellite's shape plays a major role. Hence, a more detailed characterization of the satellite's shape has to be formulated. In that sense the radius of boom and tip have to be added as detailed in Chapter 3. The aerodynamic characterization of the satellite is delivered in Table 7.1.

Mass properties	
Mass of hub M	= 3.5 kg
Density of the Boom ρ_b	= 0.08342 kg/m
Mass of tip m_t	= 100 g
Length of boom L	= 0.9 m
Total Mass M_T	= 3.6834 kg
J_1	= 0.1029 kgm ²
J_2	= 0.1263 kgm ²
J_3	= 0.0292 kgm ²
$\vec{R}_{c.m.}$	= (0,0,0.0337) m
Radius of the boom r_{boom}	= 0.0015 m
Radius of the boom r_{tip}	= 0.025 m

Table 7.1: Mass properties for aerodynamic test.

Before starting the attitude analysis, it is important to understand how the aerodynamic torque works. In order to do so, Figure 7.1 is displayed. Figure 7.1 depicts the aerodynamic forces and torques that would have been applied in a circular orbit simulation with initial $\theta_{3,t=t_0} = 15^\circ$, which is represented in Figure 5.12. In order to generate larger torques about the yaw axis, the boom has been moved slightly along the roll axis.

Figure 7.1a shows aerodynamic forces seen in the body reference frame B . The total aerodynamic force along an axis depends on the area that is exposed normal to the axis and its orientation with respect to the velocity vector of the spacecraft. Therefore, the most loaded axis is \vec{b}_1 , which represents the frontal surface of the spacecraft. If the spacecraft was aligned throughout a circular orbit, only forces along \vec{b}_1 would appear. Since this is not the case, forces along the other axes are generated. Comparing with Figure 5.12, the origin of forces can be determined. In fact, the force profile along \vec{b}_2 looks alike the angle

deviation about the yaw axis. In the same way, forces along \vec{b}_3 have the same pattern as the pitch axis motion. These forces are the source of the aerodynamic acceleration disturbances.

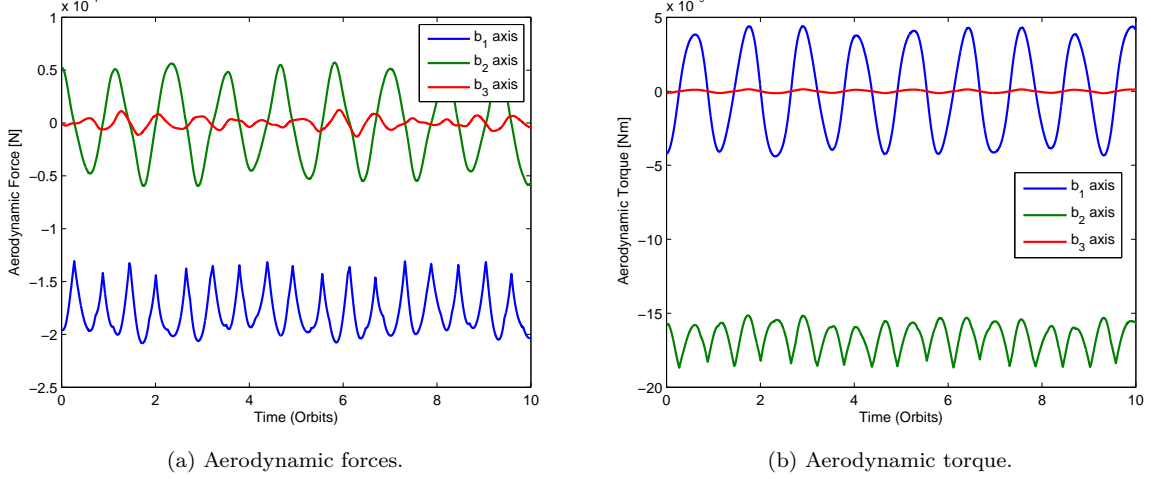


Figure 7.1: Aerodynamic force and torque profiles.

Figure 7.1b shows the aerodynamic torques seen from the body axes. Comparing to Figure 7.1a, it is noticed that the forces along \vec{b}_1 produce torques about the pitch axis, forces along \vec{b}_2 , torques about the roll axis and it is not clear where torques about the yaw axis come from. First thing to realize is that the boom and tip mass have the biggest influence in the aerodynamic torque generation. This is due to the distance from the center of pressure of the different elements to the center of gravity of the satellite. The hub surfaces are close to the center of gravity, and therefore, the distance from center of pressure to center of mass is small. On the other hand, the bottom of the boom is far from the center of mass of the spacecraft. That is why torques about the yaw axis are the lowest, because \vec{b}_3 is close to the boom and in the same direction, which does not generate large torques.

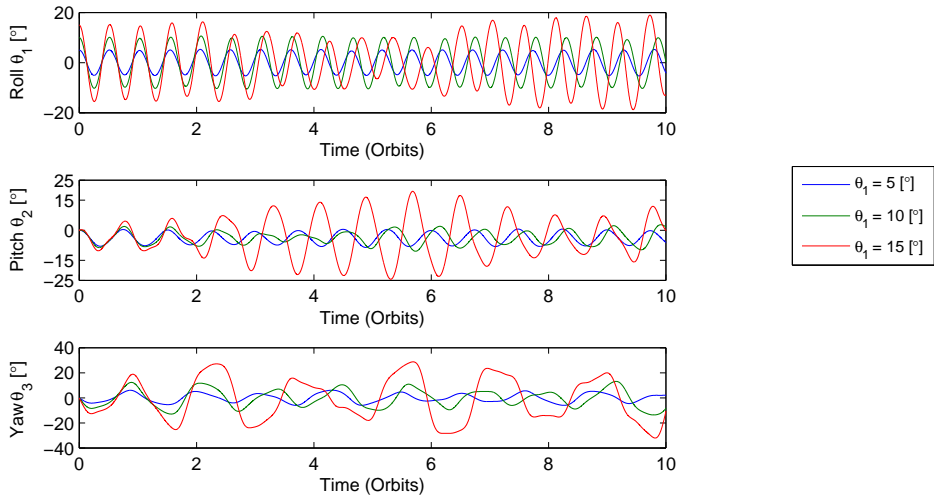


Figure 7.2: Attitude propagation with aerodynamic torque and increasing $\theta_{1,t=t_0}$.

To analyze the aerodynamic torque in the attitude motion, the same simulations as seen in Chapter

5 are run. So now, simulations are for a circular orbit with gravity gradient and aerodynamic torques.

The first simulation is for different initial angles $\theta_{1,t=t_0} = 5^\circ, 10^\circ, 15^\circ$ about the roll axis, and the equilibrium angular velocity. The attitude initial conditions are the same as in Table 6.2.

Figure 7.2 shows the angle response for initial deviations about the roll axis. For a better understanding of the aerodynamic torque effect on the angle response, it is convenient to compare Figure 7.2 with 6.3, in which the aerodynamic torque has not been applied.

The aerodynamic torque has larger magnitude about the roll and pitch axes. However, due to equation coupling, deviations spread about all axes. The main effect of the aerodynamic torque is the angle deviation about the pitch axis. The deviations with negative value about the pitch axis increase considerably. Angle deviation together with the initial deviation about the roll axis produce changes in all axes motion. These changes are small for $\theta_{1,t=t_0}$ is below 10° . In fact, the periods are very similar for all angle motions. For $\theta_{1,t=t_0} = 15^\circ$ differences are bigger. Apart from an increased of amplitude about the pitch axis, now deviations about the roll axis reaches values larger than the initial deviation. Also there is a growth of amplitude about the yaw axis, which could develop into unstable motion. In fact, for $\theta_{1,t=t_0} = 15^\circ$ there are large rotations about the yaw axis after 12 orbits, and the satellite starts rotating about this axis.

Figure 7.3 shows the angle response for different initial angles about the pitch axis with aerodynamic torque. The initial attitude conditions for the angle propagation are the same as shown in Table 6.3.

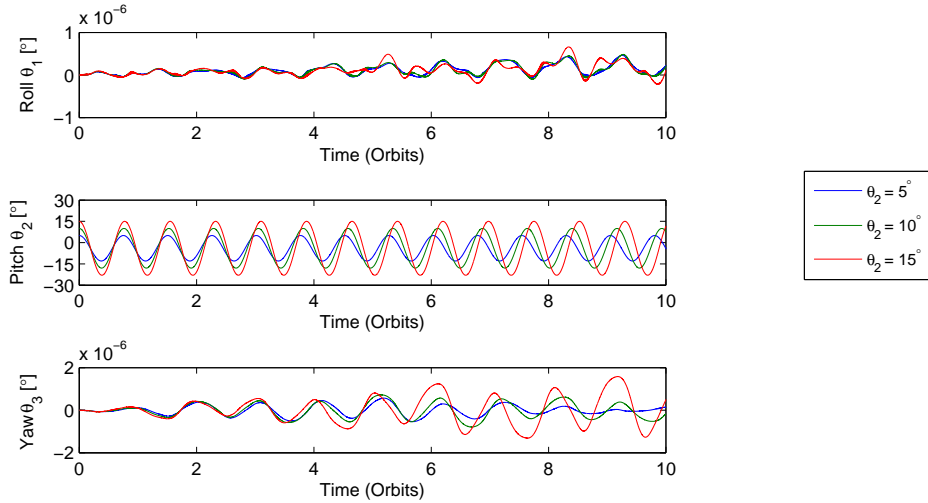


Figure 7.3: Attitude propagation with aerodynamic torque and increasing $\theta_{2,t=t_0}$.

Figure 7.2 is compared to Figure 5.3, which has same initial condition, but with no aerodynamic torque applied. First of all the roll and yaw axis can be neglected if initial conditions are deviation about the pitch axis. In this case initial deviations below 15° guarantee a stable motion of the spacecraft. The effect of the aerodynamic torque on the spacecraft motion is a slight increase in the angle motion amplitude for negative angles, whereas positive angles remain unchanged.

The pitch period is slightly larger compared with simulations with only gravity gradient torque. For example the normalized pitch period for $\theta_{2,t=t_0} = 15^\circ$ is $T_{pitch}/T_{orbit} = 0.7765$ compared to 0.7669 for only gravity gradient torque simulations.

Finally simulation for initial angles about the yaw axis is displayed in Figure 7.4. The initial attitude

conditions are shown in Table 6.4.

Figure 7.4 shows the angular response to initial deviation about the yaw axis. As previously Figure 7.4 is compared to Figure 6.5. Comparing with initial deviations about the roll and pitch axes, initial deviations about the yaw axis produce less aerodynamic effects. Matching in period between the angular response with and without aerodynamic torque is almost perfect for all initial deviation. Moreover, there are slight differences in amplitude for the roll and yaw motions. The main difference is about the pitch axis. Pitch motion amplitudes are larger when aerodynamic torques are added. These differences are around 3° to 5° in the peaks of the response. Again differences for negative angles are larger than for positive ones.

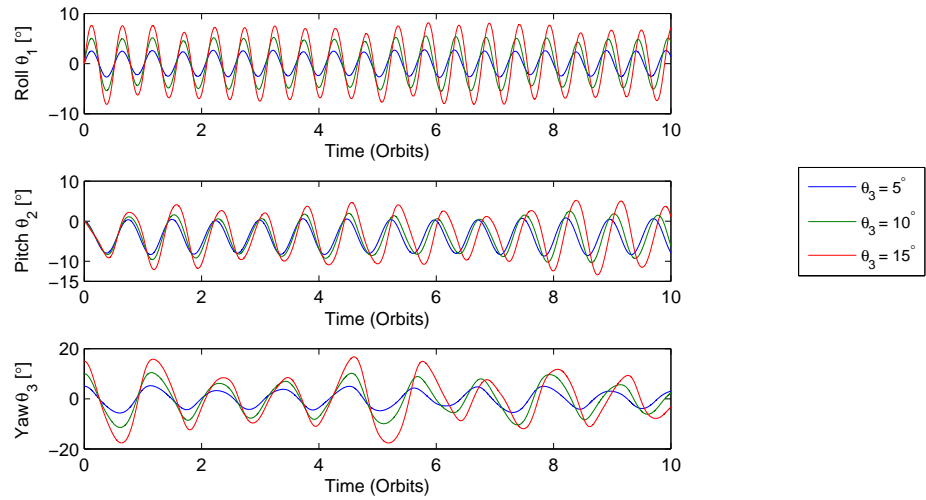
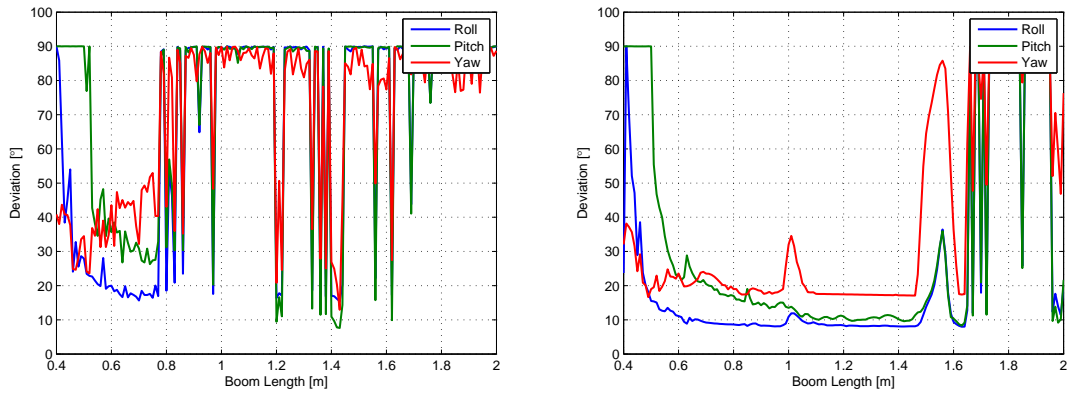


Figure 7.4: Attitude propagation with aerodynamic torque and increasing $\theta_{3,t=t_0}$.

7.1.1 Boom Length and Aerodynamic Torque

The same test regarding the boom length for gravity gradient torque is performed including the aerodynamic torque. Figure 7.5 shows the maximum angle deviation for fixed initial angles about the roll and yaw axes.



(a) $\theta_{1,t=t_0} = 15^\circ$, different boom length and aerotorque. (b) $\theta_{3,t=t_0} = 15^\circ$, different boom length and aerotorque.

Figure 7.5: Maximum deviation with aerodynamic torque with roll and yaw initial deviations.

Figure 7.5a depicts the maximum deviation for $\theta_{1,t=t_0} = 15^\circ$ versus boom length. It is not possible to see any length interval where the maximum deviations are constant. Therefore, the attitude motion is very sensitive to initial deviations about the roll axis. Between 0.6 to 0.8 meters of boom, the motion of the spacecraft is stable but deviations about the pitch and roll axes are rather large. After 0.8 meters, the motion is unstable apart from several points, which show the lowest maximum deviations. Such points are around 1.2, 1.4 and 1.6 meters of boom.

Figure 7.5b shows maximum deviation for $\theta_{3,t=t_0} = 15^\circ$ versus boom length. The motion is stable for booms below 1.6 meters, although around 1.5 there is a region of large deviations. There is a region where deviations are low and stable from 1.1 to 1.4 meters. Between 0.6 to 0.95 m there are small fluctuations with decent values of maximum deviations. For a 1 meter long boom there is a sudden peak in deviation. For all stable regions the maximum deviation about the yaw axis is the largest, followed by the pitch and roll axes.

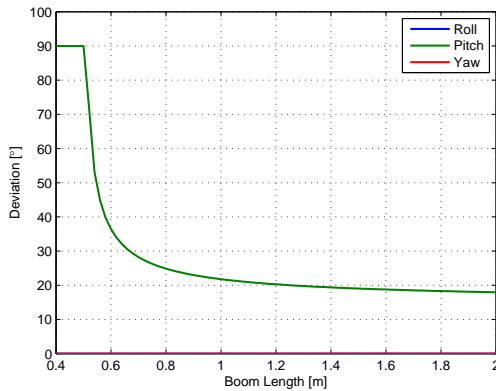


Figure 7.6: Maximum deviation for $\theta_{2,t=t_0} = 15^\circ$, different boom length and aerodynamic torque.

Figure 7.6 shows the maximum deviation for motion about the pitch axis. Pitch maximum deviation decreases with boom length approaching to initial deviation.

Boom length simulations are fixed to initial deviation of 15° , because it is considered as a large initial condition. For lower angles, results get better in terms of stability and maximum deviation. The idea behind these figures is that adverse effects cannot be solved by deploying a larger boom.

7.1.2 Aerodynamic Torque Conclusions

The principal insights of aerodynamic torque are summarized:

- The aerodynamic torque acts mainly on the roll and pitch axes. However, its effects spread to the others axes.
- The effect of aerodynamic torques about pitch axis is to increase peaks of negative angle deviations.
- Stability with aerodynamic torque is very sensitive to initial angles deviations about the roll axis.
- Stability is not reached by deploying a larger boom.

7.2 Magnetic Disturbances

The last disturbance torque to be studied is the magnetic. The magnetic torque depends on the Earth's magnetic field \vec{B}_{Earth} , the spacecraft magnetic moment $\vec{\mu}$ and the spacecraft orientation with respect to \vec{B} . The magnetic field is estimated based on the IGRF model as described in section 2.4.2. The magnetic moment of the spacecraft is unknown. Therefore, it is used as study parameter. That means that different $\vec{\mu}$ values are tested in order to check its effect on the attitude propagation. Later on, conclusions and boundaries of stable motion in terms of magnetic moment are discussed.

7.2.1 Earth's Magnetic Field

The GEOPACK library is used for estimating the Earth's Magnetic field. Magnetic field is calculated for a 600 km altitude circular orbit with 98° inclination. The initial conditions for the orbit simulation are detailed in Table 7.2.

Initial Conditions for Orbit propagation	
Orbit altitude h	= 600 km
Orbit inclination i	= 98°
Longitude of ascending node Ω	= 0°
Argument of the pericentre ω	= 0°
True anomaly θ	= 0°
Eccentricity e	= 0
Initial position vector \vec{r}	= (6978,0,0) km
Initial velocity vector \vec{v}	= (0,-1.0519,7.4844) km/s
Angular frequency n	= 1.1×10^{-3} rad/s
Orbital period T	= 5801.1 s

Table 7.2: Orbit parameters.

Figure 7.7 shows the Earth's Magnetic field components in the ECI and body reference frames. In this case the body reference frame is assumed to be aligned with the orbit frame A throughout the simulation.

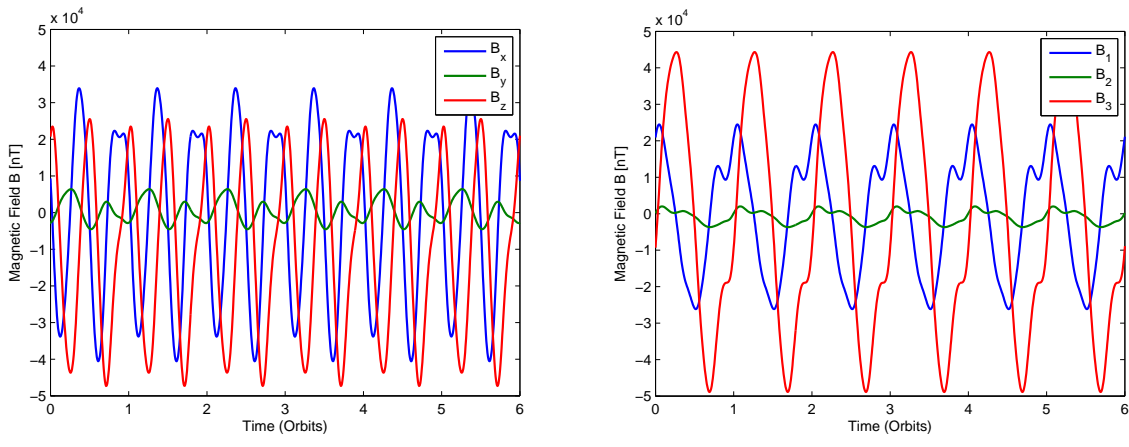


Figure 7.7: Magnetic field in ECI and body reference frame for 98° inclination orbit.

Figure 7.7a depicts Magnetic field being seen from the ECI reference frame. The major information of Figure 7.7a is the order of magnitude of the magnetic field, because its values cannot be used for calculating magnetic torque. Figure 7.7b shows magnetic field as is seen by the spacecraft, which is used for the calculation of the magnetic torque.

7.2.2 Attitude Propagation with Magnetic Torque

To find the influence of the Earth's magnetic field over the spacecraft's attitude, some simulations are displayed. This time, instead of using initial angle deviation as a parameter, the initial attitude is fixed to the equilibrium position and the magnetic moment $\vec{\mu}$ changed. Therefore, the initial conditions for attitude are $\vec{\omega}_0 = (0, -n, 0)$ and $\theta_1 = \theta_2 = \theta_3 = 0^\circ$, which in quaternions is equal to $\vec{q}_0 = (0.0493, -0.7054, -0.0493, 0.7054)$ in this orbit.

Magnetic moment is tested in the three body directions separately. That means that first values in the first body axis are tested $\mu_1 = 0.1, 0.5, 1 \text{ mAm}^2$. Later same values are used for the second (μ_2) and third (μ_3) axes simulations.

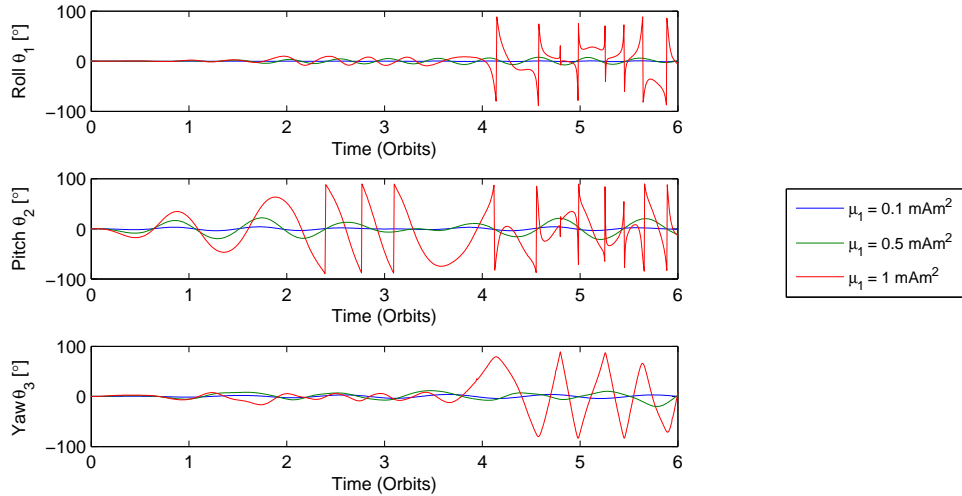


Figure 7.8: Attitude propagation for different magnetic moments μ_1 .

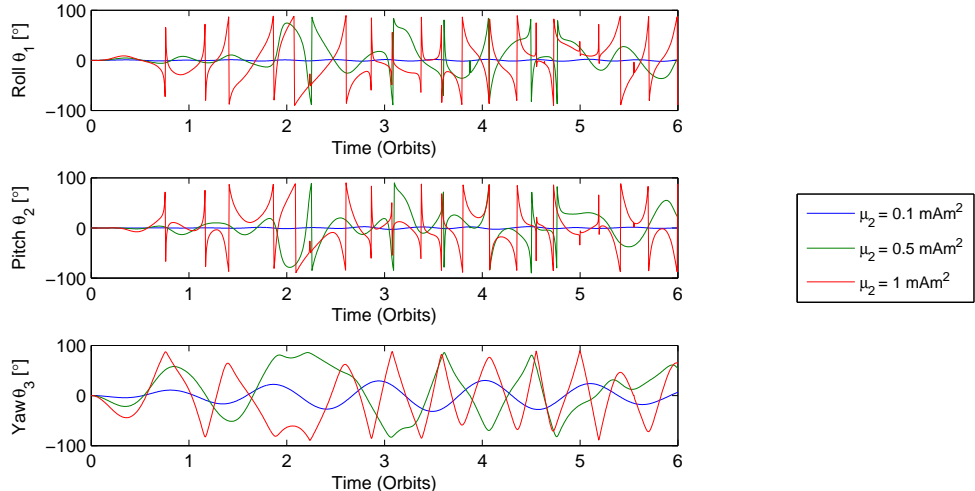


Figure 7.9: Attitude propagation for different magnetic moments μ_2 .

Figure 7.8 shows the angle response for magnetic moment in the roll axis \vec{b}_1 . Stability is guaranteed only for $\mu_1 = 0.1 \text{ mAm}^2$. For $\mu_1 = 0.5 \text{ mAm}^2$ the motion becomes unstable around the tenth orbit.

How the satellite becomes unstable for $\mu_1 = 0.1 \text{ mAm}^2$ requires special attention.

Before the fourth orbit, there are discontinuities in the pitch axis response, which could probably be avoided by deploying a larger boom or adding mass to the tip. However, after the fourth orbit angles about the yaw axis go up to 90° , which produces sharp discontinuities in the roll and pitch axes, once it happens the angle motion becomes chaotic, loosing stability.

Figure 7.9 depicts the angle motion for magnetic moment in the pitch axis \vec{b}_2 . Comparing to Figure 7.8, stability is very sensitive to magnetic moments in the second axis. In this case even $\mu_2 = 0.1 \text{ mAm}^2$ produces deviation up to 30° about the yaw axis. For $\mu_2 = 0.5$ and $\mu_2 = 1 \text{ mAm}^2$ instability comes from a large deviation about the yaw axis, which occurs when the first orbit is finished for the later case.

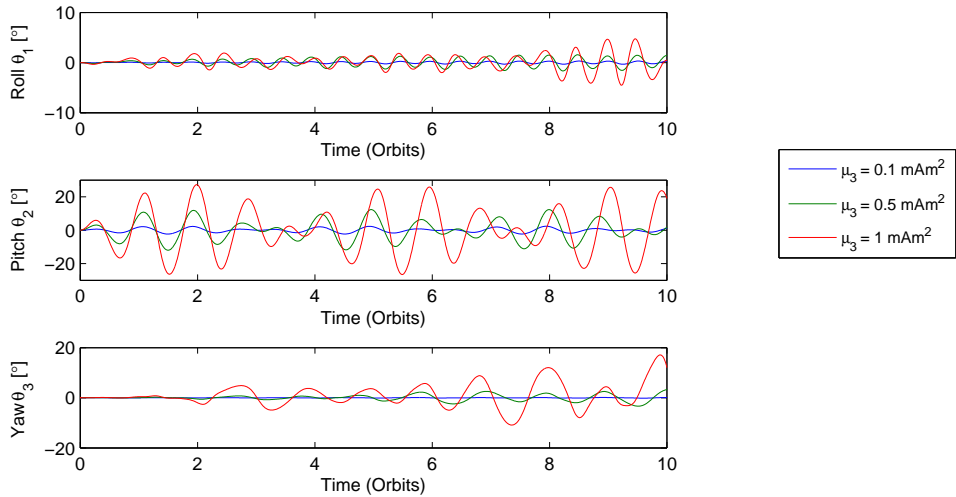


Figure 7.10: Attitude propagation for different magnetic moments μ_3 .

Figure 7.10 presents angle response to magnetic moment in the yaw axis \vec{b}_3 . Motion is stable for the three magnetic moments providing rather small amplitudes. Hence the third axis admits higher magnetic moments.

7.2.3 Magnetic Torque Discussion

The spacecraft has been designed in a way that the gravity gradient torque restores it to its equilibrium position. This is done by making gravity gradient torques larger than disturbance torques. To do so a boom is deployed in the yaw axis. As it has been discussed in Chapter 3, deploying a boom increases moments of inertia and gravity gradient torques about the roll and pitch axes. The problem appears with the yaw axis. Moment of inertia and gravity gradient torque about the yaw axis have not increased, therefore its resistance to rotation and restoring capability are lower comparing to the other axes.

Before magnetic torque was introduced perturbed orbits and aerodynamic torque had not applied significant torques about the yaw axis. Therefore, stability was a problem of initial conditions and satellite configuration. However, the magnetic torque's order of magnitude is similar about all axes, and as a result it produces large angle deviations about the yaw axis that causes instabilities.

Magnetic moment in one axis produces torques in the other two. That is why the spacecraft tolerates better magnetic moments in the yaw axis rather than in the roll and pitch axes. In order to understand better the angle response to torques Figure 7.12 shows the gravity gradient and magnetic torque profiles

for the case of $\mu_2 = 0.5 \text{ mAm}^2$. But first a good way to check the attitude response without discontinuities produced by the Euler angles trigonometric functions is to look at the magnetic field in the body reference frame from the simulation.

Figure 7.11 shows magnetic field seen from the spacecraft. Comparing to Figure 7.7b, it is seen that the third component of the magnetic fields are very similar, following same pattern, whereas second and third components have large variations. This fact signifies that the spacecraft is rotating about the third axis, the yaw axis.

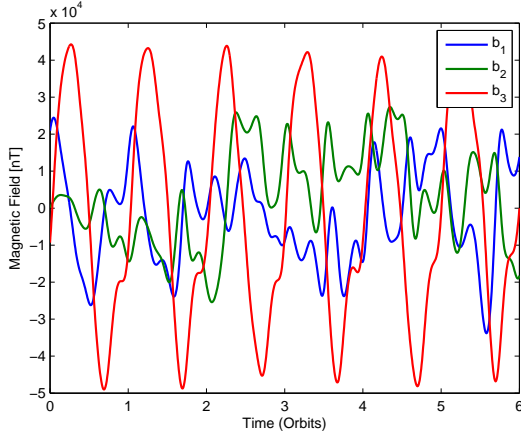
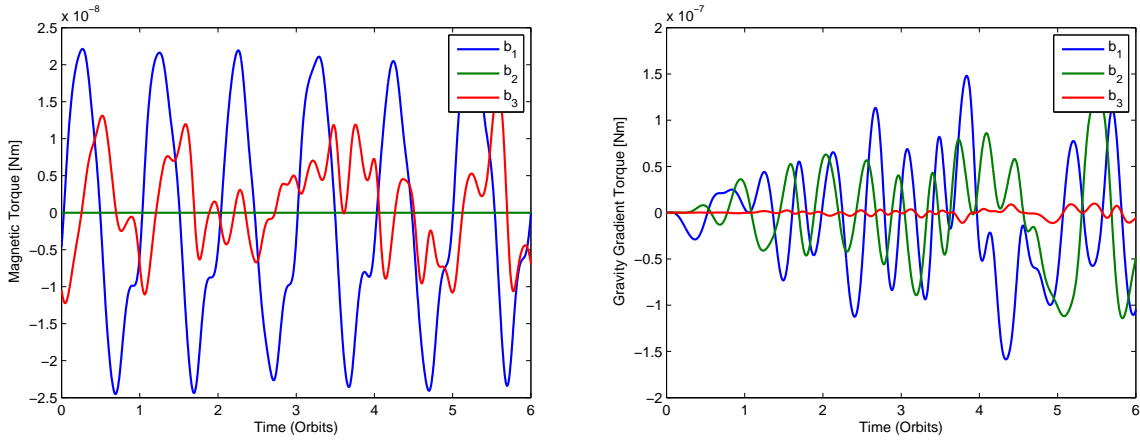


Figure 7.11: Magnetic field in body frame for $\mu_2 = 0.5 \text{ mAm}^2$.

Figure 7.12a shows magnetic torque profile. There is no torque in the second axis, whereas torque about the first axis follows the shape of the magnetic field of the first axis and the torque about the third axis has same profile as the magnetic field of the first axis with opposite sign.



(a) Magnetic torque for $\mu_2 = 0.5 \text{ mAm}^2$.

(b) Gravity gradient torque for $\mu_2 = 0.5 \text{ mAm}^2$.

Figure 7.12: Torque profiles for $\mu_2 = 0.5 \text{ mAm}^2$.

Figure 7.12b shows the gravity gradient torque. It is seen that there is a large difference in the magnitude between torques of the first two axes and the third one. Although gravity torques are one order of magnitude higher than magnetic torques, this is not the case for torques about the yaw axis. The gravity gradient torque is equal to zero at the beginning because at the equilibrium position there is no torque, but it grows with time due to satellite deviation from the orbit reference frame. Figure 7.13 shows a

comparison between the gravity and magnetic torque in the yaw axis.

Figure 7.13a shows separately the magnetic and gravity torque about the yaw axis. It is shown that the magnetic torque is generally larger than the gravity torque. Therefore, yaw motion is driven by magnetic torque. It is important to clarify that the dynamic equations are non-linear and couple, so yaw motion is not strictly driven by torques about the yaw axis. However, torques around the axis are of strong importance. For instance Figure 7.9 shows that the yaw angle is the first one to have large deviation from its equilibrium position for $\mu_2 = 0.5 \text{ mAm}^2$. Figure 7.13b shows the sum of gravity and magnetic torque. Comparing Figures 7.13a and 7.13b it is clearly seen that the magnetic torque influence is bigger than than the gravity about the yaw axis.

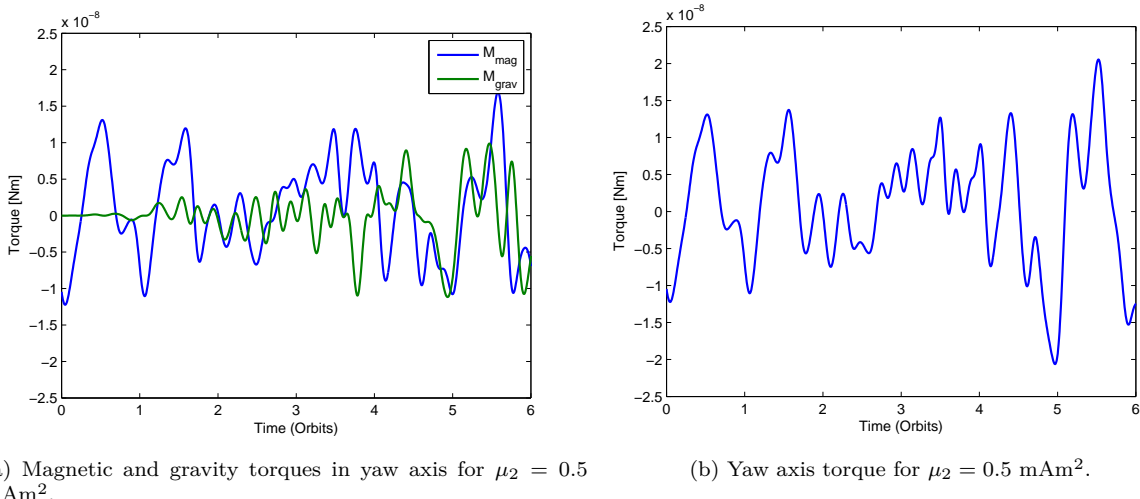


Figure 7.13: Yaw torques for $\mu_2 = 0.5 \text{ mAm}^2$.

The Earth's magnetic field seen from the spacecraft varies with the inclination of the orbit. Nevertheless, as two components of the magnetic moments produces torques about the yaw axis, it is expected that under magnetic field and large magnetic moment, the spacecraft loses stability first about the yaw axis for any inclination.

7.2.4 Magnetic Torque Conclusions

After the discussion some conclusions can be stated:

- The Earth's magnetic field produces torques about all body axes.
- The magnetic torque depends on Earth's magnetic field, and therefore orbit inclination is a fundamental parameter.
- Stability is very sensitive to the magnetic moment. For a 98° inclination orbit, μ_2 has the strongest effect, followed by μ_1 and μ_3 .
- The yaw axis has the smallest moment of inertia. That produces low resistance to rotation and small restoring capability. Therefore, stability is lost about that axis. This behavior is expected for any orbit inclination.

Chapter 8

Mission Simulation

The spacecraft attitude has been analyzed in an ideal circular orbit. Later attitude disturbances have been studied separately. The aim of this chapter is to join all disturbances and analyze a realistic attitude propagation for SWIM.

8.1 Mission Description

Missions specifications were introduced in Chapter 1. In terms of initial conditions for orbit propagation, the spacecraft will be launched into a 600 km polar circular orbit. Although mission specifications state circular orbit, a low eccentric orbit is simulated. In this sense eccentricity add more disturbances, and therefore results are more conservative.

Table 8.1 presents the initial conditions for orbit propagation in classical elements set and in Cartesian system.

Orbit Propagation Initial Conditions	
Altitude of the perigee $h_{perigee}$	= 600 km
Eccentricity e	= 0.01
True anomaly θ	= 0°
Inclination i	= 98°
Right ascension of ascending node Ω	= 0°
Argument of the perigee ω	= 0°
Position vector \vec{r}	= (6978,0,0) km
Velocity vector \vec{v}	= (0,-1.0571,7.5217) km/s
Orbit period T_{orbit}	= 5889.s seconds
Mean motion n	= 0.0011 rad/s

Table 8.1: Initial conditions for orbit propagation

In Chapter 7, it was deduced that the magnetic torque leads to uncontrolled motion about the yaw axis. So for better understanding of the spacecraft motion simulations are first without magnetic torque and then magnetic torque is added.

Analysis starts with initial deviation about the roll axis. The initial conditions for the attitude propagation are summarized in Table 8.2:

$\vec{\omega}_0$ rad/s	Roll θ_1	Pitch θ_2	Yaw θ_3	q_0
(0, -n, 0)	5°	0°	0°	(0.0800, -0.7069, -0.0185, 0.7026)
(0, -n, 0)	10°	0°	0°	(0.1106, -0.7070, 0.0123, 0.6989)
(0, -n, 0)	15°	0°	0°	(-0.0123, -0.7070, 0.0123, 0.7070)

Table 8.2: Initial conditions for roll mission analysis.

Figure 8.1 shows angle motion for initial deviation in roll. Large initial angles about the roll axis produce unstable motion. In fact, for $\theta_{1,t=t_0} = 15^\circ$, angle deviation about the yaw axis becomes very large at the beginning of the fourth orbit, leading to an unstable motion around the tenth orbit. For initial deviations below 10° the motion is stable. Oscillations of angle amplitudes appears for all motions. In general, the amplitudes are larger than in the previous simulations. All phenomena introduced by the perturbations are present. For example, deviation about the pitch axis is larger for negative angles, which is due to aerodynamic torques and the eccentricity produces angle oscillations for the pitch motion.

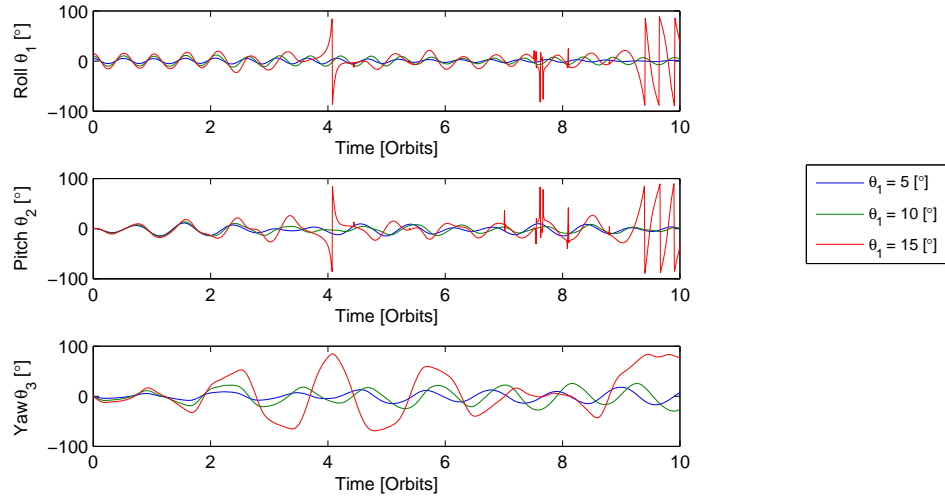


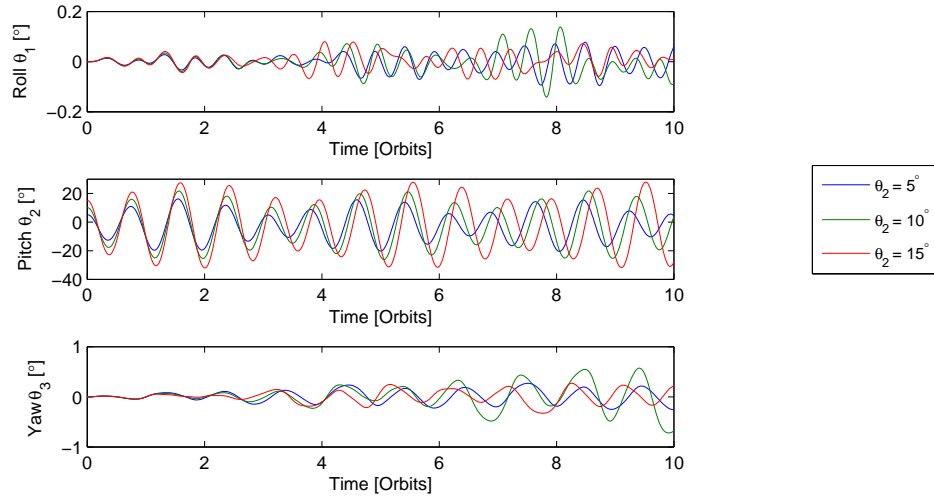
Figure 8.1: Attitude response for mission simulation with initial roll $\theta_{1,t=t_0}$.

The attitude initial conditions for initial deviation about the pitch axis are summarized in Table 8.3.

$\bar{\omega}_0$ rad/s	Roll θ_1	Pitch θ_2	Yaw θ_3	q_0
(0, $-n$, 0)	0°	5°	0°	($-0.5213, -0.4777, 0.5213, 0.4777$)
(0, $-n$, 0)	0°	10°	0°	($-0.5213, -0.4777, 0.5213, 0.4777$)
(0, $-n$, 0)	0°	15°	0°	($-0.5610, -0.4305, 0.5610, 0.4305$)

Table 8.3: Initial conditions for pitch mission analysis.

Figure 8.2 shows the angle response to initial conditions of Table 8.3. Initial deviations about the pitch axis only affects the pitch motion. Pitch response is a combination between Figures 6.4 and 7.3. Eccentricity makes pitch amplitude to oscillate and the aerodynamic torque produces negative angle deviations larger than positives. The pitch period is proportional to the initial angle deviation and larger than in a circular orbit with gravity gradient torque.

Figure 8.2: Attitude response for mission simulation with initial pitch $\theta_{2,t=t_0}$.

The initial attitude conditions for yaw angles are detailed in Table 8.4:

$\vec{\omega}_0$ rad/s	Roll θ_1	Pitch θ_2	Yaw θ_3	q_0
(0, $-n$, 0)	0°	0°	5°	(0.0185, -0.7069, -0.0185, 0.7069)
(0, $-n$, 0)	0°	0°	10°	(-0.0123, -0.7070, 0.0123, 0.7070)
(0, $-n$, 0)	0°	0°	15°	(-0.0432, -0.7058, 0.0432, 0.7058)

Table 8.4: Initial conditions for yaw mission analysis.

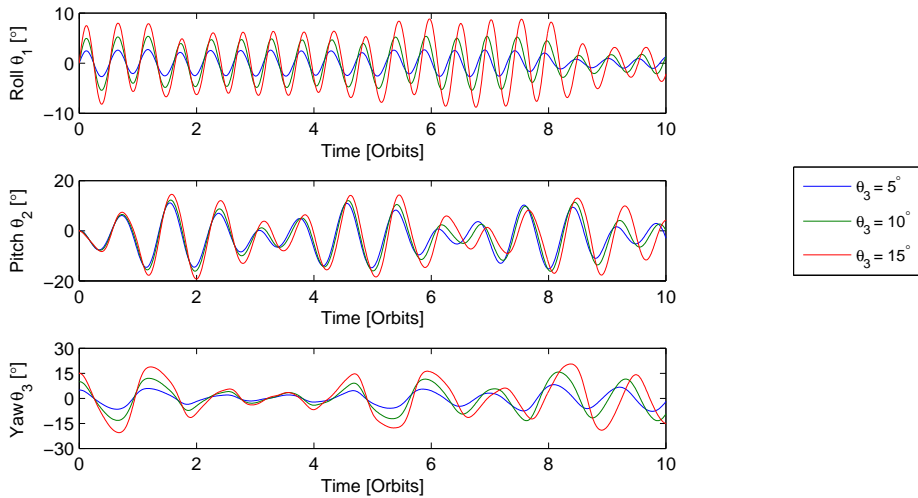
Figure 8.3: Attitude response for mission simulation with initial yaw $\theta_{3,t=t_0}$.

Figure 8.3 shows angle response to initial deviations about the yaw axis. The spacecraft motion is stable for initial angles about the yaw axis below 15° . Comparing to previous simulations with initial conditions about the yaw axis, the maximum deviations are larger for all angles, and the motion has more irregular shapes. For instance, separate disturbances do not affect much the angle amplitude for

the roll axis, but including all disturbances this is not longer the case. Adding more disturbances makes the motion to change from propagation of initial conditions to correction of deviations by the gravity gradient torque. Again eccentricity and aerodynamic effects are visible in the pitch motion.

This section finishes with an example of stable motion including all disturbances. The attitude is defined for a 600 km altitude circular polar orbit of 98° inclination. The initial conditions for orbit propagation are detailed in Table 7.2. The attitude initial state is defined by $\vec{\omega} = (0, -n, 0)$ and $q_0 = (0.0493, -0.7054, -0.0493, 0.7054)$ is the initial orientation, which corresponds to $\theta_{1,t=t_0} = \theta_{2,t=t_0} = \theta_{3,t=t_0} = 0^\circ$.

In Chapter 7, the magnetic moment was tested in all axes separately. However, the influence of three component magnetic moment is different. To investigate it, several simulations have been run with magnetic moment $\mu = 0.1$ and $\mu = 0.2 \text{ mAm}^2$. Notice that $\mu = 0.1$ means $\vec{\mu} = (0.1, 0.1, 0.1) \text{ mAm}^2$.

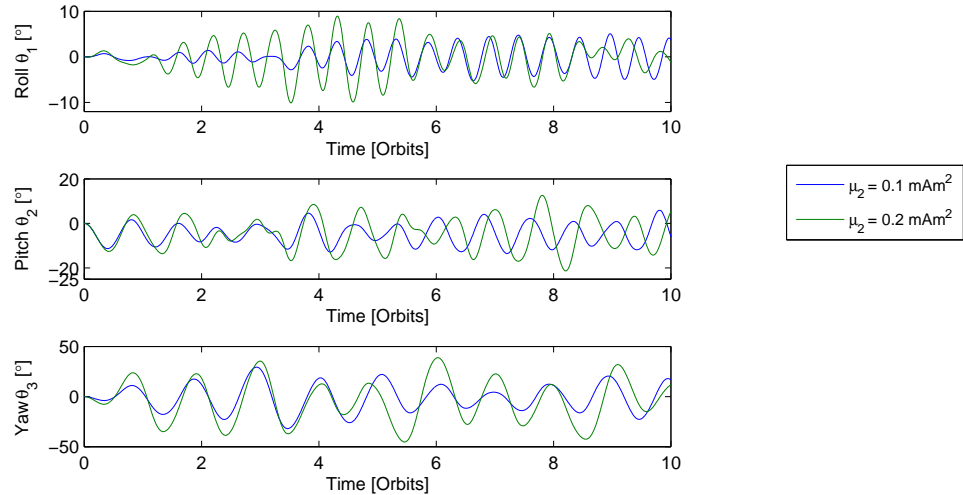


Figure 8.4: Attitude response for mission simulation with $\mu = 0.1, 0.2 \text{ mAm}^2$.

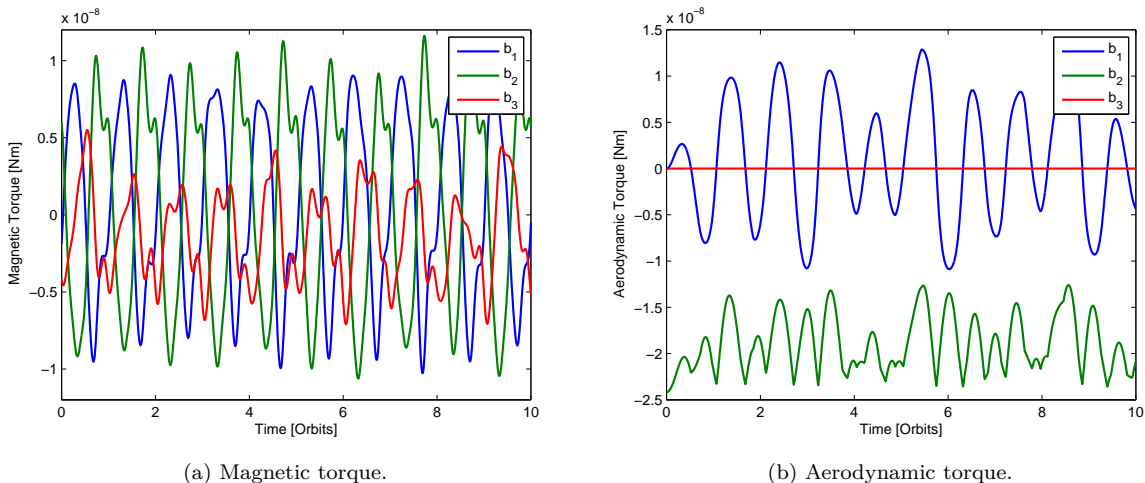


Figure 8.5: Magnetic and aerodynamic torques for $\mu = 0.2 \text{ mAm}^2$.

Figure 8.4 shows angle response to simulations with all disturbances. The angle motion is stable for $\mu = 0.1$ and $\mu = 0.2 \text{ mAm}^2$. In this case there is no propagation of initial conditions. Therefore, in order to understand the attitude, torques from different sources have to be analyzed.

Figures 8.5 and 8.6 show torques applied in the body reference frame, separated in magnetic, aerodynamic and gravity gradient and the sum of all them.

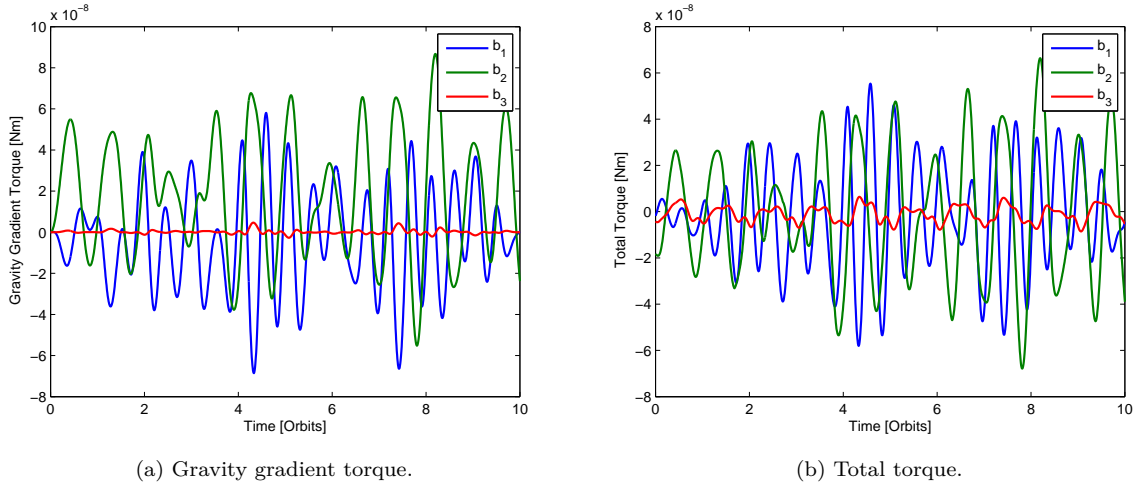


Figure 8.6: Torques for $\mu = 0.2 \text{ mAm}^2$.

The magnetic torque profile is seen in Figure 8.5a. The magnetic torque changes from previous chapter. This is because the torque about each axis depends on magnetic field seen from the spacecraft in the other two. Nevertheless, the magnetic torque about the roll and pitch axes change slightly every period. That means that the yaw axis rotates with large angles, but it does not vary much its position. This is due to the small amplitudes about the roll and pitch axes.

The aerodynamic torque is shown in Figure 8.5b. Torque about the pitch axis is always negative. That is reflected in the pitch motion, that reaches higher negative values than positive. Additionally, torque about the roll axis reaches significant values. Once again this is an effect of large rotations about the yaw axis that changes the projection of the velocity vector in the spacecraft surfaces. Finally torque around the yaw axis \vec{b}_3 , has the lowest magnitude and it does not contribute to the yaw motion.

Figure 8.6a shows the gravity gradient torque profile. The magnitude of this torque is the largest about the roll and pitch axes compared to the other torques. However, it is lower than the magnetic around the yaw axis. Consequently, the largest amplitude of motion is about the yaw axis.

Finally, Figure 8.6b depicts the sum of all torques. It is noticed that gravity torques is the one that has bigger impact on total torque. However, it is seen that the total torque about the yaw axis is similar to the magnetic torque. Hence, higher magnetic moment leads to larger torque around the yaw axis, which means uncontrolled motion about yaw. Now motion of the three axes is a consequence of disturbance torques which are restored by the gravity gradient, so propagation of initial amplitudes does not hold.

8.2 Uncontrolled Yaw Motion

In Chapter 7 and previous section has been stated that at a certain value of $\vec{m}\dot{\mu}$, the satellite becomes unstable about the yaw axis, and therefore starts rotating around it.

However, it is interesting to know how fast the satellite becomes unstable around the yaw axis. That is done by running several simulations with $\vec{\mu}$ as a parameter. The same simulations as in Figure 8.4 but with higher range of magnetic moments have been done. Figure 8.7 shows the results of these simulations for the yaw axis.

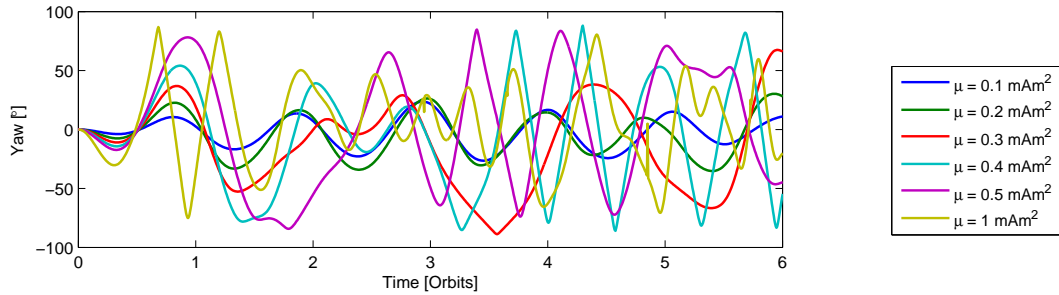


Figure 8.7: Yaw response to different μ .

Figure 8.7 shows that starting from $\mu = 0.3$ the satellite becomes unstable. It takes two orbits for the yaw angle with $\mu = 0.3$ to reach 90° and after the sixth orbit it starts spinning around \vec{b}_3 . In the case of $\mu = 0.4$ the satellite starts spinning before the fourth orbit, for $\mu = 0.5$ it occurs at the beginning of the third orbit and for $\mu = 1$ a half an orbit. Although it seems like not much time, one orbit is around 90 minutes, so for $\mu = 1$ there is more than 45 minutes to actively control the satellite before it starts to spin.

8.3 Boom Position

Finally, boom position along the roll axis \vec{b}_1 is studied. The variation of boom position produces changes in the mass distribution, which leads to changes in the attitude of the spacecraft. The boom has been located at the geometric center of the hub. The idea is to change its location along a line which is parallel to \vec{b}_1 and crossing the geometric center of the hub. The position of the boom is varied from 0.15m to the front i.e. same direction as \vec{b}_1 , and to -0.15 m. Initial Euler angles are fixed and simulations to get maximum deviations are run.

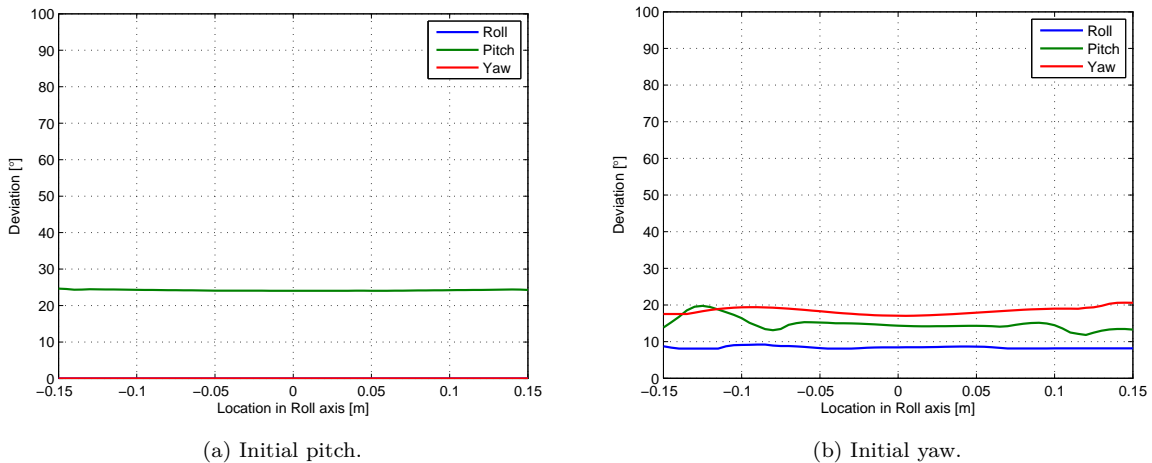


Figure 8.8: Maximum deviation with respect to boom position.

Figure 8.8 shows maximum deviation with respect to boom location for $\theta_{2,t=t_0} = 15^\circ$ and $\theta_{3,t=t_0} = 15^\circ$.

The boom location does not affect the attitude for initial deviations about the pitch axis, as seen in Figure 8.8a. Initial conditions for the yaw axis produce small variation of the maximum deviations. The smallest deviation is for the boom located at the center of the hub. Displacing the boom to the front produce slight larger deviation about the roll axis, whereas displacing it to the back produce increase in pitch angle.

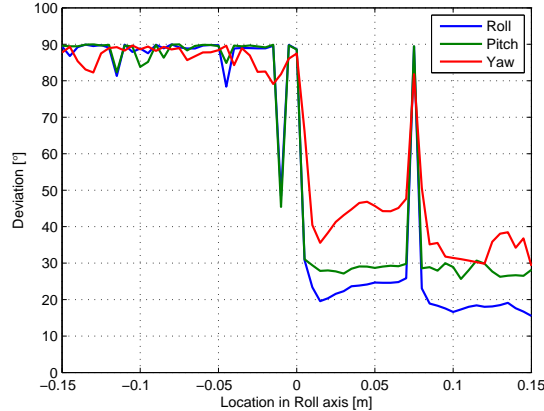


Figure 8.9: Maximum deviation with respect to boom position and initial roll.

Figure 8.9 shows the maximum deviation for 15° initial roll angle. Locating the boom backwards leads to unstable motion, whereas displacing the boom to the front produces stable motion, apart from a certain location, at 0.075 m of the hub geometric center. Further from that point maximum deviation about roll decreases, pitch remains almost constant and yaw maximum deviation fluctuates in a range of 10° .

8.4 Different Mass Configuration

For checking different possible configurations of the spacecraft, simulations with the boom deployed in one of the 10×10 cm face are run. Now the boom is deployed along what has been considered the roll axis for the normal configuration. First the new mass distribution has to be calculated. Table 8.5 shows mass properties for a 3U CubeSat with the boom deployed at the geometric center of one of the 10×10 cm face.

Mass properties	
Mass of hub M	= 3.5 kg
Density per length boom ρ_b	= 0.08342 kg/m
Mass of tip m_t	= 100 g
Length of boom L	= 0.9 m
Total mass of the spacecraft M_t	= 3.6834 kg
J_1	= 0.1654 kgm ²
J_2	= 0.1654 kgm ²
J_3	= 0.0058 kgm ²
$\vec{R}_{c.m.}$	= (0,0,0.0408) m
Linear pitch period T_{lin}	= 3.4×10^3 s

Table 8.5: Mass Properties for boom deployed in 10×10 face.

With this new model the stability criteria is not fulfilled. The satellite becomes axisymmetric. Nevertheless, what is appreciated is that now gravity gradients torques about the roll and yaw axes are larger whereas there is no restoring torque about the yaw axis. In this sense the problem presented of small restoring capabilities of the yaw axis is more severe. Therefore, the analysis with magnetic torque is skipped.

In order to check the attitude performance of the spacecraft with the boom located in a different face simulations with only gravity gradient torque, gravity gradient torque and eccentricity and gravity gradient and aerodynamic torques are run. The initial attitude conditions are 15° deviation around the three axes individually. For the eccentricity simulation $e = 0.01$ is used.

Figure 8.10 shows simulations with initial deviation about the roll axis.

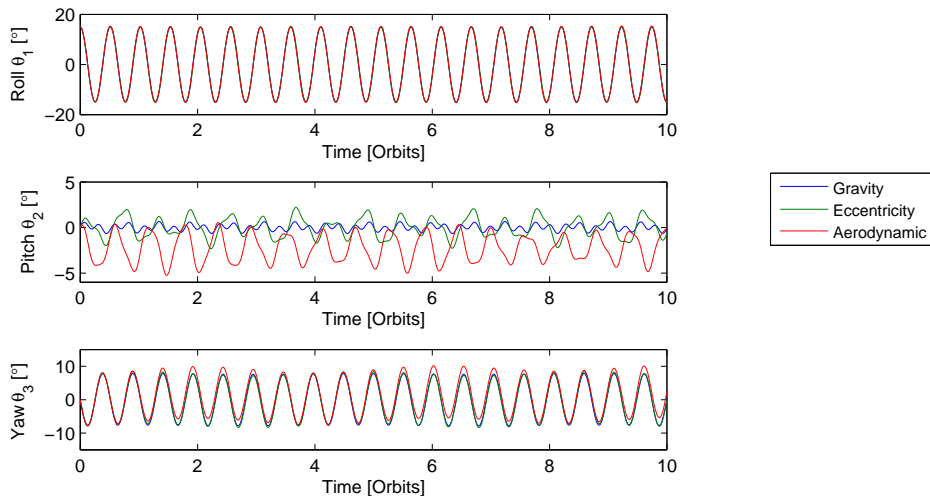


Figure 8.10: Attitude response for new boom configuration and $\theta_{1,t=t_0} = 15^\circ$.

By deploying the boom in one of the small faces the attitude motion changes significantly. Motion

around the roll axis is equivalent to an undamped harmonic oscillator. The disturbances do not affect much the roll axis and the three simulation responses superpose each other. For this mass configuration the linear pitch period is much lower and so is the coupling of the pitch equation of motion with the roll and yaw equations. As a consequence pitch motion has small amplitude with large frequency comparing to the original configuration of the SWIM CubeSat. The simulation with the eccentric orbit delivers a response with larger amplitude and period. The simulation that includes the aerodynamic torque has larger negative angle deviations about the pitch axis. Yaw response is also more decoupled to the roll and pitch one than the original configuration and looks as an undamped harmonic oscillator. The disturbances do not affect much the response about the yaw axis. Therefore, this configuration shows more stiffness to disturbances and non-linearities.

Figure 8.11 shows angular response for $\theta_{2,t=t_0} = 15^\circ$. The pitch equation of motion is also decoupled to the other axis, and therefore, only response about the pitch axis is affected for these simulations. The angular motion is similar to the original configuration but with higher frequency. The gravity gradient torque is larger about the pitch axis, so the disturbances affect less the motion.

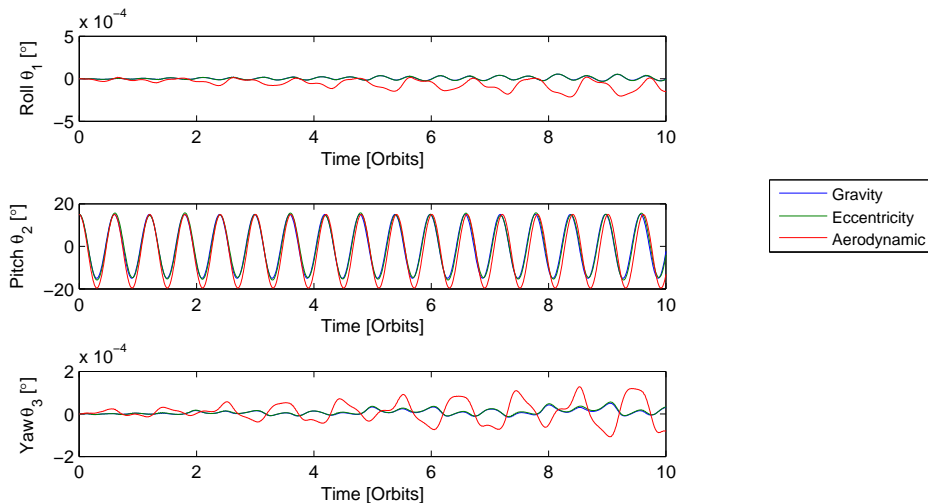


Figure 8.11: Attitude response for new boom configuration and $\theta_{2,t=t_0} = 15^\circ$.

Figure 8.12 shows the angle response for initial deviation of $\theta_{3,t=t_0} = 15^\circ$. The most interesting behavior is for the yaw axis. Since the spacecraft is axisymmetric there is no gravity torque about the yaw axis and its motion is driven by the coupling of Euler's equations. The fact of no gravity gradient torque produces that the angle deviation never reaches the equilibrium zero angle. However, motion of the spacecraft is stable for short time simulations. Moreover, the angle amplitude of the motion about the yaw axis is smaller than for the original configuration, being less than half the initial deviation. The response about the roll axis looks like an undamped harmonic oscillator and same features as in other simulations hold for the pitch axis.

If the boom is deployed from one of the 10×10 cm faces of the hub the attitude of the spacecraft changes. It is appreciated that coupling of equations is less than for the original configuration and the satellite is stiffer against non-linearities and disturbances about the roll and pitch axis. However, there is no opposition to disturbance torques about the yaw axis, and therefore, it is expected to have uncontrolled motion about the yaw axis once magnetic torque is added. Hence, this configuration only works if the yaw motion can be controlled by another mechanism rather than the gravity gradient torque.

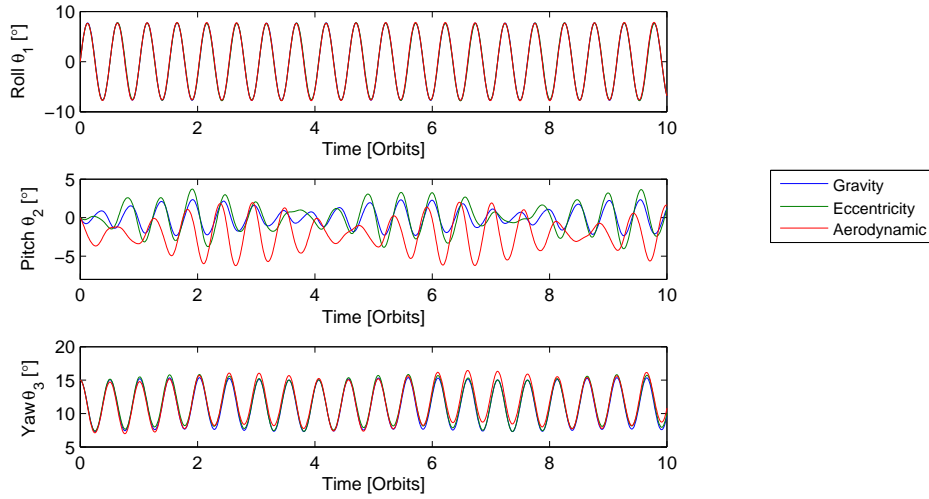


Figure 8.12: Attitude response for mission new boom configuration and $\theta_{3,t=t_0} = 15^\circ$.

8.5 Mission Conclusions

After the analysis of the mission some conclusions can be summarized for the selected orbit:

- The motion of the spacecraft differs from propagation of initial conditions when all sources of disturbance are taking into account. Instead the motion is driven by external torques.
- If initial deviations are small and the satellite is rotating with same frequency as the orbit, the LHLV position is conserved for a magnetically clean spacecraft.
- Special attention must be taken for initial deviation about the roll axis, which could lead to unstable motion. However, this could be solved by deploying the boom in the front position.
- Magnetic moments larger than 0.2 mAm^2 make the satellite rotate around its yaw axis and eventually lose the LHLV position.
- It takes a certain time for the satellite to become unstable, so active control is possible.
- The attitude of the spacecraft changes by deploying the boom along an axis perpendicular to the $10 \times 10 \text{ cm}$ face of the hub. However, there is no controlled of the yaw axis by the gravity gradient torque.

Chapter 9

Aerostable Spacecraft

It is already known that the gravity gradient torque does not control the yaw axis. It is possible to control passively a satellite using magnetic torque. This is done by placing a magnetic rod in one of the axis and aligned it with Earth's magnetic field. However, that mechanism is not compatible with a LHLV pointing nor with accurate magnetic field measurements. Nevertheless, it is possible to provide stabilization with aerodynamic torque [14]. In this case the aerodynamic torque could control passively the yaw axis.

This chapter proposes a way to stabilize the yaw axis with aerodynamic torque.

9.1 New Mass Distribution

Aerodynamic stability about the yaw axis is reached by deploying two solar panels. These solar panels have to be deployed in the faces that are perpendicular to the one where the boom is deployed. In other words, in the faces with normal vector parallel to \vec{b}_2 .

The idea of stability around the yaw axis comes from the shadowing of the panels due to yaw deviation. Considered SWIM CubeSat to have its center of mass in the geometric center of the hub. If the spacecraft is aligned with orbit reference frame, aerodynamic forces in both panels cancel each other, with no aerodynamic torque as a result. However, when some deviation occurs about the yaw axis, one of the panels gets partially shadowed, creating a torque about the yaw axis. If the center of mass is located at the front of the center of pressure of the panels, the aerodynamic torque restores the satellite to its equilibrium position as depicted in Figure 9.1.

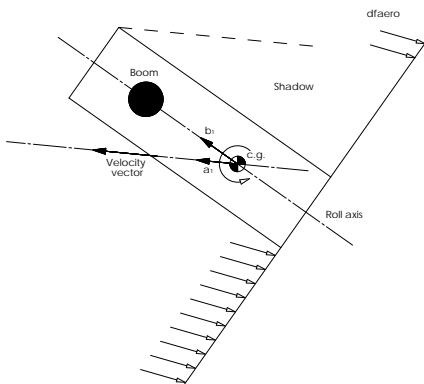


Figure 9.1: Aerodynamic torque about the yaw axis.

The solar panels create also aerodynamic torques about the roll and pitch axes. For the pitch axis, aerodynamic torques of the panels are opposite to the aerodynamic torques of the boom, therefore, it is not a bad configuration. The aerodynamic torques around the roll axis are not restoring. However, it is expected the gravity gradient torques to be larger than aerodynamics.

Deploying solar panels changes the mass distribution of the spacecraft. Considered the length of the solar panel to be $a = 20$ cm and its width to be $b = 10$ cm. Table 9.1 delivers the mass distribution information for an aerostable satellite.

Mass properties		
Mass of hub M	=	3.2 kg
Density of the Boom ρ_b	=	0.08342 kg/m
Mass of tip m_t	=	100 g
Length of boom L	=	0.9 m
Mass of a panel m_p	=	0.14 kg
Panel length a	=	20 cm
Panel width b	=	10 cm
Total Mass M_T	=	3.6551 kg
J_1	=	0.1099 kgm ²
J_2	=	0.1298 kgm ²
J_3	=	0.0406 kgm ²
Linear pitch period T_{lin}	=	4242.5 seconds
$\vec{R}_{c.m.}$	=	(-0.0115, 0, 0.0337) m
Radius of the boom r_{boom}	=	0.0015 m
Radius of the boom r_{tip}	=	0.025 m

Table 9.1: Mass properties aerodynamic test.

The main differences in mass distribution is an increased in moment of inertia of the yaw axis and displacement of the center of mass. Besides other moments of inertia also have changed, but the stability criteria is satisfied:

$$0.1298 > 0.1099 > 0.0406 \quad \text{and} \quad 0.1298 < 0.1099 + 0.0406 = 0.1505$$

9.2 Attitude Propagation

The new mass distribution after deploying solar panels leads to changes in the attitude propagation. In order to find the new behavior of the spacecraft simulations are run, starting with a circular orbit with only gravity gradient torque. Therefore, as it was done in Chapter 5, a 600 km altitude circular orbit defines trajectory. Orbital parameters are detailed in Table 5.2.

The attitude initial conditions are initial deviation about the three axes of 15°. Simulation with angles below 15° are skipped. This is because it is interesting to look at the behavior of large deviations, which are the ones that lead to unstable motion. Table 9.2 shows the initial attitude conditions for the three simulations. Non-linear equations are used in the simulations.

$\vec{\omega}_0$ rad/s	Roll θ_1	Pitch θ_2	Yaw θ_3	q_0
(0, -n, 0)	15°	0°	0°	(0.1305, 0, 0, 0.9914)
(0, -n, 0)	0°	15°	0°	(0, 0.1305, 0, 0.9914)
(0, -n, 0)	0°	0°	15°	(0, 0, 0.1305, 0.9914)

Table 9.2: Initial attitude conditions for new mass distribution.

Figure 9.2 shows the angle and angular velocity response for initial deviation of 15° about the roll axis. In comparison with the mass model of Chapter 5 in Figure 5.8, amplitudes of angle response oscillate less for the new model. In fact, the roll response is similar to an undamped harmonic oscillator, deviation about the pitch is of small magnitude and an interesting fact occurs to the yaw motion. The yaw response is the combination of two modes, one with large period of about 2 orbits and a lower period

motion of a quarter of orbit. That means that this new mass distribution produces more coupled results, and therefore it makes no sense to calculate quasi-linear periods, but it is stiffer to non-linear effects. That is because there is not such a big difference between J_3 and the other moments of inertia.

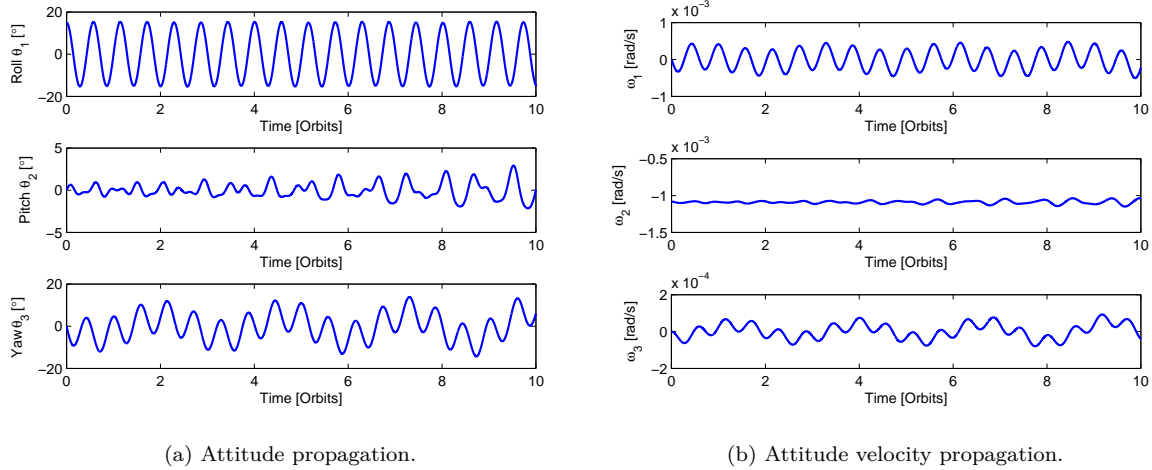


Figure 9.2: Attitude and angular velocity propagation for $\theta_{1,t=t_0} = 15^\circ$ in circular orbit.

Figure 9.2b depicts the angular velocity response. Compare to the former mass model amplitudes of angular velocities remain constant, and therefore smaller. Here coupling of modes in the roll and yaw responses can be observed.

Figure 9.3 shows the angle and angular velocity response to initial deviation about the pitch axis. As with the former mass model, pitch response is like an undamped oscillator with period slightly large than linear period, which normalized is $T_{lin}/T_{orbit} = 0.713$ and in Figure 9.3a is $T_{pitch}/T_{orbit} = 0.7421$. However, the difference between linear and non-linear is expected to be lower with smaller initial deviation. Figure 9.3b shows the angular velocity response. The energy exchange mechanism is again observed for the pitch motion.

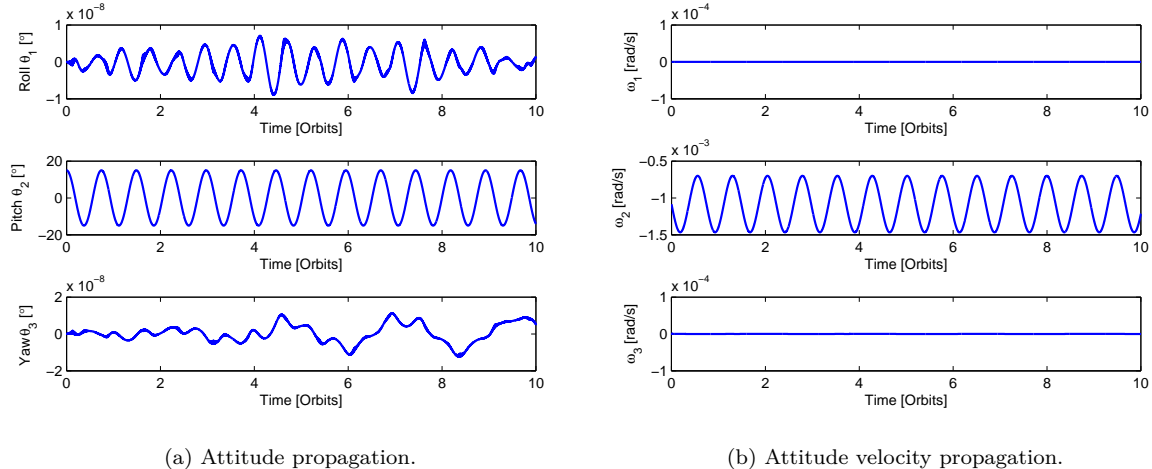


Figure 9.3: Attitude and angular velocity propagation for $\theta_{2,t=t_0} = 15^\circ$ in circular orbit.

Figure 9.4 presents the attitude and angular velocity propagation for initial deviations about the yaw axis. Comparing to propagation with initial deviation about the roll, now it is seen two modes in the roll response. This is seen better in the angular velocity response. Deviations about the pitch axis are of smaller amplitude compared to former mass model. The angular velocities components in Figure 9.4b have lower amplitudes than for the former mass model.

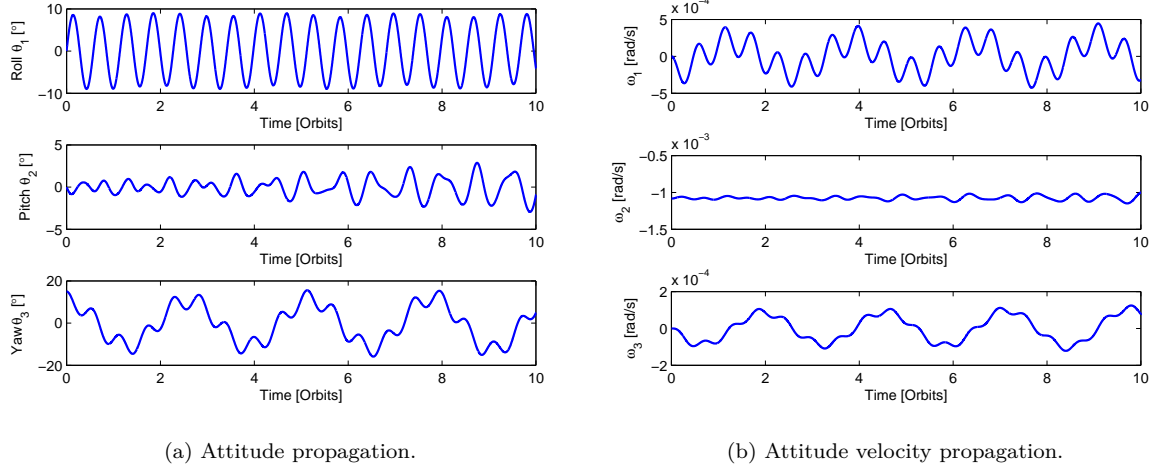


Figure 9.4: Attitude and angular velocity propagation for $\theta_{3,t=t_0} = 15^\circ$ in circular orbit.

After analyzing the attitude responses for initial deviation about the three axes it can be concluded that the mass model with deployed panels produces more coupled solutions, which are stiffer to non-linear effects.

9.2.1 Attitude with Aerodynamic Torque

After analyzing mass distribution changes, the aerodynamic torque has to be included in propagation. The idea of deploying solar panels is to provide yaw passive stabilization. First new distribution of aerodynamic forces and torques has to be explained. Figure 9.5 shows the aerodynamic forces and torques for $\theta_{3,t=t_0} = 15^\circ$ simulation in the previous section.

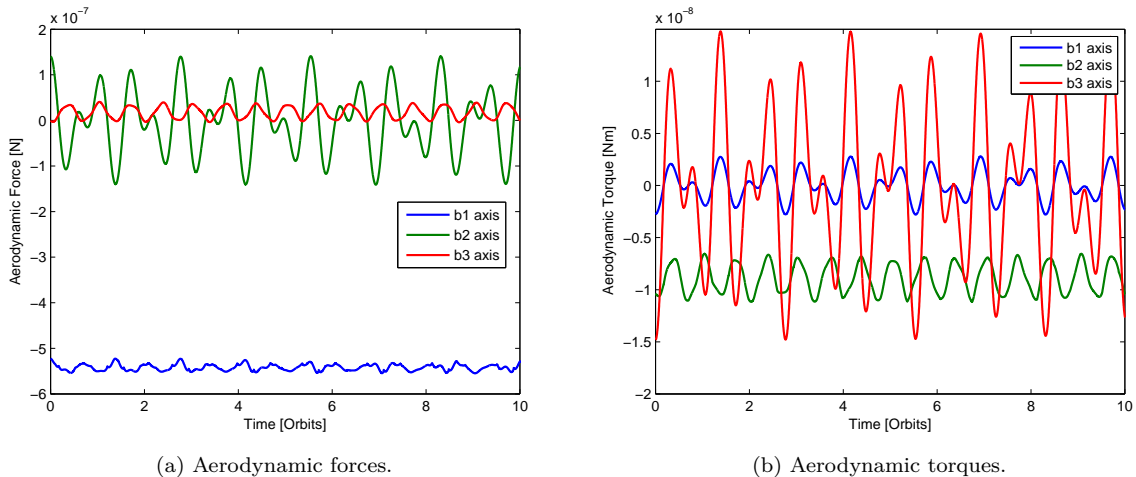


Figure 9.5: Aerodynamic forces and torques for $\theta_{3,t=t_0} = 15^\circ$.

Figure 9.5a shows the sum of aerodynamic forces in the body axes. Comparing to the spacecraft with no deployed panels in Figure 7.1a the aerodynamic forces are twice as large along \vec{b}_2 and \vec{b}_3 with panels deployed, and the increase of aerodynamic forces is higher along \vec{b}_1 . This is because frontal area of the spacecraft is much larger with the panels. Very important is the aerodynamic torque profile shown in Figure 9.5b. Now the largest torque is around the yaw axis. This torque pushes the spacecraft to the equilibrium position for any disturbance about the yaw axis. Additionally torque around the pitch axis has decreased its value, if it is compared to Figure 7.1a. Aerodynamic torque about the roll axis is of small magnitude and the gravity gradient torque exceeds it.

Figure 9.6 shows a comparison between simulations with only gravity gradient torque and simulations with gravity and aerodynamic torques.

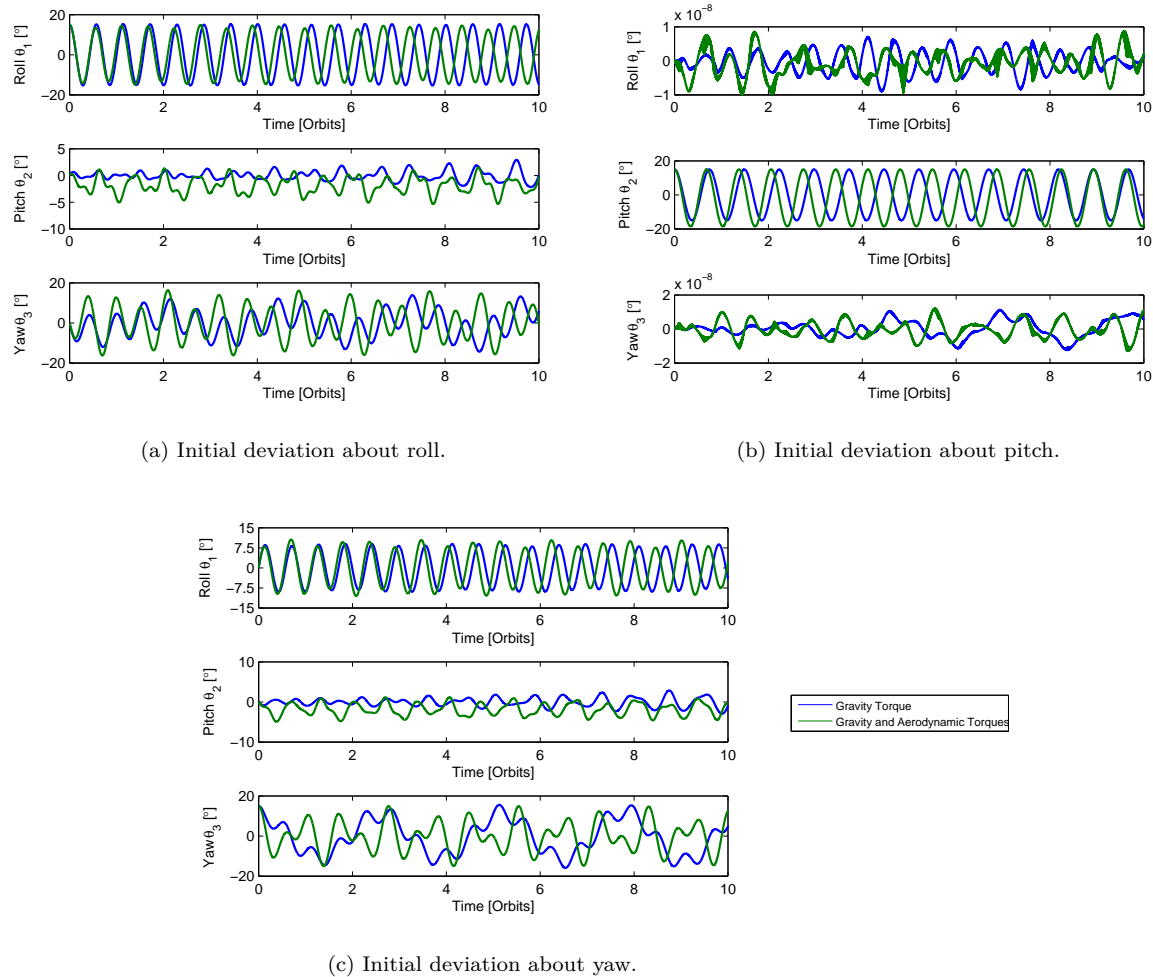


Figure 9.6: Attitude with aerodynamic torque.

Figure 9.6a shows angle response with initial deviation about the roll axis. Aerodynamic torques produce slightly smaller amplitude in roll response with shorter period. Deviation about the pitch axis increases for negative angles as it occurred without the panels deployed. Yaw motion is driven by aerodynamic torque. Initially the spacecraft takes negative deviation about the yaw axis, which is rapidly corrected by the aerodynamic torque. Later amplitude reaches deviation close to initial condition about the yaw axis and propagates. Now motion cannot be seen as two different modes.

Figure 9.6b shows simulations with initial deviation about the pitch axis. The aerodynamic torque produces oscillations with slightly larger amplitudes for negative angles and shorter period. The difference in amplitude is very small compared to simulations without panels deployed. Deviations about the roll and yaw axes are negligible.

Figure 9.6c depicts the attitude propagation for initial deviations about yaw. Roll axis response increases slightly in amplitude and decreases in period. Amplitude oscillates compared to the simulations without the aerodynamic torque. Pitch axis response has larger values for negative angles. Yaw response changes significantly. As with the initial conditions for the roll axis, response of the yaw axis is driven by the aerodynamic torque. Initial conditions are propagated and slightly reduced with time, in a periodic oscillation with changes in the amplitude.

The general behavior of aerodynamic torque is to increase oscillation frequency compared to only gravity gradient, in a propagation of initial deviations.

9.2.2 Attitude with Magnetic Torque

Now is time to check the new satellite configuration with the magnetic torque. Same procedure as with previous chapters is followed. The satellite is inserted into a 98° inclination polar orbit and starts the attitude aligned with orbit reference frame and $\omega_2 = (0, -n, 0)$. Different magnetic moments are tested and also different length of the solar panels as delivered in Table 9.3.

a [m]	Panel length		
	J_1 [kgm 2]	J_2 [kgm 2]	J_3 [kgm 2]
0.2	0.1099	0.1298	0.0406
0.25	0.1127	0.1298	0.0457
0.3	0.1159	0.1298	0.0516

Table 9.3: Moments of inertia for different panel length.

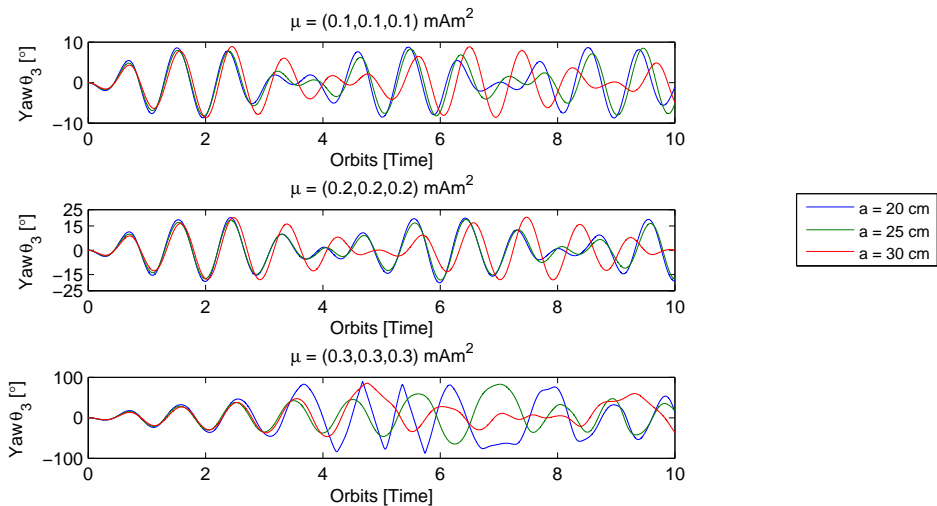


Figure 9.7: Yaw for different μ and panel length.

Figure 9.7 shows yaw deviation for different panels length and magnetic moment. All solar panels selected stabilized correctly for $\mu = 0.1$ mAm 2 magnetic moment for the three axes. Deviations due to magnetic torque are corrected by the aerodynamic torque producing amplitudes of less than 10° regardless of panel length. This is an improvement of performance, because without deployed panels amplitudes

reach 20° . Larger panels deliver larger periods for the yaw response. For $\mu = 0.2 \text{ mAm}^2$ magnetic moment, the yaw response is similar to $\mu = 0.1$, with larger amplitude of deviations, around 20° . The same behavior remains for the periods.

For $\mu = 0.3 \text{ mAm}^2$ large deviations appear. The spacecraft with 20 cm panels loses stability about the yaw axis after the fourth orbit. For 25 and 30 cm panels large angle deviation about the yaw axis appears after the fourth orbit. Therefore, stable motion is not assured for 0.3 mAm^2 .

At this altitude, the aerodynamic torque do no exceed the magnetic torque as much as it is needed for relative small magnetic moments. Therefore, active control of the spacecraft is required. Besides the atmospheric density is taken as average mean value. But there are density fluctuations which depend on solar wind [8]. Therefore, the aerodynamic stabilization needs to be studied, a more accurate atmospheric model has to be implemented. MSIS-86 and HWM-93 are empirical models which provide atmospheric disturbances $\rho(t)$, [14].

9.3 Propagation at Lower Altitude

In previous section has been seen that the aerodynamic torque does not provided stability for $\mu = (0.3, 0.3, 0.3)$. However, as long as the spacecraft gets closer to the Earth, the aerodynamic torque magnitude increases. Therefore, it is expected that at lower altitude, the attitude performance improves. Figure 9.8 shows similar simulations than in previous section with different magnetics moments at 550 km altitude.

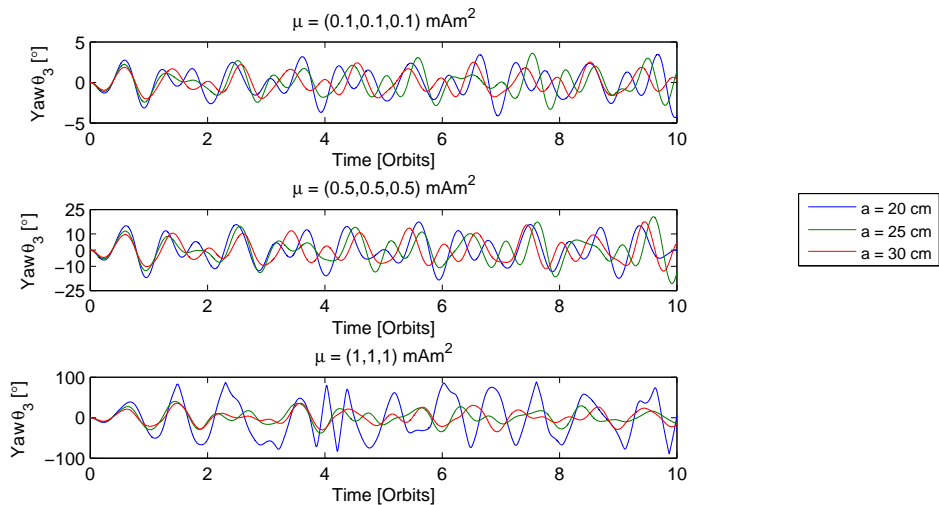


Figure 9.8: Yaw for different μ and panel length at 550 km.

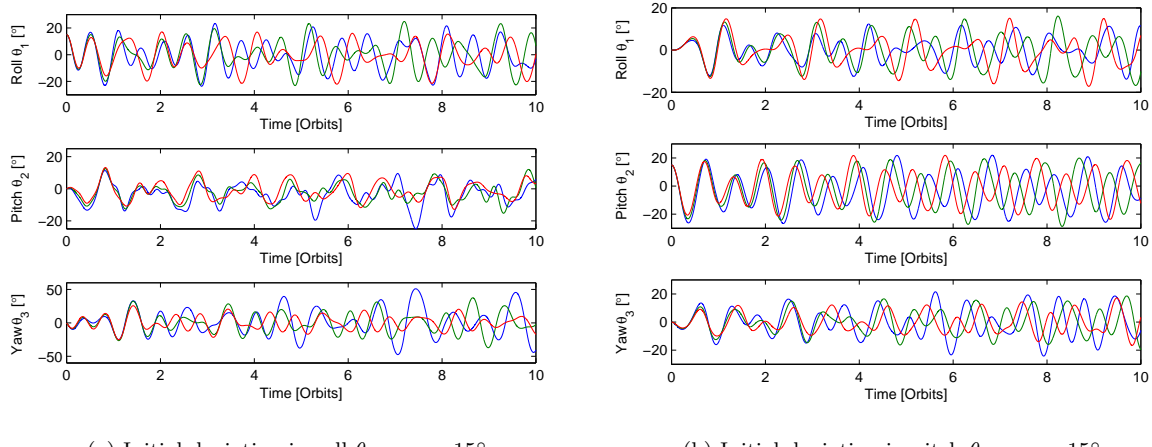
Figure 9.8 shows that the satellite is stable in yaw for a circular orbit at 550 km altitude with deployed panes of length 0.25 cm for a magnetic moment of $\mu = (1, 1, 1)$, which is three times larger than the one that produces unstable motion at a 600 km circular orbit. The reason why it happens is the variation of density in the upper atmosphere. Figure 2.2 shows the atmospheric density variation with altitude. For a 600 km altitude, the atmospheric density $\rho = 1.5 \times 10^{-13} \text{ kgm}^{-3}$, whereas for 550 km is $3.3 \times 10^{-13} \text{ kgm}^{-3}$, which is more than twice the value. Therefore, the aerodynamic torque doubles its value. The atmospheric density increases when the satellite approaches the Earth and so does its effect on the solar panels. Hence, it is possible to have a three axes passive stable satellite with gravity gradient and aerodynamic torques.

9.3.1 Initial Deviations and Magnetic Torque

So far magnetic torque has been tested without initial angle deviation. Without the aerodynamic stabilization it does not make sense due to large deviation starting aligned with the orbit reference frame. Nevertheless, once this problem is solved, it is interesting to visualize the attitude propagation with all torques and initial deviations. This is done by inserting the spacecraft into a 500 km altitude 98° inclination orbit, with an initial position vector $\vec{r} = (6928, 0, 0)$ km, velocity vector $\vec{v} = (0, -1.05, 7.54)$ km/s and mean orbital motion $n = 1.1 \times 10^{-3}$. Table 9.4 shows initial values for propagation. The satellite has magnetic torque $\mu = (0.5, 0.5, 0.5)$ mAm².

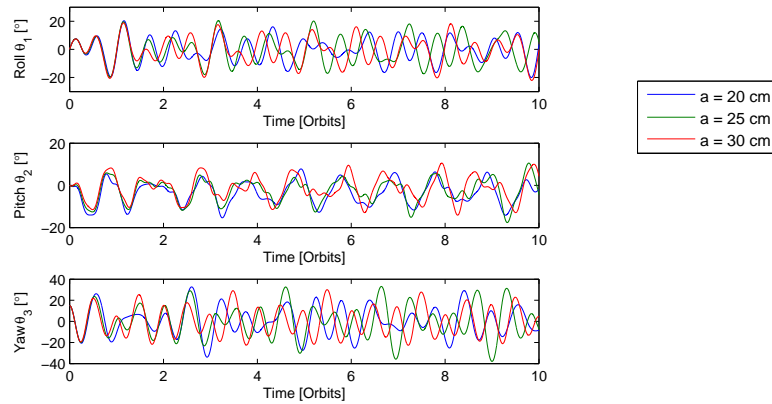
$\bar{\omega}_0$ rad/s	Roll θ_1	Pitch θ_2	Yaw θ_3	q_0
(0, $-n$, 0)	15°	0°	0°	(0.1410, -0.7058, 0.0432, 0.6920)
(0, $-n$, 0)	0°	15°	0°	(0.0553, -0.6073, -0.0425, 0.7914)
(0, $-n$, 0)	0°	0°	15°	(-0.0432, -0.7058, 0.0432, 0.7058)

Table 9.4: Initial conditions for attitude propagation with magnetic torque.



(a) Initial deviation in roll $\theta_{1,t=0} = 15^\circ$.

(b) Initial deviation in pitch $\theta_{2,t=0} = 15^\circ$.



(c) Initial deviation in yaw $\theta_{3,t=0} = 15^\circ$.

Figure 9.9: Attitude with magnetic torque and initial deviation.

Figure 9.9 represents the attitude propagation for different initial deviations and length of panel. Now the attitude is not a propagation of initial deviations, instead motion is driven by torques. The gravity gradient torques are restoring about the three axes. However, gravity torque around the yaw axis is of small magnitude. The aerodynamic torque restores position about the yaw axis. On the other hand aerodynamic torque causes deviation around the roll and pitch axes, and magnetic about the three axes.

Deviation is proportional to the panel length. This is because a 20 cm panel produces larger deviations about the yaw which are spread to the other axes. In general for 25 cm and 30 cm angle amplitudes are around 20° regardless of initial deviations.

9.3.2 Aerodynamic Damping

There is a final feature of the aerodynamic torque. The aerodynamic torque comes from aerodynamic forces, which are non-conservative and produce energy dissipation. That applied to an aerodynamic stable spacecraft means damping of angular deviation.

In order to illustrate aerodynamic damping a simulation in a polar 98° inclination 500 km altitude circular orbit is displayed. The initial position vector is $\vec{r} = (6878, 0, 0)$ km and initial velocity vector $\vec{v} = (0, -1.0595, 7.5380)$ km/s. The orbital period is 5.676×10^3 and mean motion $n = 1.1 \times 10^{-3}$. The satellite initiates attitude with 60° deviation about the yaw axis which gives an initial quaternion $q_0 = (-0.3100, -0.6355, 0.3100, 0.6355)$. The initial angular velocity is equal to $\vec{\omega} = (0, -n, 0)$.

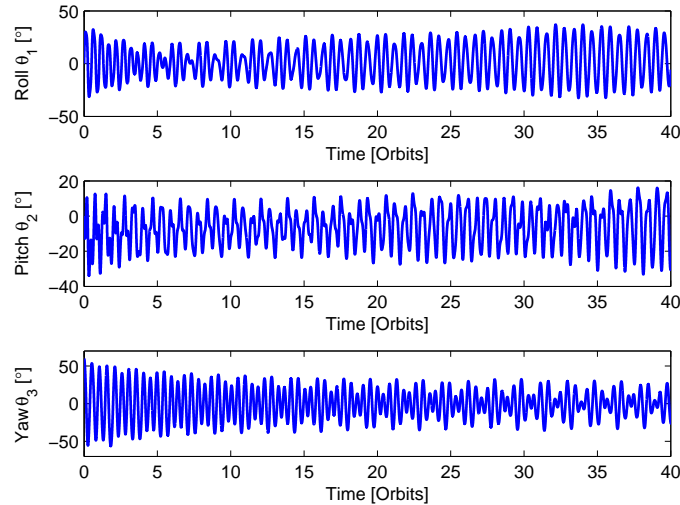


Figure 9.10: Attitude propagation at 500 km.

Figure 9.10 shows how initial deviation about the yaw axis is damped from initial amplitude of 60° to 25°. Initial deviation about yaw spreads to the other axes, producing amplitudes of 30° about the roll and 20° about the pitch axes. These amplitudes are not damped and they propagate and even increase slightly. However, the satellite has stable motion despite large initial deviation.

9.4 Conclusions

The aerodynamic stabilization is not enough to control passively the spacecraft at 600 km altitude. Nevertheless, it delays unstable motion.

On the other hand if the orbit altitude is decreased, control in the three axes can be obtained with a combination of a gravity boom and aerodynamic stabilization. The aerodynamic stabilization works better with proximity to the Earth. In this sense ,from 550 km to lower orbits, deploying two panels of 20 or 25 centimeters and the boom assures stable motion.

Chapter 10

Conclusions

During this master thesis an extensive analysis of the attitude dynamics of the SWIM CubeSat has been carried out. The main conclusion is that the spacecraft cannot be kept in a LVLH position using the gravity torque alone. Moreover, a combination between aerodynamic and gravity gradient torques may not guarantee pointing requirements for a 600 km circular orbit. In this case active control is required for optimum performance of the mission.

Gravity gradient stabilization makes the satellite propagate initial conditions with constant periods. Depending on the mass properties of the spacecraft, the motion shows more coupling effects between the different axes or stiffness to non-linear effects. The disturbance torques i.e. aerodynamic and magnetic torques increase deviation in the motion, which spread out to the different axes. When this happens the motion of the spacecraft depends more on the external torques than initial deviations, and periodic motion disappears. If the external torques are large enough, instability is reached and the spacecraft starts rotating in an uncontrolled fashion. The first axis to become unstable is the yaw, due to mass distribution properties. Since the gravity gradient torque comes from a conservative force there is no energy dissipation, and therefore no damping of motion.

It is possible to make the spacecraft aerodynamically stable around the yaw axis by deploying two solar panels. At the same time the spacecraft mass model changes, becoming stiffer to non-linear effects and showing more coupled response between the roll and yaw axes. By deploying the solar panels, significant restoring torques are produced about the yaw axis. The aerodynamic forces are non-conservative, and therefore the aerodynamic torque produces damping of angular motion about the yaw axis. However, aerodynamic performance works better at lower altitudes and 600 km seems to be too high to guarantee three axes stabilization.

After general analysis of the satellite's motion more specific conclusions and proposed future work are detailed in the following sections.

10.1 Boom Length and Position

Gravity gradient depends strongly on the mass distribution, which is modified by deploying a boom. Therefore, the boom length and its position relative to the spacecraft are important parameters to work with. Homogeneous mass distribution has been assumed for modeling of the spacecraft.

Performance depending on boom length has been studied, and it has been seen that a 1.2 meters boom length delivers satisfactory results in terms of maximum deviation.

The boom location changes the position of the satellite's center of mass, which also affects the dynamics of the spacecraft. Pitch and yaw motion are not significantly affected by the boom position. This is different for the roll motion. Moving the boom's location to the front of the spacecraft produces smaller

angle deviation about the roll axis, but to move it 7.5 mm to the front has to be avoided.

10.2 Dynamic Constraints

For the correct performance of the satellite, it is of essential that the satellite is correctly detumbled. It has been demonstrated that deviations in angular velocity from its equilibrium value of $\vec{\omega} = (0, -n, 0)$ lead to large deviations. If the correct angular velocity is not achieved a damping mechanism would be required.

Additionally, once the boom is deployed, the deviation from the orbit reference frame has to be as small as possible. If only gravity gradient stabilization is used the motion will propagate the initial deviation. Special attention is required by the roll axis, which has delivered the worst results in term of maximum deviation.

10.3 Future Work

After concluding this master thesis the design process of SWIM continues. Several aspects concerning the dynamics have to be taken into account for future actions.

The boom has been modeled as a solid rigid body. However, this is a simplification. Compared to the hub, the boom is expected to behave as an elastic body. In further stages of the project this aspect has to be taken into account and the boom has to be modeled as a flexible appendage.

An homogeneous mass distribution model has been assumed. However, as soon as it is decided where the different experiments are located, a more realistic mass model can be generated, and more realistic simulations can be performed.

Further investigation is required if it is decided that aerodynamic stabilization should be included in the model. First of all the atmospheric density model needs to be more accurate as mentioned in Chapter 9. Similarly more investigation about the solar panels deployment is required. Panels have been deployed perpendicular to one of the faces of the hub. However, if the panels are deployed with a certain angle with respect to the velocity direction, the aerodynamic performance can be improved. Doing so the protection of the velocity vector when there is deviation about the yaw axis is larger, and therefore, so is the aerodynamic force and torque. Resulting on a higher restoring capability.

Finally the satellite can be actively controlled using the Earth's magnetic field. That would require the insertion of torque coils without magnetic cores in the satellite. Besides a control algorithm needs to be implemented. This technique would affect power requirements and experiment measurements.

Bibliography

- [1] <http://www.cubesat.org>(accessed August 25, 2011).
- [2] *CubeSat Design Specification Rev.12* The CubeSat Program, Cal Poly SLO http://www.cubesat.org/images/developers/cds_rev12.pdf(accessed August 25, 2011).
- [3] Yen-Hsun Chen, Zuu-Chang Hong, Chung-Hsien Lin *Aerodynamic and Gravity Gradient Stabilization for Microsatellites* Acta Astronautic Vol.46, No. 7, pp.491-499, 2000 Great Britain
- [4] Bong, Wie *Space vehicles dynamics and control* AIAA, 1998
- [5] Vladimir A. Chobotov *Orbital Mechanics* AIAA Education Series, Washington, 1991
- [6] Hanspeter Schaub, John L.Junkins *Analytical Methods of Space Systems* AIAA Education Series, 2003
- [7] James Wertz. *Spacecraft Attitude Determination and Control* D. Reidel Publishing Co., Dordrecht, 1978
- [8] C-G. Fälthammar *Space Physics compendium* KTH, Space and Plasma Physics department, 2009
- [9] Willian E. Wiesel. *Spaceflight Dynamics* The McGraw-Hill Companies, Inc 1997 Second edition
- [10] Carlos A. Felippa, *The Mathematics of Finite Rotations* , Appendix R in Non-Linear Finite Element Methods, Available from Internet <http://www.colorado.edu/engineering/cas/courses/d/NFEM.d/>(accessed September 1, 2011).
- [11] Jack B. Kuipers. *Quaternions and Rotation Sequences* Princeton University Press, 1999
- [12] Sidi M. J. *Spacecraft Dynamic and Control* Cambridge University Press, 1999
- [13] M. H. Acuña *The Design, Construction and Test of Magnetically Clean Spacecraft - A Practical Guide* April 1994
- [14] T. Bak, R.Wisniewski *Passive Aerodynamics Stabilization of Low Earth Satellite Orbit* Third International Conference on Spacecraft Guidance, Navigation and Control Systems, ESTEC, Noordwijk, The Netherlands, 26-29 November 1996, ESA SP-381 (February 1997)
- [15] J.L. Meriam, L.G. Kraige *Engineering Mechanics Dynamics VI edition* John Wiley and Sons, Inc S, 2008
- [16] www.cubesatkit.com(accessed September 16, 2011).
- [17] L. Edsberg *Introduction to Computation and Modeling for Differential Equations* John Wiley and Sons, 2008
- [18] The MathWorks,Inc. *MATLAB[®] Mathematics* 1984-2011 The MathWorks,Inc.
- [19] Å. Forslund, N. Ivchenko, G. Olsson, T. Edberg and A. Marusenkov *Miniaturized digital fluxgate magnetometer for small spacecraft applications* Science and Tecnology 19 015202, 2008

- [20] S. K. Jeon, T. W. Murphey *Desing and analysis of a meter-class CubeSat boom with a motor-less deployment by bi-stable tape springs* 52nd AIAA/ASME/ASCE/AHS/ASC Structures, Structural Dynamics and Materials Conference, 4-7 April 2011, Denver, Colorado
- [21] A. Sim, M. Santer *Analysis of a Segmented Compliant Deployable Boom for CubeSat Magnetometer Missions* 51st AIAA/ASME/ASCE/AHS/ASC Structures, Structural Dynamics and Materials Conference, 12-15 April 2010, Orlando, Florida
- [22] <http://mem.drexel.edu/satellite/dragonsat1.htm>(accessed September 15, 2011).
- [23] GEOPACK library, Available from Internet <http://www.igpp.ucla.edu/public/tpoi/Pliny/MATLAB/Tsyg/>(accessed March 15, 2011).
- [24] C. Arduini, P. Baiocco *Active Magnetic Damping Attitude Control for Gravity Gradient Stabilized Spacecraft* Journal of Guidance, Control and Dynamics, Vol. 20, No. 1, January-February 1997

XR-EE-SPP 2011:006